

Mechanistic Insights with Homogeneous Pd and Pt Complexes for the Oxidative Coupling of Methane

by

Monica D. Lotz

A dissertation submitted in partial fulfillment
of the requirements for the degree of
Doctor of Philosophy
(Chemistry)
in the University of Michigan
2015

Doctoral Committee:

Professor Melanie S. Sanford, Chair
Professor Mark M. Banaszak Holl
Professor Suljo Linic
Professor John Montgomery

Dedicated To Barbara and Don

Acknowledgements

In my graduate career, I have learned many important lessons – both in life and in my scientific career. I am thankful for all the people who not only helped me to learn these lessons but also continued to support me throughout this journey. This has been an extremely rewarding experience, and it certainly would not have been possible without the contributions of my teachers, peers, friends and family.

Throughout my scientific education, I have had a number of amazing educators who have undoubtedly made me the passionate and dedicated scientist I am today. My high school chemistry teacher, Mr. Powell, had an inspirational way of teaching chemistry with his chemistry caroling and reenactments of the Hindenburg explosion. He taught me about the exciting aspects of chemistry and to have confidence in myself as a scientist. During my undergraduate studies at the University of Texas, I joined the research lab of Professor Stephen Martin, under the guidance of Dr. John Delorbe. They both taught me a significant amount about conducting research and presenting my work to a scientific community, which ultimately helped me get a position at Bristol-Myers Squibb. At BMS, I had the privilege to work under Dr. Christine Tarby. She was a great role model, demonstrating how to be a successful female scientist while remaining dedicated to her family. She also encouraged me to further my career by pursuing a Ph.D., even guiding me to apply to the University of Michigan. I am extremely thankful to all of these people who impacted my career early on and led me to continue my studies in graduate school.

At the University of Michigan, I had the opportunity to work in the group of Professor John Montgomery. Professor Montgomery was extremely supportive of my passion for organometallic chemistry, even allowing me to take my project in a direction less commonly pursued by his group. Additionally, a number of students in his group really encouraged me as a young student to ask questions and expand my organic synthesis knowledge.

Ultimately, I joined Professor Melanie Sanford's research group to pursue my graduate studies. Melanie was really an inspiration for me – through her infectious passion for science to her amazing ability to engage any audience during scientific presentations. I have no doubt that the lessons she has taught me will be invaluable in my future career, and I greatly appreciate her continued support in my graduate studies.

During my graduate work, I also had the opportunity to be a part of a NSF collaboration, CENTC. This collaboration provided a highly supportive environment to share my chemistry with the leading professors in the field, along with many of their students. Everyone in the center has impacted my education, specifically Professor James Mayer, who collaborated on my project. Jim has been like a second advisor to me, giving me advice on my chemistry and in my career, which has proven invaluable to my growth as a scientist.

My committee, Professor John Montgomery, Professor Mark Banaszak Holl, and Professor Suljo Linic, have provided advice and guidance throughout my graduate career, from candidacy to my defense. Furthermore, a number of professors and students throughout the department have been really helpful in everything from poster sessions to casual conversations in the hallway. I am very fortunate to have worked in such a collaborative atmosphere that encouraged me to excel in my science.

While in the Sanford group, I had the pleasure to work with many talented students from diverse backgrounds. Although a number of them taught me invaluable lessons, I interacted with a few very closely and would like to acknowledge their contributions. Dr. Matt Remy taught me how to be an inorganic chemist, and I am very grateful for his patience and encouragement. Dr. Amanda Hickman, an early deskmate, gave me significant advice early in my career which really helped me to persevere through graduate school. I also had the opportunity to work with Lily Hale and Diana Cox, providing experiences in mentoring which will help me significantly in the future.

Through CENTC, I was able to interact with a number of scientists across the country, including direct collaborations with Dr. David Lao, Professor Johanna Blaquiere, and Dr. Brad McKeown. I really enjoyed the opportunity to discuss ideas with these students and the guidance they provided in troubleshooting problems that arose in my chemistry.

Lastly, my friends and family have provided endless support throughout my graduate studies. Friends, both near and far, have been amazing in this whole process, but there are too many people to thank for all of their distractions, encouragement, and support, so I would like to mention a few. Much thanks to: Tamara, Colin, and Nicki for never letting me forget my Texan roots, Emily for keeping me on track, Jennifer for always being there to lend an ear, Mal for keeping me grounded, Noah and Serina for the walks and coffee, and Leslie for being my cheerleader – it wouldn't have been as easy without you. Tyler – your understanding and patience is endless. And to my family, Allison, Mom and Dad, I can't put into words how much I have appreciated your unwavering love, support and kindness throughout this process.

Table of Contents

Dedication.....	ii
Acknowledgements	iii
List of Schemes	viii
List of Tables.....	x
List of Figures	xii
List of Abbreviations.....	xv
Abstract	xvii
CHAPTER 1.....	1
Upconversion of Natural Gas to Access Value-Added Products.....	1
References	9
CHAPTER 2.....	12
Mechanistic Studies of Methyl Transfer and Reductive Elimination of Palladium Methyl Complexes.....	12

Background	12
Results and Discussion.....	16
Conclusions	32
General Experimental Procedures and Characterization	33
References	51
 CHAPTER 3.....	 54
Investigating C–H Activation at Palladium: Studies with Arene Model Substrates	54
Background	54
Results and Discussion.....	57
Conclusions	72
General Experimental Procedures and Characterization of Data.....	73
References	97
 CHAPTER 4.....	 101
Conversion of Methane to Ethane: High Throughput Experimentation and Resulting Studies	101
Background	101
Results and Discussion.....	104
Conclusions	121
Future Directions.....	122
General Experimental Procedures and Characterization	125
References	135

List of Schemes

Scheme 1.1 Industrial Methods to Functionalize Methane.....	3
Scheme 1.2 Potential Routes to Methane Functionalization	4
Scheme 1.3 Leading Heterogeneous Process for the Oxidative Coupling of Methane	5
Scheme 1.4 Selected Pd/Pt Catalysts Shown to Perform Partial Oxidation of Methane	6
Scheme 1.5 Ethane-Forming Reductive Elimination via High-Valent Intermediates	7
Scheme 1.6. Proposed Route to Oxidative Coupling of Methane	8
Scheme 2.1. Proof-of-Principle for Oxidative Coupling Generate Ethane.....	15
Scheme 2.2. Degenerative Exchange of Methyl Groups with Pt.....	15
Scheme 2.3. Thermolysis of Mono-methyl Complex 3.....	16
Scheme 2.4. Oxidation of 3 with AcFcBF ₄ and NFTPT.....	18
Scheme 2.5. Prior Studies to Observe Organometallic Intermediate 2 via ¹ H NMR Spectroscopy	20
Scheme 2.6. Proposed Mechanism for Ethane-Formation from 3.....	20
Scheme 2.7. Thermolysis of Mono-methyl Complex 9.....	24
Scheme 2.8. Proposed Mechanism of Reaction of 9 with NFTPT	28
Scheme 3.1. Proposed Catalytic Cycle for Methane Functionalization.....	55

Scheme 3.2. Proposed Catalytic Cycle for Methane Functionalization.....	56
Scheme 3.3. Activation of C ₆ F ₅ H with 1-Cl to Generate 2 and 3.....	57
Scheme 3.4. H/D Exchange with C ₆ F ₅ H and Various MOPiv Sources.....	83
Scheme 4.1. Proposed Catalytic Cycle for Methane Dimerization	103
Scheme 4.2. Representative Control Reaction under 10 bar CH ₄	107
Scheme 4.3. Ethylene Generated from Palladium Salts, Under CH ₄ and N ₂ Pressures	114
Scheme 4.4. Yields of C ₂ H ₆ and C ₂ H ₄ from K ₂ PtCl ₆ and a Biscarbene Ligand.....	114
Scheme 4.5. Yields of C ₂ H ₄ and C ₂ H ₆ Using (bipyrimidine)Pt ^{II} Cl ₂	115
Scheme 4.6. Generation of C ₂ H ₆ and C ₂ H ₄ Using (DAB)PtCl ₂ Complexes	115
Scheme 4.7. A Tandem Catalytic Approach to Methane Coupling.....	122
Scheme 4.8. Tandem Catalysis to Convert Methane to Ethane	124
Scheme 4.9. Ethane and Ethylene Generated from 6 Under Pressure of CH ₄ or N ₂	132
Scheme 4.10. Ethane and Ethylene Generation from Complex 6 at Reduced Times.....	133
Scheme 4.11. Ethane and Ethylene Generation Using CsOPiv or Cs ₂ CO ₃ with Complex 6	134
Scheme 4.12. Generation of Ethane and Ethylene from Pt Complexes Under N ₂	134

List of Tables

Table 2.1. Oxidation of 3 with $1e^-$ and $2e^-$ Oxidants ^a	17
Table 2.2. Influence of Cyclohexadiene (CHD) and Light on Oxidative Ethane Formation from 3	19
Table 2.3. Reaction of 9 with AcFcBF ₄ and NFTPT	25
Table 2.4. Reaction of Mono-methyl Complexes with AcFcBF ₄	32
Table 2.5. Results from Thermolysis of 3 and 9.....	40
Table 3.1. Probing Carboxylate Complexes in C ₆ F ₅ H Activation.....	58
Table 3.2. Developing a Model System to Investigate C–H Activation.....	59
Table 3.3. Reactivity of Mono-Aryl Palladium Complex 2.....	67
Table 3.4. Dimerization of Thiophenes Under Optimized Conditions.....	70
Table 3.5. Deuterium Incorporation of 2-substituted Thiophenes	72
Table 3.6. Dimerization of 2-R-Thiophene with 1-OAc Under Stoichiometric Conditions	88
Table 3.7. Crystal Data and Structure Refinement for (dtbpy)Pd ^{II} (C ₆ F ₅)(I).....	94
Table 3.8. Crystal Data and Structure Refinement for 3.....	96
Table 4.1. HTE Hits Generating Ethane and Ethylene	108
Table 4.2. Ethane and Ethylene Generated using Palladium Complexes	113

Table 4.3. Modifying Conditions to Impede Formation of Ethane Under N ₂	117
Table 4.4. Ethane and Ethylene Observed from 12 and 13 under CH ₄ and N ₂	121
Table 4.5. Ethane and Ethylene Formed at Reduced Temperatures	133

List of Figures

Figure 1.1. U.S. Energy Production by Fuel, 1980 - 2040 ¹	2
Figure 2.1. Homogeneous Pd-Catalyzed Arene Oxidative Dimerization to Generate Industrial Precursor to Upilex® Resin	13
Figure 2.2. Proposed Catalytic Cycle for Pd-Catalyzed Methane Oxidative Dimerization	14
Figure 2.3. Monitoring the Oxidation of 3 with AcFcBF ₄ at -80 °C	21
Figure 2.4. Energy Profile for the Oxidation of (bpy)Pd(CH ₃)(CF ₃) (3') with NFTPT	23
Figure 2.5. Energy Profile for the Oxidation of (bpy)Pd(CH ₃)(CF ₃) (9') with NFTPT	26
Figure 2.6. Energy Profile for the Formation of H ₃ C–OAc and H ₃ C–CF ₃ from 8' and 13', respectively	27
Figure 2.7. Oxidation of 9 with AcFcBF ₄ Upon Addition of CD ₃ CN.....	29
Figure 2.8. New Pd ^{IV} Intermediates Formed <i>In Situ</i> Upon Oxidation of 9 with AcFcBF ₄	30
Figure 2.9. Authentic Synthesis of Pd ^{IV} Intermediate 13-CD ₃ CN.....	31
Figure 2.10. ¹ H NMR Spectra for Low Temperature Oxidation of 9 with AcFcBF	43
Figure 2.11. ¹⁹ F NMR Spectra for Low Temperature Oxidation of 9 with AcFcBF ₄	44
Figure 2.12. ¹ H- ¹ H ROESY NMR Spectra	45
Figure 2.13. ¹ H- ¹ H ROESY NMR Spectra	46

Figure 2.14. ¹ H NMR Spectra for Independent Synthesis of Proposed Intermediates 13-CD ₃ CN and 13-isomer.....	48
Figure 2.15. DFT Calculations for the Low Energy Pathway for Oxidation of (dtbpy)Pd(CH ₃)(Cl).	49
Figure 2.16. DFT Calculations for the Low Energy Pathway for Competing Reductive Elimination with the Chloride Complex.....	50
Figure 3.1. Monitoring the Reaction by ¹⁹ F NMR Spectroscopy	61
Figure 3.2. Overlapping ¹⁹ F NMR Spectra for <i>In Situ</i> Observation of 4.....	62
Figure 3.3. H/D Exchange Studies with C ₆ F ₅ H and Various MOPiv Sources	63
Figure 3.4. Comparison of <i>In Situ</i> Formation of 4 with Authentically Synthesized 4	64
Figure 3.5. Observance of Shifting ¹⁹ F NMR Resonances in Isolated Ag Species (4) With Acetate and Pivalate Anions	65
Figure 3.6. Monitoring the Reaction of 1-OAc with Preformed 4 by ¹⁹ F NMR	66
Figure 3.8. ¹⁹ F NMR Experiment of Dimerization of 2-Trifluoromethyl Thiophene	71
Figure 3.9. Plot of the Reaction of 1-OAc with C ₆ F ₅ H Upon Addition of AgOPiv.....	82
Figure 3.10. Plot of the Reaction of 1-OAc with 4.....	85
Figure 3.11. Plot of the Reaction Progress Upon Treatment of 2 with C ₆ F ₅ H/AgOPiv.....	86
Figure 3.12. Plot for the Reaction Upon Treatment of 2 with AgC ₆ F ₅ (4).	87
Figure 3.13. Overlaped Spectra for H/D Exchange of 2-methyl thiophene and MOPiv.....	90
Figure 3.14. Overlaped Spectra for H/D Exchange of 2-trifluoromethyl thiophene and MOPiv.....	91
Figure 4.1. Industrial Process for Accessing Alkanes from Methane.....	102
Figure 4.2. Potential Routes to Functionalization of Methane	103
Figure 4.3. High Throughput Experiment – Reactor Setup.....	104
Figure 4.4. Representative Conditions for the Conversion of Methane to Ethane	105
Figure 4.5. Sampling of Reaction Headspace from Parallel Reactor to Gas Bag.....	107
Figure 4.6. Setup for Sampling of Gaseous Products From Pressure Vessel	110

Figure 4.7. Reproducibility of Sampling and Calibration of System	111
Figure 4.8. Modifications to Pressure Vessel to Enable Solution Phase Sampling.....	112
Figure 4.9. Ethane Generated Using Complex 6 under Pressures of CH ₄ and N ₂	116
Figure 4.10. Probing the Background Reaction – Modification of the Base	118
Figure 4.11. Methods for Modification of the Aryl Substituent of 6 to Inhibit the Observed Background Reaction.....	119
Figure 4.12. Modifications in the Backbone of the Ligand Scaffold for 6 to Minimize the Background Ethane Observed.....	120
Figure 4.13. Precedents for Cobalt Mediated C–H Functionalization and H ₃ C–CH ₃ Coupling	125
Figure 4.14. HTE Generating C ₂ Products.....	131
Figure 4.15. Diagram of the Sample Loop on the GC-2010 Plus.....	132

List of Abbreviations

AcFcBF ₄	Acetylferrocenium tetrafluoroborate
Ar	Aryl
BF ₄ ⁻	Tetrafluoroborate
bpm	bipyrimidine
bpy	4,4'-bipyridine
BQ	1,4-benzoquinone
CAN	Ceric ammonium nitrate
CHD	1,4-cyclohexadiene
COSY	Correlation spectroscopy
DAB	Diazabutadiene (diarybutane diimine)
DFT	Density functional theory
DMSO	Dimethyl sulfoxide or (H ₃ C) ₂ SO
dtbpy	2,2'-di- <i>tert</i> -butyl-4,4'-bipyridine
<i>e</i> ⁻	electron
Fc ⁺	ferrocenium
FcBF ₄	Ferrocenium tetrafluoroborate
GC	Gas chromatography
GTL	Gas-to-liquids
HMBC	Heteronuclear multiple bond correlation

HOMO	Highest occupied molecular orbital
HSQC	Heteronuclear single quantum coherence spectroscopy
HTE	High throughput experimentation
LUMO	Lowest unoccupied molecular orbital
Me	Methyl or CH ₃
MeOH	Methanol or CH ₃ OH
NCS	N-Chloro-succinimide
NFPBF ₄	N-fluoropyridinium tetrafluoroborate
NFTPT	<i>N</i> -fluoropyridinium triflate
NMR	Nuclear magnetic resonance
OAc	Acetate or CH ₃ COO ⁻
OPiv	Pivalate or (CH ₃) ₃ COO ⁻
ORTEP	Oak Ridge thermal ellipsoid
OTf ⁻	Triflate or CF ₃ O ₂ SO ⁻
OTFA	Trifluoroacetate or CF ₃ COO ⁻
Oxone	Potassium peroxymonosulfate
Pd ^X or Pt ^X	Palladium or platinum with the oxidation state of X
PhI(OAc) ₂	Iodobenzene diacetate
PhI(OTFA) ₂	Iodobenzene ditrifluoroacetate
ppm	Parts per million
^R DAB ^{R'}	DAB ligand where R = aryl substituents and R' is substitution on the backbone
ROESY	Rotating frame Overhauser effect spectroscopy
TFE	2,2,2-trifluoroethanol
TMEDA	Tetramethylethylenediamine or (CH ₃) ₂ N(CH ₂) ₂ N(CH ₃) ₂
TMS	Trimethyl silyl or (CH ₃) ₃ Si
TP	2,4,6-trimethylpyridine

Abstract

The domestic production of natural gas has significantly increased in recent years. As a result, there is a demand to utilize its main component, methane, as a C1 source for value-added products, such as gasoline or diesel fuels. The industrial conversion of methane to liquid fuels uses multi-step processes with heterogeneous catalysts, which require high energy input and result in poor selectivity for the desired products. An attractive alternative to this method employs homogeneous catalysts to perform the oxidative coupling of methane. This approach could directly access higher alkanes at lower temperatures to achieve a more mild and selective process. Additionally, mechanistic insight gained from well-established solution-phase techniques could help improve the yield and selectivity in such homogeneous reactions. The proposed mechanism to form the initial product ethane from methane involves: (i) C–H activation of methane to generate a M–CH₃ intermediate, (ii) oxidatively-induced disproportionation between M–CH₃ intermediates to form a M–(CH₃)₂ species, and (iii) reductive elimination from M–(CH₃)₂ to liberate ethane.

Chapter 2 describes the stoichiometric oxidation of homogeneous mono-methyl Pd^{II} complexes to selectively generate ethane. Experimental and computational studies support the formation of a dimethyl Pd^{IV} intermediate from methyl transfer. These studies demonstrate steps ii and iii of our proposed catalytic cycle.

In Chapter 3, C–H activation, step i, is examined using a model system. Pd^{II} complexes and AgOPiv are employed in the C–H activation of pentafluorobenzene, via a Ag–C₆F₅ intermediate.

Experimental evidence supports a Ag-mediated activation of pentafluorobenzene to form Ag-C₆F₅, followed by transmetalation to Pd, affording the Pd^{II} product.

Chapter 4 explores the conversion of methane to ethane based on mechanistic information gained in the aforementioned stoichiometric studies of steps i, ii, and iii. High throughput experimentation demonstrates ethane generation from several reactions containing Pd or Pt complexes, which are further pursued upon the development of a method to quantify the gaseous products. These studies reveal that a decomposition pathway to form ethane arises from ligand degradation, and that ligand modification suppresses this side reaction. Further studies with these modifications are being pursued to achieve methane coupling.

Chapter 4 explores the conversion of methane to ethane based on mechanistic information gained in the aforementioned stoichiometric studies of steps i, ii, and iii. High throughput experimentation demonstrates the formation of ethane from several reactions containing Pd or Pt catalysts, which are further pursued upon the development of a method to quantify the gaseous products. These studies reveal that a significant decomposition pathway to form ethane arises from ligand decomposition, and that ligand modification suppresses this side reaction. Further studies with these modifications are being pursued in order to achieve methane coupling.

CHAPTER 1

Upconversion of Natural Gas to Access Value-Added Products

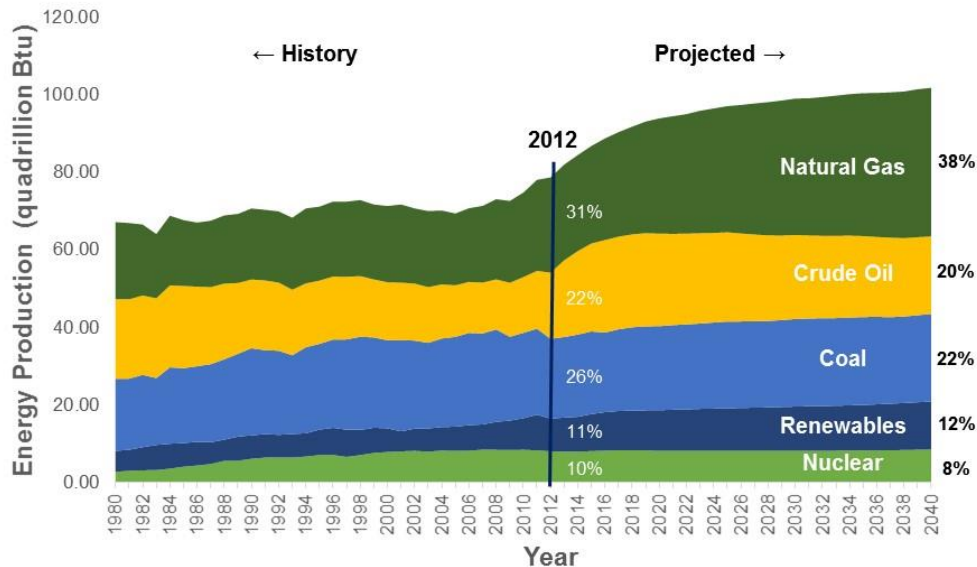
1.1 Overview

As natural gas production increases in the United States, methods to efficiently utilize this abundant resource have gained growing attention. Natural gas is most often burned to generate heat and electricity for industrial and residential applications. However, a major inefficiency associated with this process is the transportation of this gas. To circumvent this challenge, the main component, methane, could be converted into liquid fuels or commodity chemicals. This introduction discusses several relevant approaches to the functionalization of methane, from established industrial processes to recent advances of individual steps in this transformation.

1.2 Increasing Natural Gas and Common Utilization

Since 2005, domestic natural gas production has dramatically increased, mainly as a result of improved hydraulic fracturing techniques for accessing shale gas. As shown in Figure 1.1, the U.S. Energy and Information Administration projects dramatically rising supplies of natural gas, making domestic natural gas production by 2040 nearly equal to coal and crude oil combined.¹ As natural gas has become more abundant, the price has dropped by almost 50% since 2008.² Thus, increased effort has focused on developing strategies to utilize this cheap, abundant carbon source in place of traditional crude oil feedstocks, thereby reducing our dependence on foreign oil.

Figure 1.1. U.S. Energy Production by Fuel, 1980 - 2040¹



In the U.S., natural gas is typically burned to generate heat and power, as transporting natural gas from drilling or fracking sites to homes and businesses is highly energetically wasteful. Natural gas is most commonly transported by pressurization in pipelines, but it can also be condensed into liquefied natural gas and shipped in tanker trucks. Both of these methods are much less efficient than shipping liquid alkanes. Due to the significant transportation cost and/or limited pipeline infrastructure, excess natural gas from crude oil production and processing is often flared, or burned off, in more remote areas. Although flaring reduces the negative environmental impact of this potent greenhouse gas, this process wastes significant amounts of natural gas and generates environmentally detrimental CO₂ in the process.³ Thus, an efficient method for converting natural gas into a liquid form could provide a more transportable form of energy.

Natural gas is composed of 70 to 90% methane, which provides an attractive carbon source for liquid transportation fuels and commodity chemicals.⁴ The chemical conversion of methane could circumvent the associated inefficiencies of transporting natural gas and could provide access to products traditionally arising from crude oil. Thus, methane functionalization would be a useful alternative to typical methods to burn natural gas.

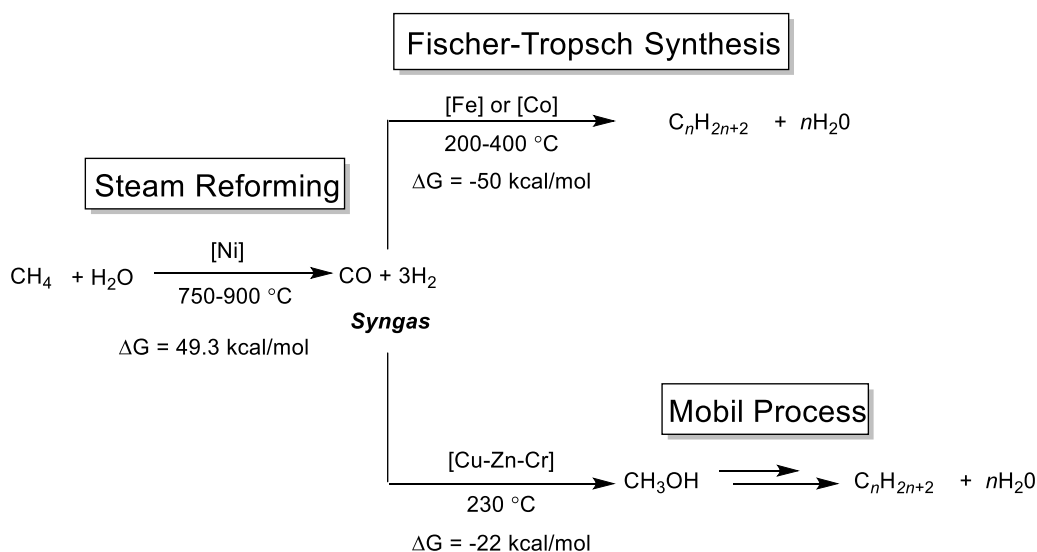
1.3 Chemical Conversion of Methane

Methane functionalization ($\text{H}_3\text{C-H} \rightarrow \text{H}_3\text{C-X}$) is a challenging process due to the inert nature of this molecule. Thus, selective functionalization of methane and other alkanes, is often considered the “holy grail” reaction for chemists.⁵ Methane contains very strong C–H bonds of 105 kcal/mol, has poor solubility in many polar solvents, and has poor coordinative abilities. To overcome the unreactive nature of methane, many approaches employ harsh conditions with high temperatures and pressures.^{6–9} However, all of these conditions introduce a series of new challenges that must be addressed to achieve an industrially viable process.

1.4 Industrial Approaches to Methane Upconversion

Currently, several methods to convert methane into value-added products are conducted on an industrial scale. The most well established process involves an initial steam reforming step to generate syngas, comprised of a mixture of CO and H_2 .⁶ Syngas can then be converted into methanol and ultimately gasoline through the Mobil process, or proceed directly to higher alkanes through the Fischer-Tropsch synthesis (Scheme 1.1).¹⁰ However, a number of limitations are associated with these methods to upconvert methane.

Scheme 1.1 Industrial Methods to Functionalize Methane



Both the Mobil Process and Fischer-Tropsch synthesis require high temperatures to generate the syngas intermediate, which is a highly energy intensive step.⁶ The Fischer-Tropsch step also

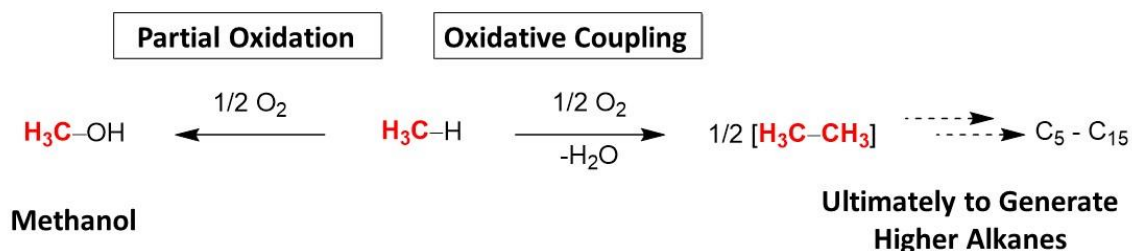
results in a mixture of products, further reducing the overall efficiency of the process.¹⁰ Furthermore, the gas-to-liquid (GTL) plants to convert methane into liquid fuels require high capital investments, often upwards of billions of dollars. Despite these limitations, globally five GTL plants were operational as of early 2014 with four additional plants in planning or construction phases.¹¹ This is likely a result of the low price and increasing abundance of natural gas.

1.5 Direct Routes to Methane Functionalization

To avoid the challenges associated with the multi-step GTL process, extensive research has been focused on direct routes to convert methane into value-added products. In nature, methane monooxygenase performs the selective partial oxidation of methane to generate methanol through the use of an iron active site.¹² Although this process provides a direct and selective route to methane functionalization, performing this transformation on an industrial scale is currently challenging.¹³

Similar approaches have been widely studied in catalysis research, in which the C–O bond in methanol is formed via activation of methane (Scheme 1.2).^{9,14–20} An inherent challenge in the catalytic conversion of methane to methanol is the propensity for over-oxidation, which converts the desired product, methanol, to the thermodynamically favored product CO₂. Several reports^{17,19,21–23} have taken various strategies to overcome this challenge, using unique reaction conditions, oxidants and solvents, however, none of these processes can outperform current GTL methods.

Scheme 1.2 Potential Routes to Methane Functionalization



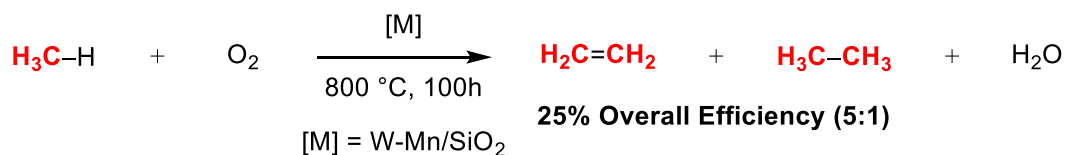
An alternate method for the functionalization of methane would be through oxidative coupling to generate the C–C bond in ethane (Scheme 1.2). Upon subsequent couplings, higher liquid

alkanes could access transportation fuels such as gasoline or diesel fuel. Additionally, olefins such as ethylene or butadiene, valuable precursors to a wide array of polymers, could be formed through oxidative coupling of methane. Moreover, this process could replace traditional petroleum feedstocks, as both higher alkanes and olefins are predominantly synthesized from cracking of crude oil.

1.6 Current Advances in Oxidative Coupling of Methane

Significant research on the oxidative coupling of methane has focused on the use of heterogeneous metal oxide catalysts to generate ethane and ethylene (Scheme 1.3).^{7,24–27} The leading reports employ mixed catalyst systems with lithium and magnesium²⁸ or tungsten and manganese.²⁵ These transformations are proposed to proceed through homolytic cleavage of the C–H bond, to generate methyl radical, which recombines with another methyl radical to generate ethane or ethylene. To make these processes industrially viable, approximately 30% overall efficiency is required; however, after years of research on catalyst design, leading catalysts still do not meet this standard.²⁶ Some relevant limitations include: (1) poor selectivity due to significant overoxidation to form CO and CO₂; (2) harsh reaction conditions with temperatures over 700 °C required to achieve reactivity of methane; and (3) heat transfer issues resulting in hot spots in the catalyst bed that lead to catalyst degradation.²⁶ Additionally, similar transformation with alkanes higher than methane could result in regioselectivity issues, as secondary C–H bonds are more easily functionalized due to lower bond dissociation energies.²⁹ To address these challenges of heterogeneous catalysts, significant efforts in catalyst design and modifications have been pursued, such as the process currently being commercialized by Siluria using nanowire catalysts.^{30,31} To further address these challenges, a better mechanistic understanding of reactivity at the metal center is required to inform both chemical and engineering modifications to these systems.

Scheme 1.3 Leading Heterogeneous Process for the Oxidative Coupling of Methane³²

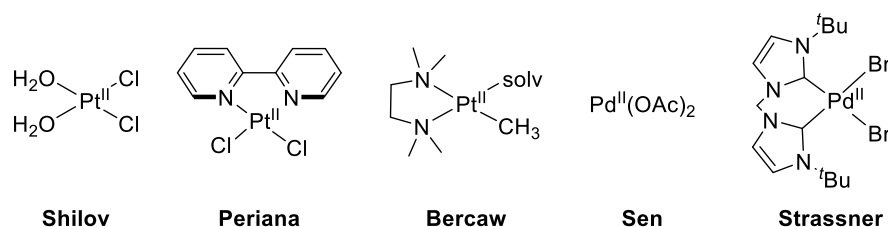


In our approach for the oxidative coupling of methane, we sought to address some issues faced in heterogeneous systems by exploring the use of homogeneous catalysts. Typically, homogeneous systems operate at lower temperatures, which provides opportunities for mitigating catalyst deactivation and overoxidation pathways that are commonly observed at the high temperatures required for the heterogeneous systems.³³ Furthermore, mechanistic experimental techniques are well established with homogeneous catalysts, facilitating efforts to obtain the mechanistic insights necessary to rationally improve the reactivity and selectivity of the catalyst. Despite these benefits, prior examples of homogeneous catalytic alkane/alkane coupling reactions are scarce.^{34–37}

1.7 Prior Studies on Methane Activation or Methyl Coupling with Pd and Pt

Precedents for the methane activation with homogeneous Pd^{II} and Pt^{II} catalysts and ethane generation from palladium or platinum methyl complexes support the potential feasibility of the oxidative coupling of methane using homogeneous Pd and Pt catalysts. For example, partial oxidation of methane to methanol has been shown by Shilov¹⁴ with homogeneous platinum salts. Numerous subsequent studies^{9,15,20,38–43} have established the detailed mechanism of the C–H activation step in this system. Periana also performed methane functionalization with a homogeneous palladium or platinum catalyst to generate methyl bisulfate or acetic acid.^{17,21,44} Additional reports on the partial oxidation of methane have also been shown with palladium salts⁴⁵ and biscarbene palladium complexes, as shown in Scheme 1.4. We drew inspiration from these examples of homogeneous Pd and Pt catalysts that are known to activate methane for our studies into the oxidative coupling of methane (Scheme 1.4).

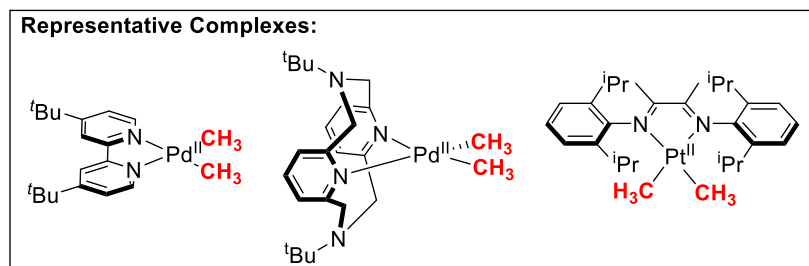
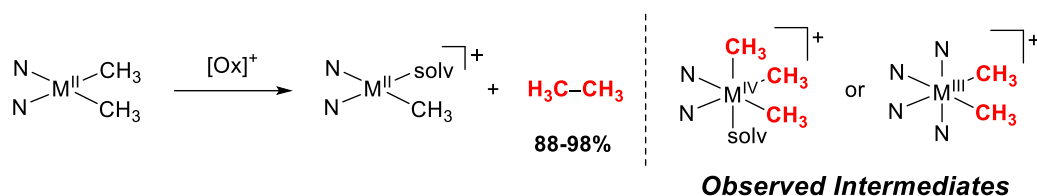
Scheme 1.4 Selected Pd/Pt Catalysts Shown to Perform Partial Oxidation of Methane



In the late 1980s, Canty demonstrated the first example of the reductive elimination from a high-valent Pd^{IV}–CH₃ species to generate ethane. More recently, several reports from our group^{46–}

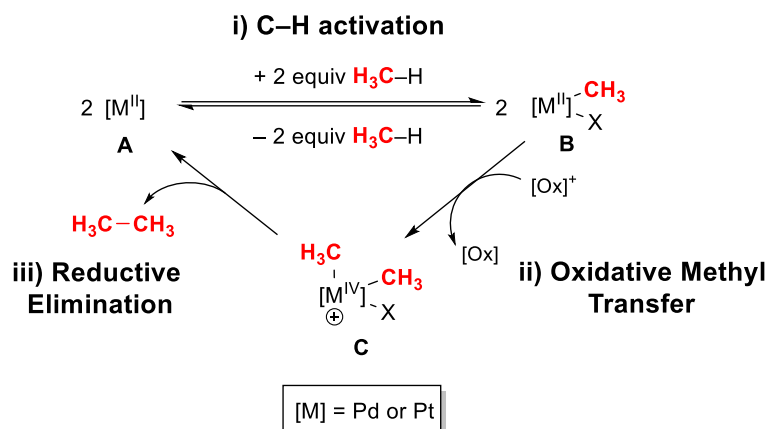
⁴⁹ and others^{50–59} have shown the oxidation of similar low-valent Pd^{II} and Pt^{II} dimethyl complexes to access high-valent intermediates, followed by selective formation of ethane under mild reactions conditions (Scheme 1.5). Based on these studies, we propose a similar reaction for ethane formation from reductive elimination using Pd or Pt methyl complexes

Scheme 1.5 Ethane-Forming Reductive Elimination via High-Valent Intermediates



Collectively, these reports of methane activation and H₃C-CH₃ coupling at palladium and platinum metal centers help to inform our catalytic cycle for oxidative coupling of methane (Scheme 1.6). Our proposed catalytic cycle involves: (i) activation of methane by a Pd or Pt metal center, **A**, to form **B**; (ii) methyl transfer between two molecules of **B** to generate 0.5 equiv of **C**; and (iii) reductive elimination at **C** to liberate ethane and regenerate **A**. The following chapters outline mechanistic studies related to each of the steps of the proposed catalytic cycle. Mechanistic studies on the oxidation and reductive elimination, steps *ii* and *iii*, are discussed in Chapter 2 (Scheme 1.6). Mechanistic studies of C–H activation at Pd, shown as step *i*, are described in Chapter 3 using a model system. Finally, we explore the generation of C₂ products from methane in Chapter 4, combining all three steps of our proposed catalytic cycle. These studies could have direct implications for the development of a catalytic homogeneous approach to the oxidative coupling of methane.

Scheme 1.6. Proposed Route to Oxidative Coupling of Methane



1.8 Collaborations in Our Efforts towards Oxidative Coupling of Methane

Studies in the Sanford lab on the oxidative coupling of methane were in collaboration with Professor James Mayer, and much of the work shown from the high throughput experiments in Chapter 4 were performed with Dr. Johanna Blaquiere from the Mayer lab. Dr. Matthew Remy, a previous member of the Sanford lab, provided initial studies on the generation of ethane from mono-methyl palladium complexes, although his results are not discussed in detail in Chapter 2. All of the computational work shown in Chapter 2 was conducted by Prof. Allan Canty from the University of Tasmania, and all of the crystal structures were resolved by Dr. Jeff Kampf.

References

- (1) EIA - Annual Energy Outlook 2014 Early Release http://www.eia.gov/forecasts/aeo/er/early_production.cfm (accessed Mar 26, 2015).
- (2) Monthly Energy Review - Energy Information Administration <http://www.eia.gov/totalenergy/data/monthly/index.cfm#prices> (accessed Mar 26, 2015).
- (3) Sustainable Development - World Bank, GGFR Partners Unlock Value of Wasted Gas <http://web.worldbank.org/WBSITE/EXTERNAL/TOPICS/EXTSDNET/0,,contentMDK:22416844~menuPK:64885113~pagePK:64885161~piPK:64884432~theSitePK:5929282,00.html> (accessed Mar 27, 2015).
- (4) McFarland, E. *Science* **2012**, *338*, 340.
- (5) Arndtsen, B. a.; Bergman, R. G.; Mobley, T. A.; Peterson, T. H. *Acc. Chem. Res.* **1995**, *28*, 154.
- (6) Crabtree, R. H. *Chem. Rev.* **1995**, *95*, 987.
- (7) Lunsford, J. H. *Catal. Today* **2000**, *63*, 165.
- (8) Arakawa, H.; Aresta, M.; Armor, J. N.; Barteau, M. a.; Beckman, E. J.; Bell, A. T.; Bercaw, J. E.; Creutz, C.; Dinjus, E.; Dixon, D. a.; Domen, K.; DuBois, D. L.; Eckert, J.; Fujita, E.; Gibson, D. H.; Goddard, W. a.; Goodman, D. W.; Keller, J.; Kubas, G. J.; Kung, H. H.; Lyons, J. E.; Manzer, L. E.; Marks, T. J.; Morokuma, K.; Nicholas, K. M.; Periana, R.; Que, L.; Rostrup-Nielsen, J.; Sachtler, W. M. H.; Schmidt, L. D.; Sen, A.; Somorjai, G. a.; Stair, P. C.; Ray Stults, B.; Tumas, W. *Chem. Rev.* **2001**, *101*, 953.
- (9) Labinger, J. a.; Bercaw, J. E. *J. Organomet. Chem.* **2015**.
- (10) Kaneko, T.; Derbyshire, F.; Makino, E.; Gray, D.; Tamura, M.; Li, K. In *Ullmann's Encyclopedia of Industrial Chemistry*; Wiley-VCH, 2000.
- (11) Gas-to-liquids plants face challenges in the U.S. market - Today in Energy - U.S. Energy Information Administration (EIA) <http://www.eia.gov/todayinenergy/detail.cfm?id=15071> (accessed Mar 27, 2015).
- (12) Baik, M.-H.; Newcomb, M.; Friesner, R. A.; Lippard, S. J. *Chem. Rev.* **2003**, *103*, 2385.
- (13) Holmen, A. *Catal. Today* **2009**, *142*, 2.
- (14) Shilov, A. E.; Shul, G. B. *Chem. Rev.* **1997**, *97*, 2879.
- (15) Stahl, S. S.; Labinger, J. a; Bercaw, J. E. *J. Am. Chem. Soc.* **1996**, *118*, 5961.
- (16) Lin, M.; Hogan, T.; Sen, A. *J. Am. Chem. Soc.* **1997**, *119*, 6048.
- (17) Periana, R. A. *Science* **1998**, *280*, 560.
- (18) Muehlhofer, M.; Strassner, T.; Herrmann, W. A. *Angew. Chem. Int. Ed.* **2002**, *41*, 1745.
- (19) Kao, L. C.; Hutson, A. C.; Sen, A. *J. Am. Chem. Soc.* **1991**, *113*, 700.

- (20) Balcells, D.; Clot, E.; Eisenstein, O. *Chem. Rev.* **2010**, *110*, 749.
- (21) Periana, R. A.; Mironov, O.; Taube, D.; Bhalla, G.; Jones, C. J. *Science* **2003**, *301*, 814.
- (22) Soulivong, D.; Copéret, C.; Thivolle-Cazat, J.; Basset, J. M.; Maunders, B. M.; Pardy, R. B. a; Sunley, G. J. *Angew. Chem. Int. Ed.* **2004**, *43*, 5366.
- (23) Munz, D.; Strassner, T. *Chem. - A Eur. J.* **2014**, *20*, 14872.
- (24) Keller, G. E.; Bhasin, M. M. *J. Catal.* **1982**, *73*, 9.
- (25) Lunsford, J. H. *Angew. Chem. Int. Ed. English* **1995**, *34*, 970.
- (26) Hammond, C.; Conrad, S.; Hermans, I. *ChemSusChem* **2012**, *5*, 1668.
- (27) Ma, D. *Energy Environ. Sci.* **2014**, *7*, 2580.
- (28) Guo, X.; Fang, G.; Li, G.; Ma, H.; Fan, H.; Yu, L.; Ma, C.; Wu, X.; Deng, D.; Wei, M.; Tan, D.; Si, R.; Zhang, S.; Li, J.; Sun, L.; Tang, Z.; Pan, X.; Bao, X. *Science* **2014**, *344*, 616.
- (29) Labinger, J. A. *J. Mol. Catal. A: Chem.* **2004**, *220*, 27.
- (30) Tullo, A. *C E News* **2014**, *92*, 20.
- (31) Noon, D.; Seubsai, A.; Senkan, S. *ChemCatChem* **2013**, *5*, 146.
- (32) Liu, H.; Wang, X.; Yang, D.; Gao, R.; Wang, Z.; Yang, J. *J. Nat. Gas Chem.* **2008**, *17*, 59.
- (33) Hartwig, J. *Transition* **2010**, 2010.
- (34) Li, Z.; Li, C.-J. *J. Am. Chem. Soc.* **2005**, *127*, 3672.
- (35) Li, Z.; Li, C.-J. *J. Am. Chem. Soc.* **2006**, *128*, 56.
- (36) Xie, J.; Li, H.; Zhou, J.; Cheng, Y.; Zhu, C. *Angew. Chem. Int. Ed. Engl.* **2012**, *51*, 1252.
- (37) Nobuta, T.; Tada, N.; Fujiya, A.; Kariya, A.; Miura, T.; Itoh, A. *Org. Lett.* **2013**, *15*, 574.
- (38) Wick, D. D.; Goldberg, K. I. *Organometallics* **1997**, *39*, 10235.
- (39) Siegbahn, P. E. M.; Crabtree, R. H. *J. Am. Chem. Soc.* **1996**, *118*, 4442.
- (40) Holtcamp, M. *J. Am. Chem. Soc.* **1997**, *5*, 848.
- (41) Scollard, J. D.; Day, M.; Labinger, J. a.; Bercaw, J. E. *Helv. Chim. Acta* **2001**, *84*, 3247.
- (42) Vedernikov, A. N.; Wang, D. In *Abstracts of Papers, 248th ACS National Meeting & Exposition, San Francisco, CA, United States, August 10-14, 2014*; American Chemical Society, 2014; p INOR – 394.
- (43) Vedernikov, A. N. *Acc. Chem. Res.* **2012**, *45*, 803.

- (44) Periana, R. A.; Mironov, O.; Taube, D.; Bhalla, G.; Jones, C. J. *Top. Catal.* **2005**, *32*, 169.
- (45) Lin, M.; Sen, A. *J. Am. Chem. Soc.* **1992**, *114*, 7307.
- (46) Lotz, M. D.; Remy, M. S.; Lao, D. B.; Ariafard, A.; Yates, B. F.; Canty, A. J.; Mayer, J. M.; Sanford, M. S. *J. Am. Chem. Soc.* **2014**, *136*, 8237.
- (47) Lanci, M. P.; Remy, M. S.; Kaminsky, W.; Mayer, J. M.; Sanford, M. S. *J. Am. Chem. Soc.* **2009**, *131*, 15618.
- (48) Lanci, M. P.; Remy, M. S.; Lao, D. B.; Sanford, M. S.; Mayer, J. M. *Organometallics* **2011**, *30*, 3704.
- (49) Lanci, M. P.; McKeown, B. a.; Lao, D. B.; Spettel, K. E.; Mayer, J. M. *Polyhedron* **2014**, *84*, 44.
- (50) Luo, J.; Rath, N. P.; Mirica, L. M. *Organometallics* **2013**, *32*, 3343.
- (51) Khusnutdinova, J. R.; Qu, F.; Zhang, Y.; Rath, N. P.; Mirica, L. M. *Organometallics* **2012**, *31*, 4627.
- (52) Khusnutdinova, J.; Rath, N.; Mirica, L. *J. Am. Chem. Soc.* **2010**, *132*, 7303.
- (53) Khusnutdinova, J. R.; Qu, F.; Zhang, Y.; Rath, N. P.; Mirica, L. M. *Organometallics* **2012**, *31*, 4627.
- (54) Khusnutdinova, J. R.; Rath, N. P.; Mirica, L. M. *Angew. Chem. Int. Ed.* **2011**, *50*, 5532.
- (55) Mirica, L. M.; Khusnutdinova, J. R. *Coord. Chem. Rev.* **2013**, *257*, 299.
- (56) Tang, F.; Qu, F.; Khusnutdinova, J. R.; Rath, N. P.; Mirica, L. M. *Dalt. Trans.* **2012**, 1.
- (57) Khusnutdinova, J. R.; Rath, N. P.; Mirica, L. M. *J. Am. Chem. Soc.* **2012**, *134*, 2414.
- (58) Luo, J.; Khusnutdinova, J. R.; Rath, N. P.; Mirica, L. M. *Chem. Commun.* **2012**, *48*, 1532.
- (59) Tang, F.; Zhang, Y.; Rath, N. P.; Mirica, L. M. *Organometallics* **2012**, *31*, 6690.

CHAPTER 2

Mechanistic Studies of Methyl Transfer and Reductive Elimination of Palladium Methyl Complexes¹

Background

Natural gas is an abundant domestic resource, and its main component, methane, provides an attractive C₁ feedstock for both fuels and commodity chemicals.¹⁻³ Thus, there is high demand for efficient routes to methane functionalization. A number of heterogeneous catalysts have been utilized in methane functionalization, however, these processes often require high temperatures which result in poor selectivity.⁴ Thus, we envisioned a pathway using homogeneous catalysts operating at lower temperatures to circumvent these challenges.

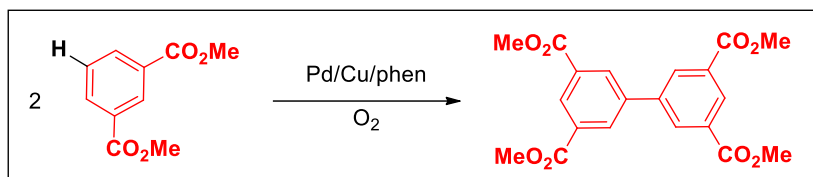
Prior work by Shilov and others provides precedence for methane functionalization with homogeneous group 10 metals through the formation of C–O bonds.^{1-3,5,6} However, this approach faces an inherent challenge due to facile overfunctionalization of the product MeOH to generate thermodynamically favored CO₂.^{2,4} Thus, we propose an alternate route via formation of C–C

¹The majority of the chemistry described in this chapter has been published in the following Article: Lotz, M. D.; Remy, M. S.; Lao, D. B.; Canty, A. J.; Mayer, J. M.; Sanford, M. S. "Formation of Ethane from Mono-Methyl Palladium(II) Complexes," *J. Am. Chem. Soc.* **2014**, *136*, 8237-8242.

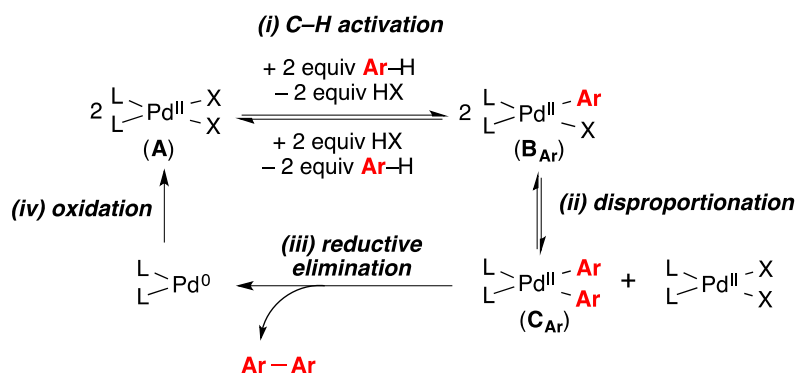
bonds to ultimately access higher alkanes.⁷⁻⁹ We focused on the first step in this methane oligomerization process by studying the initial C–C bond formation to generate ethane from methane. Examples of catalytic methane coupling to liberate ethane remain rare in homogeneous catalysis.^{1-3,5,6,10-13} Thus, we sought to demonstrate the key step in this process, C–C bond formation to generate ethane from mono-methyl Pd^{II} species.

For our approach to catalytic coupling of methane, we envisioned a process analogous to well established arene C–H oxidative coupling reactions.¹⁴ One such example is the dimerization of dimethyl phthalate, used industrially to access a monomer precursor to the commercial resin Upilex® (Figure 2.1).^{15,16} The catalytic cycle for this reaction is proposed to involve the following steps: (i) arene C–H activation by **A** to generate mono-aryl Pd^{II} complex **B**_{Ar} (Ar = aryl), (ii) disproportionation to form bis-aryl Pd^{II} adduct **C**_{Ar}, (iii) C–C bond-forming reductive elimination to release the biaryl product and Pd⁰, and (iv) oxidation of Pd⁰ to regenerate the Pd^{II} catalyst (Figure 2.1).

Figure 2.1. Homogeneous Pd-Catalyzed Arene Oxidative Dimerization to Generate Industrial Precursor to Upilex® Resin



Proposed Mechanism:

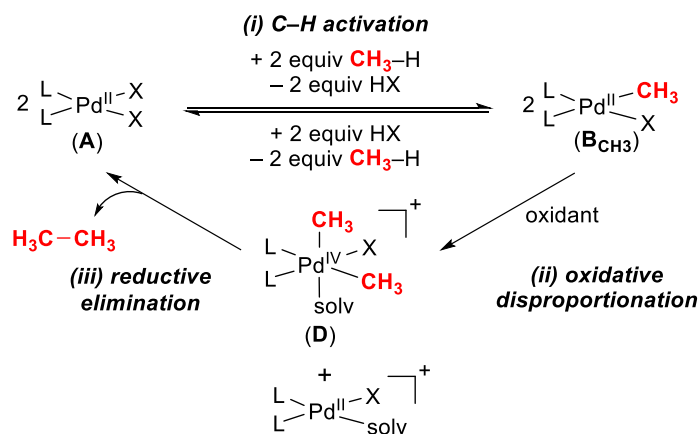


Based on this precedent for arene dimerization, we envisioned a similar process for methane coupling. Prior studies have demonstrated C–H activation of methane (Figure 2.1, step i) at Pd^{II}

complexes to form mono-methyl complexes similar to \mathbf{B}_{Ar} .^{5,17–23} However, generation of ethane has not been reported from mono-methyl complexes analogous to \mathbf{B}_{Ar} (steps *ii* and *iii*).^{24,25} The main challenges in disproportionation/reductive elimination from mono-methyl Pd^{II} complexes are: (a) disproportionation has been shown to be highly energetically unfavorable at Pd^{II} (step *ii*)²⁶ and (b) the subsequent C–C coupling step at dimethyl Pd^{II} complexes typically results in poor yields of ethane, even under forcing conditions.²⁶

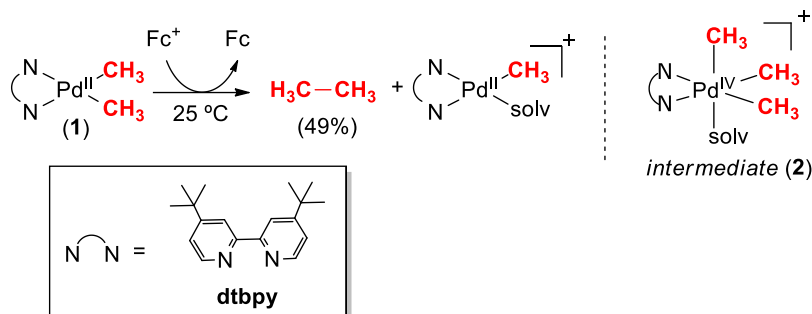
$\text{CH}_3\text{--CH}_3$ coupling at high valent palladium dimethyl species is known to occur more readily than at the analogous Pd^{II} species.^{7,27–32} Thus, we hypothesized that the oxidation of Pd^{II} methyl complexes to Pd^{IV} dimethyl intermediates might induce a more facile reductive elimination. Our newly proposed catalytic cycle would involve: (i) CH_4 activation at Pd^{II} to generate mono-methyl complex \mathbf{B}_{CH_3} , (ii) oxidatively-induced disproportionation to form dimethyl Pd^{IV} species \mathbf{D} , and (iii) C–C coupling from \mathbf{D} to regenerate the Pd^{II} catalyst (Figure 2.2).^{15,16}

Figure 2.2. Proposed Catalytic Cycle for Pd-Catalyzed Methane Oxidative Dimerization



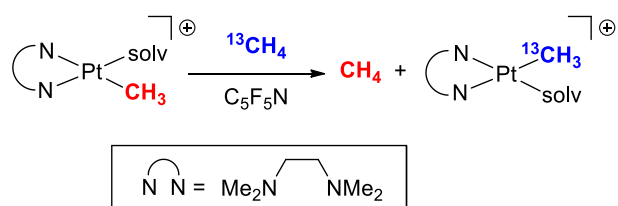
Previously, our group provided proof-of-principle for the feasibility of the proposed oxidatively-induced generation of ethane from dimethyl Pd^{II} complex $(\text{dtbpy})\text{Pd}(\text{CH}_3)_2$ (**1**, dtbpy = 4,4'-di-*tert*-butyl-2,2'-bipyridine, Scheme 2.1).⁷ The treatment of **1** with 1.1 equiv of ferrocenium (Fc^+) yielded ethane in 49% yield (maximum theoretical yield = 50%). This reaction was shown to proceed through trimethyl Pd^{IV} intermediate **2** (Scheme 2.1), and upon warming the reaction to 25 °C, liberation of ethane was observed.

Scheme 2.1. Proof-of-Principle for Oxidative Coupling Generate Ethane



These studies with the dimethyl Pd^{II} species **1** demonstrated steps *ii* and *iii* of our proposed cycle. However, Pd^{II} dimethyl complexes such as **1** could prove challenging to access catalytically through CH₄ activation. For instance, prior work by Bercaw has shown similar mono-methyl metal species react with methane via degenerative exchange of the methyl ligand rather than the formation of a dimethyl intermediate (Scheme 2.2).³³ Thus, a mono-methyl intermediate such as **B**CH₃, where X represents anionic ligands such as Cl, OAc, OTFA, would be a more catalytically relevant species.

Scheme 2.2. Degenerative Exchange of Methyl Groups with Pt^{II}



To support our proposed catalytic cycle, it was crucial to demonstrate the key step of ethane formation from such a mono-methyl Pd^{II} species. Thus, our goals were to (a) achieve high yielding, selective generation of ethane from mono-methyl Pd^{II} complexes in the presence of an oxidant and (b) to provide mechanistic insight to support our proposal of oxidative disproportionation in this reaction.

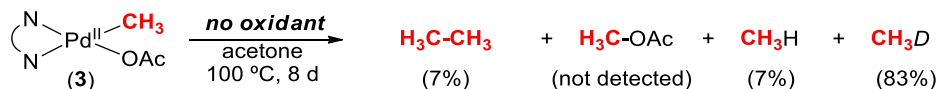
Results and Discussion

Reactivity of Mono-methyl Pd^{II} Complex 3: Thermolysis Studies

Our initial studies focused on the generation of ethane from mono-methyl Pd^{II} complex (dtbpy)Pd(CH₃)(OAc) (**3**). Notably, acetate and other carboxylate ligands have been widely employed in catalytic methane functionalization reactions with Pd^{II}.³⁴⁻³⁷ Thus, complex **3** is a more catalytically relevant intermediate than dimethyl species **1**.

Complex **3** was synthesized by halide abstraction from previously reported³⁸ (dtbpy)Pd^{II}(CH₃)(Cl) with AgOAc and was characterized by NMR spectroscopy and elemental analysis. This complex is remarkably stable in the absence of an oxidant. It can be stored in the solid state at -33 °C for several months without detectable decomposition. It is also stable in acetone at room temperature under N₂ for at least 24 h. Upon heating to 100 °C, **3** decomposed after 21 h in acetone-*d*₆ to predominantly generate CH₃D (83% yield) along with only small amounts of ethane (Scheme 2.3).

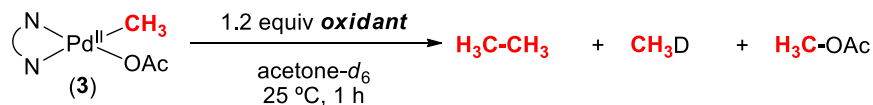
Scheme 2.3. Thermolysis of Mono-methyl Complex 3



Reactivity of Mono-methyl Pd^{II} Complex 3: Oxidation

Complex **3** was subjected to oxidation with several 1 and 2 *e*⁻ oxidants at 25 °C in acetone-*d*₆. Complex **3** reacted rapidly with several of these oxidants to form ethane in modest yield (Table 2.1²). Notably, the maximum theoretical yield of ethane in these experiments is 50%. Only trace CH₃D (or CH₄) was observed with most oxidants (≤1% in all cases except with hypervalent iodide oxidants, entries 5-6).

² This ethane-forming reaction of **3** with AcFcBF₄ was initially discovered by Dr. Matthew Remy.

Table 2.1. Oxidation of **3 with $1e^-$ and $2e^-$ Oxidants^a**

Entry	Oxidant	% Yield $C_2H_6^b$	% Yield CH_3D/CH_4^c	% Yield CH_3OAc
1	$K_2S_2O_8$	11	<1	<1
2	BQ	<1	<1	<1
3	Oxone	<1	<1	<1
4	NCS	11	<1	10
5	$PhI(OAc)_2$	15	31	37
6	$PhI(TFA)_2$	28	3	49 ^d
7	CAN	17	<1	<1
8	$AgBF_4$	22	1	<1
9	$AcFcBF_4$	36	<1	<1
10	NFTPT	32	<1	<1
11 ^e	NFTPT	37	1	<1

^aConditions: **3** (4 μ mol, 1 equiv), oxidant (4.8 μ mol, 1.2 equiv), 1,1,2-trichloroethane (4 μ mol, 1 equiv, standard), acetone- d_6 (5 mM), 25 °C, 24 h. ^bTheoretical maximum yield of ethane is 50%. ^cTheoretical maximum yield of CH_4 and CH_3OAc is 100%. ^d CH_3OTFA is formed in 49% yield this reaction. ^eConditions: **3** (4 μ mol, 1 equiv), NFTPT (20 μ mol, 5 equiv), 1,1,2-trichloroethane (4 μ mol, 1 equiv, standard), acetone- d_6 (5 mM), 25 °C, 1 h.

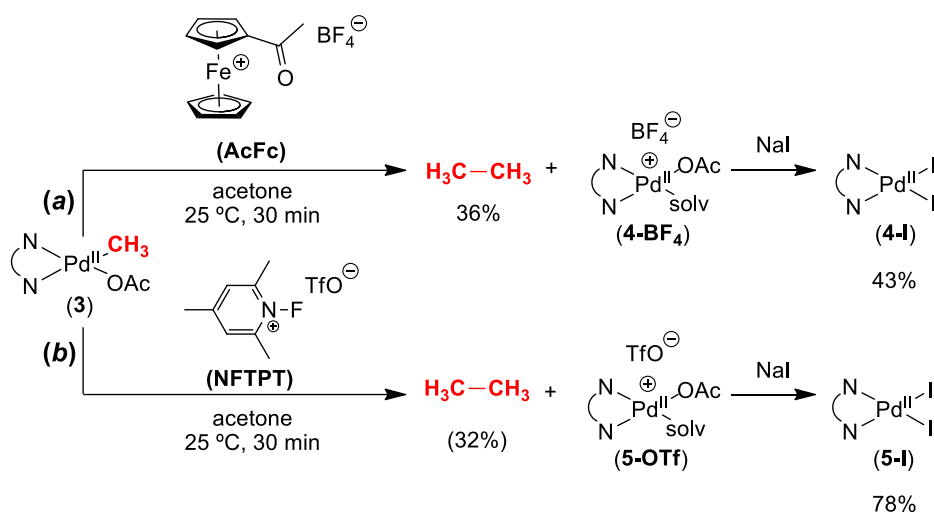
The yield of ethane varies significantly as a function of oxidant. In some cases, this is due to competitive C–X reductive elimination. For example, $PhI(OAc)_2$ and $PhI(OTFA)_2$ afforded significant quantities of CH_3OAc and CH_3OTFA , respectively, as well as CH_3D (Table 2.1, entries 5 and 6). Many of these oxidants exhibited poor reactivity, generating little or no ethane.

The highest yields of ethane and cleanest reactions were observed with the $1e^-$ oxidant acetylferrocenium tetrafluoroborate ($AcFcBF_4$) and the $2e^-$ oxidant *N*-fluoropyridinium triflate (NFTPT) (Table 2.1, entries 9 and 10). The reaction of **3** with 1.2 equiv of each of these oxidants afforded ethane in 36 and 32% yield, respectively. With 1.2 equiv of NFTPT, there was ~15% of a $Pd^{II}(CH_3)$ species remaining at the end of this reaction, potentially due to loss of the acetate ligand over the course of the reaction. However, the use of excess oxidant (5 equiv) could be used to push

the reaction to full conversion. Under these conditions, ethane was formed in 37% yield (Table 2.1, entry 11).

The inorganic by-products of these transformations are $(dtbpy)Pd^{II}(OAc)(BF_4)$ (**4**) with $AcFcBF_4$ and $(dtbpy)Pd^{II}(OAc)(X)^+$ [$X = F^-$ (**5-F**); $X = 2,4,6$ -trimethylpyridine (**5-TP**)] with NFTPT. The X-type ligands of **4** and **5** (BF_4^- , F^- , and TP) are in rapid exchange with solvent (acetone or water); thus, the complexes were converted to the corresponding iodide salts to determine yields. This procedure established that the yield of **4** is 43% and the yield of **5** is 78% under our standard reaction conditions (Scheme 2.4).

Scheme 2.4. Oxidation of 3 with $AcFcBF_4$ and NFTPT

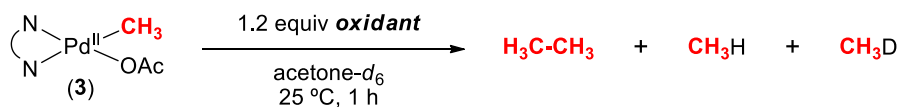


Mechanistic Studies: Probing the Potential Intermediacy of $CH_3\bullet$

We next sought to gain insights into the mechanism of ethane formation with mono-methyl complexes. Initial studies investigated the potential intermediacy of methyl radicals ($CH_3\bullet$) in ethane generation upon oxidation of **3**. The oxidation of complex **3** was performed in the presence of 40 equiv of the H-atom donor 1,4-cyclohexadiene (CHD). Based on our prior studies,⁷ $CH_3\bullet$ intermediates would be expected to participate in rapid H• abstraction from cyclohexadiene to afford CH_4 in high yield under these conditions. As shown in Table 2.2, $\leq 6\%$ methane was detected (entries 3 and 4). Additionally, only a small decrease in the yield of ethane was observed upon reaction with both NFTPT and $AcFcBF_4$ in the presence of CHD. Based on these results, $CH_3\bullet$ formation does not appear to be a major pathway to ethane under these conditions. Additionally,

reactions of **3** with AcFcBF₄ and NFTPT were conducted in foil-wrapped NMR tubes to exclude any light-mediated reactivity. Nearly identical yields were observed in both the absence of light as compared to in ambient light, suggesting against mechanisms involving light-induced homolysis of the Pd–CH₃ bonds (Table 2.2, entries 5 and 6).

Table 2.2. Influence of Cyclohexadiene (CHD) and Light on Oxidative Ethane Formation from **3^a**



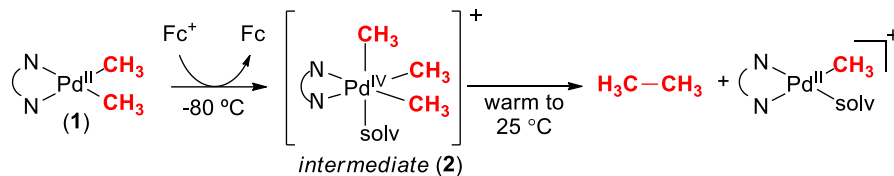
Entry	Oxidant	Conditions	% Yield C ₂ H ₆	% Yield CH ₄
1	AcFcBF ₄	standard	36	<1
2	NFTPT	standard	37	1
3 ^b	AcFcBF ₄	CHD	29	2
4 ^b	NFTPT	CHD	35	6
5 ^c	AcFcBF ₄	no light	38	<1
6 ^c	NFTPT	no light	39	<1

^aConditions: **3** (4 μmol, 1 equiv), AcFcBF₄ (4.8 μmol, 1.2 equiv) or NFTPT (20 μmol, 5 equiv), 1,1,2-trichloroethane (4 μmol, 1 equiv, standard), acetone-*d*₆ (5 mM), 25 °C, 1 h under ambient light. ^b40 mmol of 1,4-cyclohexadiene (CHD) added under the standard conditions. ^cReaction conducted under standard conditions but in a foil-wrapped NMR tube to exclude ambient light.

Mechanistic Studies of **3**: Intermediates in the Oxidation of **3** *In Situ*

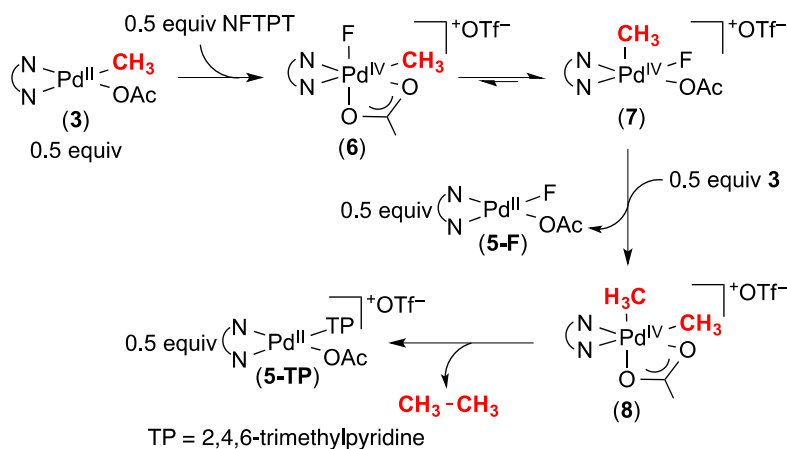
We next conducted low temperature NMR spectroscopy experiments in an attempt to observe organometallic intermediates during the oxidation of complex **3**. Previously, our group observed high-valent Pd intermediate **2** at -80 °C upon the treatment of complex **1** with FcBF₄ (Scheme 2.5).⁷ Intermediate **2** was proposed to form via initial oxidation of **1** followed by subsequent methyl group transmetalation. This species (**2**) was detected via low temperature ¹H NMR spectroscopy due to enhanced stabilization from three strongly electron donating methyl groups.^{27,28,30,39}

Scheme 2.5. Prior Studies to Observe Organometallic Intermediate 2 via ^1H NMR Spectroscopy



We envisioned an analogous methyl group transmetalation process could be occurring during the oxidation of **3** (Scheme 2.6). However, in this reaction, the organometallic intermediate would be the dimethyl Pd^{IV} species **8**, which is expected to be significantly less stable than its trimethyl analogue.^{27–30} Indeed, broad, uninterpretable signals were observed by ^1H NMR spectroscopy upon the treatment of **3** with NFTPT or AcFcBF_4 at $-78\text{ }^\circ\text{C}$ in CD_2Cl_2 . Generation of ethane was observed upon warming the reaction mixture to $-60\text{ }^\circ\text{C}$. This is consistent with the lower stability of the putative high valent Pd intermediates in this transformation compared to previously observed **2**.

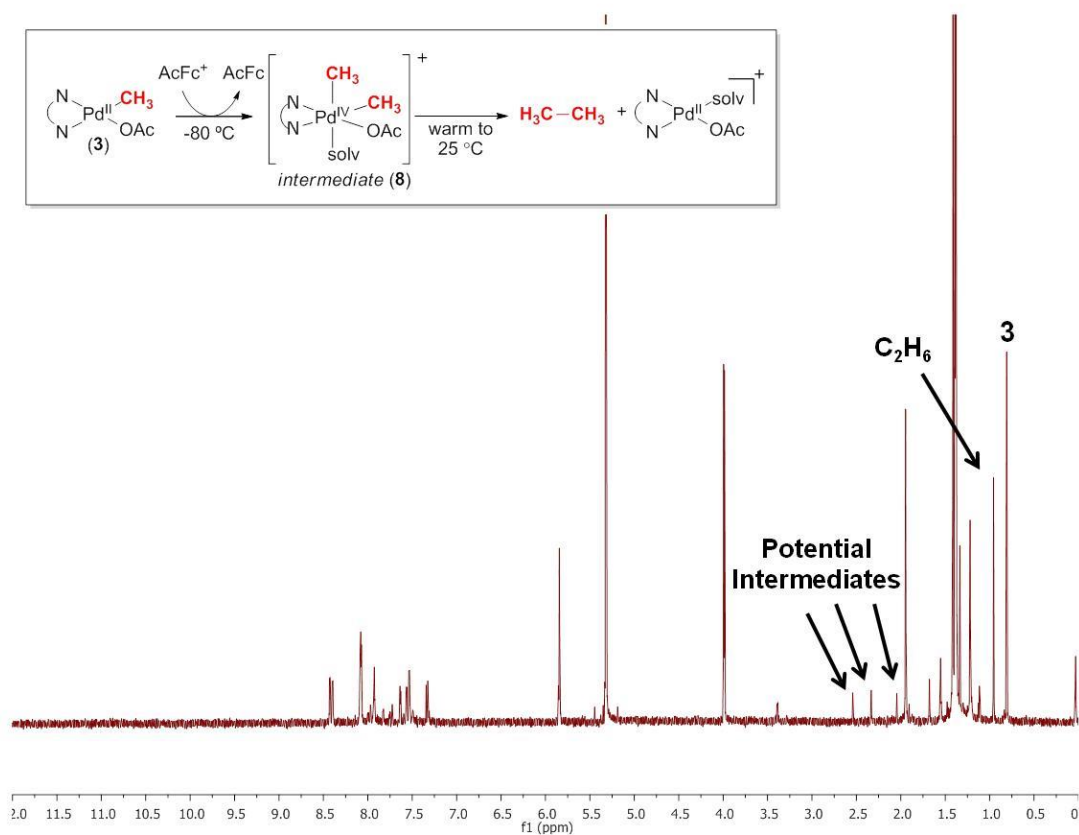
Scheme 2.6. Proposed Mechanism for Ethane-Formation from **3**



We hypothesized that further stabilization of the putative Pd^{IV} intermediate **8** was necessary to obtain a clearer mechanistic picture of the intermediates in this transformation. Previous work has shown facile C–C reductive elimination from similar octahedral complexes to proceed through an initial ligand loss to generate a pentacoordinate intermediate.⁴⁰ Based on previous studies with dimethyl species **1**, we envisioned a similar pentacoordinate Pd^{IV} intermediate (**8**) is formed during the reaction with **3** (Scheme 2.6). This species is likely partially stabilized by fluxional κ^2 coordination of the acetate. However, we hypothesized the addition of a more strongly

coordinating axial ligand, such as CD_3CN , could trap intermediate **8** in an octahedral conformation, and thus, slow reductive elimination.^{27–30} Upon addition of 100 equiv of CH_3CN to the reaction, only marginal enhancements in stability of the intermediates were observed by ^1H NMR experiments at $-80\text{ }^\circ\text{C}$. However, the spectra showed a complex mixture of ^1H NMR signals. Additionally, this mixture concomitantly resulted in the rapid liberation of ethane at $-80\text{ }^\circ\text{C}$, in the presence of CD_3CN (Figure 2.3).

Figure 2.3. Monitoring the Oxidation of 3 with AcFcBF_4 at $-80\text{ }^\circ\text{C}$



Mechanistic Studies of 3: Computational Modeling

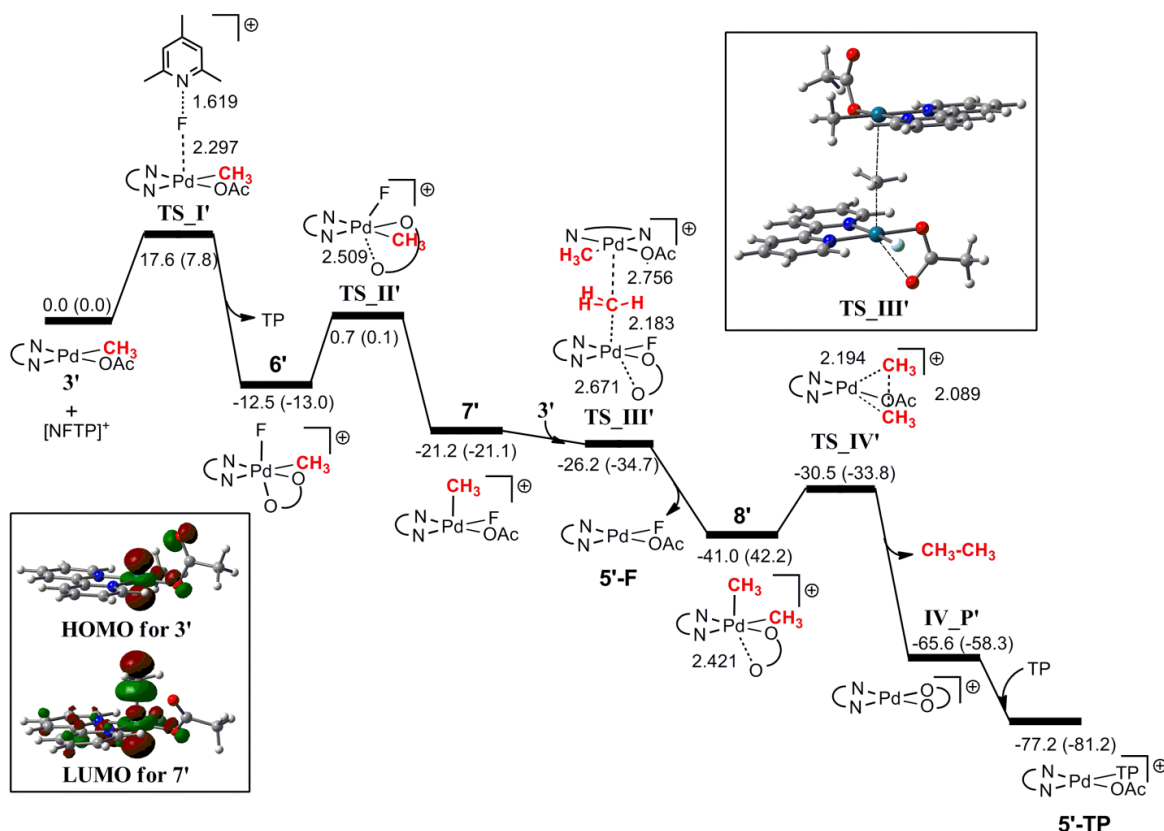
As *in situ* NMR experiments highlighted the complexity of the system, we utilized DFT studies as a tool to gain a better mechanistic picture of this transformation. These computational studies, performed by Professor Allan Canty, probed the reactivity of **3** with oxidants. The oxidation of **3** with NFTPT was chosen for DFT calculations as it affords the highest yield of ethane compared to other oxidants in Table 2.1. Additionally, NFTPT is a well studied $2e^-$ oxidant,^{41–45} thus limiting the likelihood of more computationally challenging $1e^-$ outer sphere oxidation pathways.

Bipyridine (bpy) was used in place of dtbpy to simplify calculations. The analogous bpy intermediates are denoted with a prime (i.e. **3'** vs **3**). Additionally, all calculations were performed in dichloromethane at the B3LYP level for geometry optimization, using the SDD basis set on Pd and the 6-31G(d) basis set for other atoms.

These calculations show a low energy $2e^-$ oxidation path that has three steps in the overall conversion of **3'** + NFTPT to **5'-F/5'-TP** and ethane. These steps are: (1) oxidation of 0.5 equiv of **3'** by NFTPT to generate Pd^{IV} isomers **6'** and **7'**, (2) methyl group transmetalation between **7'** and the remaining 0.5 equiv of Pd^{II} starting material **3'** to form **8'** and **5-F'**,^{19,20} and (3) reductive elimination from **8'** to release ethane and inorganic products. Oxidation by NFTPT is the highest energy step in the pathway, occurring through F⁺ transfer (via TS_1', Figure 2.4) to the Pd^{II} starting complex (**3**) with a barrier of 17.6 kcal/mol. The resulting Pd^{IV} complex **6'** then proceeds through a thermodynamically downhill isomerization ($\Delta G = -8.7$ kcal/mol) to achieve **7'**. This step occurs with a low barrier as a result of dissociation (from a κ^2 to κ^1 coordination) of the labile acetate ligand to access a five-coordinate Pd^{IV} intermediate.²⁷⁻³⁰

Figure 2.4. Energy Profile for the Oxidation of (bpy)Pd(CH₃)(CF₃) (3') with NFTPT

(TP = 2,4,6-trimethylpyridine. Energies ΔG (ΔH) in kcal/mol.)



The next step involves transmetalation of a methyl ligand from Pd^{IV} species **7'** to Pd^{II} starting complex (**3'**). This step occurs via an early transition state, reflected in the bond distance of the Pd^{IV}-Me (2.183 Å) as compared to the Pd^{II}-Me (2.756 Å), shown in Figure 2.4 (**TS_III'**). The geometry at the carbon of the bridging methyl ligand is not fully trigonal bipyramidal, as reflected in CH₂ angles (117.4-117.9°). The structure shows a single imaginary frequency, with an "umbrella" motion for the methyl group. Excellent orbital overlap between the LUMO of nucleophilic Pd^{II} species **3'** and the HOMO of Pd^{IV} methyl species (**7'**) facilitates a barrierless transmetalation that is highly thermodynamically downhill (ΔG = -19.8 kcal/mol). This transmetalation produces Pd^{IV} intermediate **8'**, which is analogous to the trimethyl Pd^{IV} intermediate experimentally observed in the oxidation of dimethyl Pd^{II} species (**1**).⁷

Finally, reductive elimination occurs from five-coordinate complex **8'** to generate ethane with a relatively low barrier of 10.5 kcal/mol. Formation of CH₃OAc, via an alternate reductive elimination pathway, has a much higher barrier (ΔG[‡] = 32.4 kcal/mol), consistent with the

selectivity for ethane observed in this oxidation. These results provide computational evidence to support our propose mechanism. In parallel with these DFT studiess, we were concurrently investigating alternative approaches to experimentally characterize intermediates formed during the reaction.

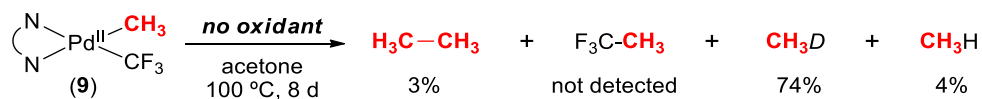
Reactivity of Model Complex 9: Thermolysis Studies

We anticipated that replacement of the acetate ligand of **3** with a more stabilizing X-type ligand might enable detection of some of the transient intermediates. CF₃ ligands have been shown to stabilize related Pd^{IV} intermediates.^{46,47} Additionally, these ligands are relatively unreactive in reductive elimination, minimizing any potential reactions such as competing F₃C–CH₃ reductive elimination. Therefore, an analogous CF₃ complex, (dtbpy)Pd^{II}(CH₃)(CF₃) (**9**), was utilized in further studies to observe intermediates and obtain mechanistic insight for the formation of ethane from palladium methyl complexes.

Reactivity of Model Complex 9: Oxidation

Complex **9** was prepared by treating (tmeda)Pd^{II}(CH₃)(I) with CsF and Rupert’s reagent, TMSCF₃, to generate (tmeda)Pd^{II}(CH₃)(CF₃), followed by ligand exchange with dtbpy to achieve **9**. This complex was characterized by NMR spectroscopy and elemental analysis. As anticipated, palladium (II) complex **9** was even more stable than **3** in the absence of oxidants. It can be stored under N₂ in the solid state for >6 months without detectable decomposition and is stable at 25 °C in acetone for at least 2 d under N₂. Even at 100 °C in acetone, complex **9** only decomposes completely after 8 d, yielding CH₃D as the major organic product in 74% yield. Trace ethane (<5%) and no F₃C–CH₃ were detected (Scheme 2.7).

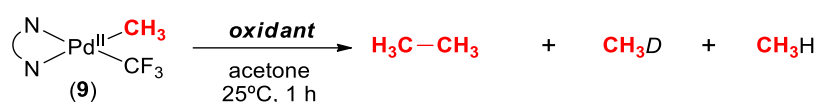
Scheme 2.7. Thermolysis of Mono-methyl Complex 9



Complex **9** reacts rapidly with AcFcBF₄ and NFTPT at 25 °C in acetone-*d*₆ to afford ethane in 34 and 41% yield, respectively (Table 2.3, entries 1 and 2). As with complex **3**, oxidation of **9** is highly selective with both oxidants, generating ≤2% yield of methane in these reactions. The inorganic by-product of both of these reactions is (dtbpy)Pd^{II}(CF₃)(X)⁺ (**10**, X = solvent, F⁻, or

TP), which is formed in 95% and 93% yield, respectively. To fully quantify the inorganic products, NaI was added to the reaction upon completion to displace labile ligands present in solution (F^- , TP, BF_4^-). The reactions of **9** with AcFcBF₄ and NFTPT were unaffected by the exclusion of light (entries 5 and 6), indicating that light-induced Pd–CH₃ bond homolysis is not a major pathway in generating ethane. Additionally, only trace amounts of CH₄ were observed upon oxidation of **9** in the presence of the H• donor CHD, providing evidence against CH₃• intermediates as a major pathway to ethane formation.

Table 2.3. Reaction of **9 with AcFcBF₄ and NFTPT^a**



Entry	Oxidant	Conditions	% Yield C ₂ H ₆	% Yield CH ₄ or CH ₃ D
1	AcFcBF ₄	none	34	2
2	NFTPT	none	41	<1
3 ^b	AcFcBF ₄	CHD	29	2
4 ^b	NFTPT	CHD	42	2
5 ^c	AcFcBF ₄	no light	39	<1
6 ^c	NFTPT	no light	42	<1

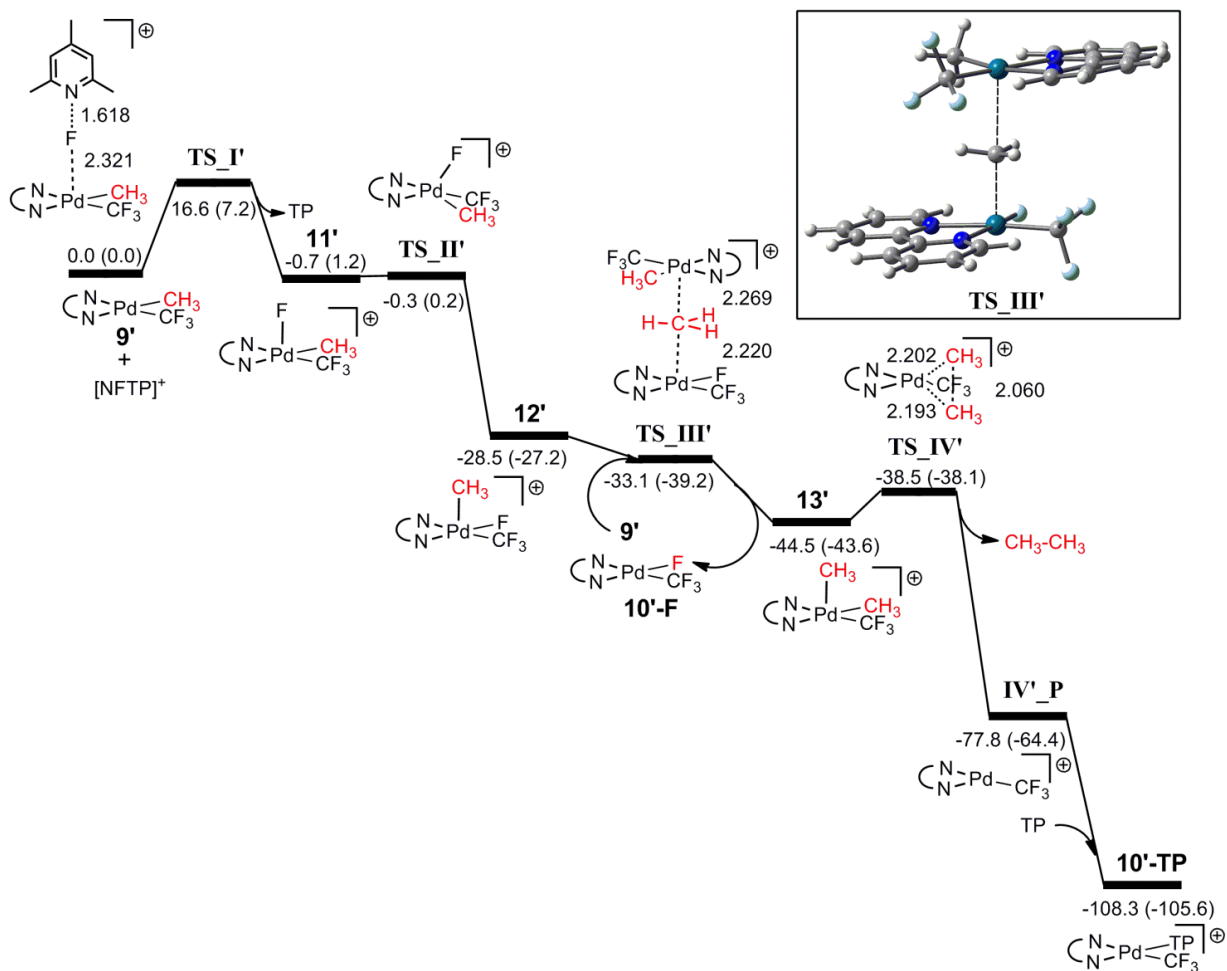
^aConditions: **9** (4 μmol, 1 equiv), AcFcBF₄ (4.8 μmol, 1.2 equiv) or NFTPT (20 μmol, 5 equiv), 1,1,2-trichloroethane (4 μmol, 1 equiv, standard), acetone-*d*₆ (5 mM), 25 °C, 1 h. ^b 40 mmol of 1,4-cyclohexadiene (CHD) added under otherwise standard conditions. ^cReaction conducted under standard conditions but in a foil-wrapped NMR tube to exclude ambient light).

Mechanistic Studies of **9**: Computation

Next, we computationally modeled the oxidation of **9** with NFTPT, to test the feasibility of a similar low energy pathway as with **3**. DFT calculations show that the lowest energy path for the reaction of **9'** (bipyridine analogue of **9**) with NFTPT directly parallels that of the aforementioned calculations with **3'**. It involves three steps: (1) oxidation of 0.5 equiv of **9'** by NFTPT to generate Pd^{IV} isomers **11'** and **12'**, (2) methyl group transmetalation between **12'** and the remaining 0.5 equiv of Pd^{II} starting material **9'** to form 1 equiv of **13'**,^{39,48–53} and (3) ethane reductive elimination from **13'** to release the products (Figure 2.5). Initial oxidation of **9'** via F⁺ transfer to Pd^{II} is the highest energy step for the entire sequence, albeit slightly lower than that of the acetate system with a $\Delta G^\ddagger = 16.6$ kcal/mol versus 17.6 kcal/mol for the oxidation of **3'**. The following

isomerization of **11'** (via **TS_II'**) and methyl transfer from **12'** to **9'** (via **TS_III'**) are both thermodynamically favorable steps. The methyl transfer of the acetate complex (in the oxidation with **3'**) proceeded through an early transition state. However, in the oxidation of **9'**, **TS_III'** appears to have much more closely matched Pd^{IV}-Me and Pd^{II}-Me bond distances of 2.22 and 2.27 Å, respectively (Figure 2.5). This suggests that methyl transfer proceeds through more of a central transition state with **9'** compared to the analogous system with **3'**.

Figure 2.5. Energy Profile for the Oxidation of (bpy)Pd(CH₃)(CF₃) (9'**) with NFPTP (TP=2, 4, 6-trimethylpyridine. Energies ΔG (ΔH) in kcal/mol.)**

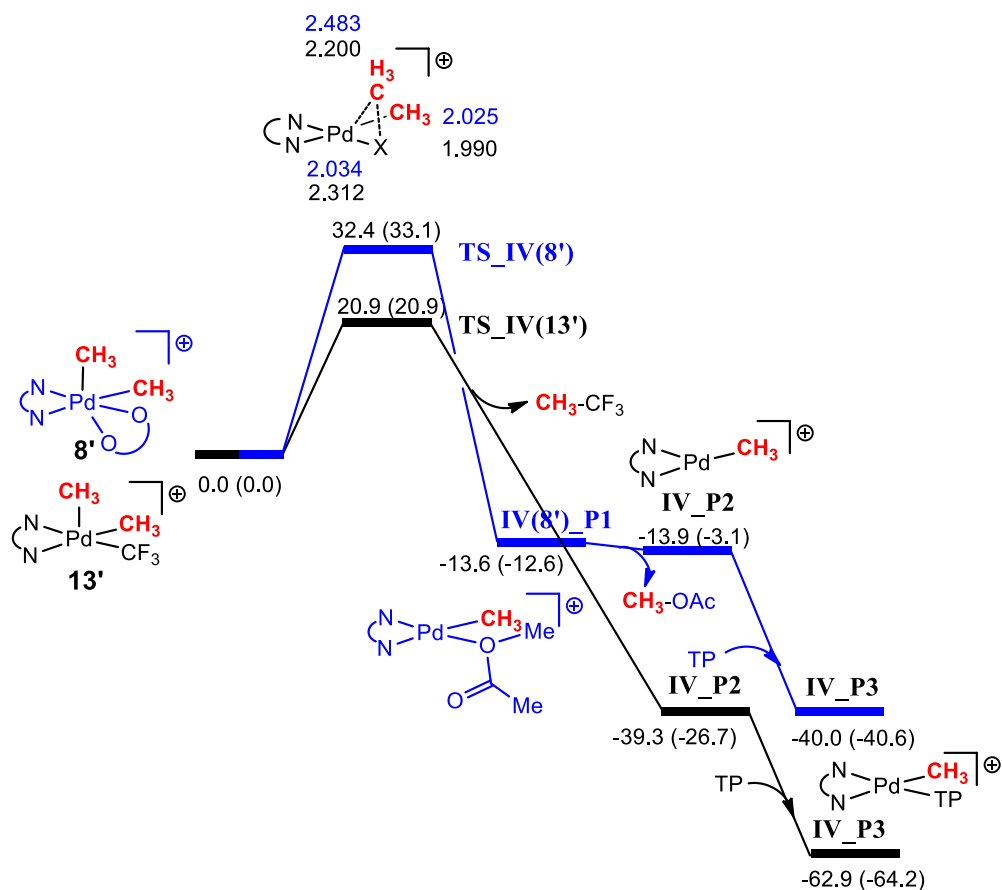


The barrier for ethane reductive elimination from CF₃ intermediate **13'** (Figure 2.5) is computed to be lower than that from OAc intermediate **8'** (6.0 versus 10.5 kcal/mol, respectively). This difference can be attributed to the six-coordinate nature of **8'**, as the acetate ligand of **8'** can

participate in κ^1 and κ^2 coordination. Generally, reductive elimination from five-coordinate complexes has been shown favored over six-coordinate complexes.^{40,54} Thus, this fluxional behavior of the acetate ligand increases the barrier for reductive elimination.

Furthermore, the observed selectivity for $\text{H}_3\text{C}-\text{CH}_3$ reductive elimination over competing $\text{H}_3\text{C}-\text{CF}_3$ can be explained based on a much higher energy barrier for $\text{H}_3\text{C}-\text{CF}_3$ of 20.9 kcal/mol (Figure 2.6). Similar trends in reactivity with the acetate complex **3'** can be supported with a high barrier for $\text{H}_3\text{C}-\text{OAc}$ reductive elimination, with $\text{H}_3\text{C}-\text{OAc}$ proceeding through an even higher barrier of 32.4 kcal/mol.

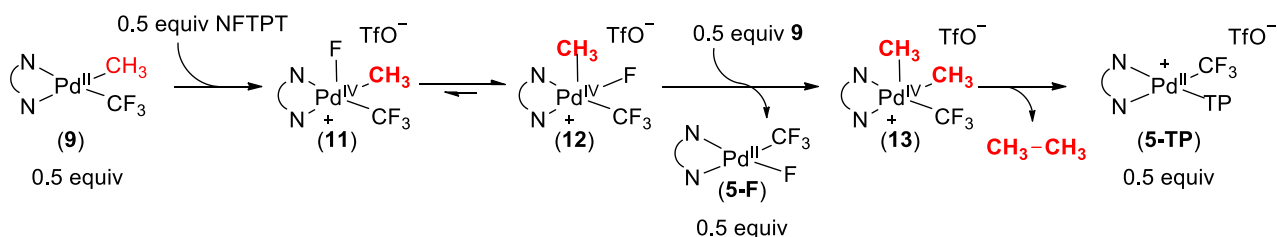
Figure 2.6. Energy Profile for the Formation of $\text{H}_3\text{C}-\text{OAc}$ and $\text{H}_3\text{C}-\text{CF}_3$ from **8' and **13'**, respectively** (TP= 2, 4, 6-trimethylpyridine. Energies ΔG (ΔH) in kcal/mol.)



Mechanistic Studies of 9: Experimental

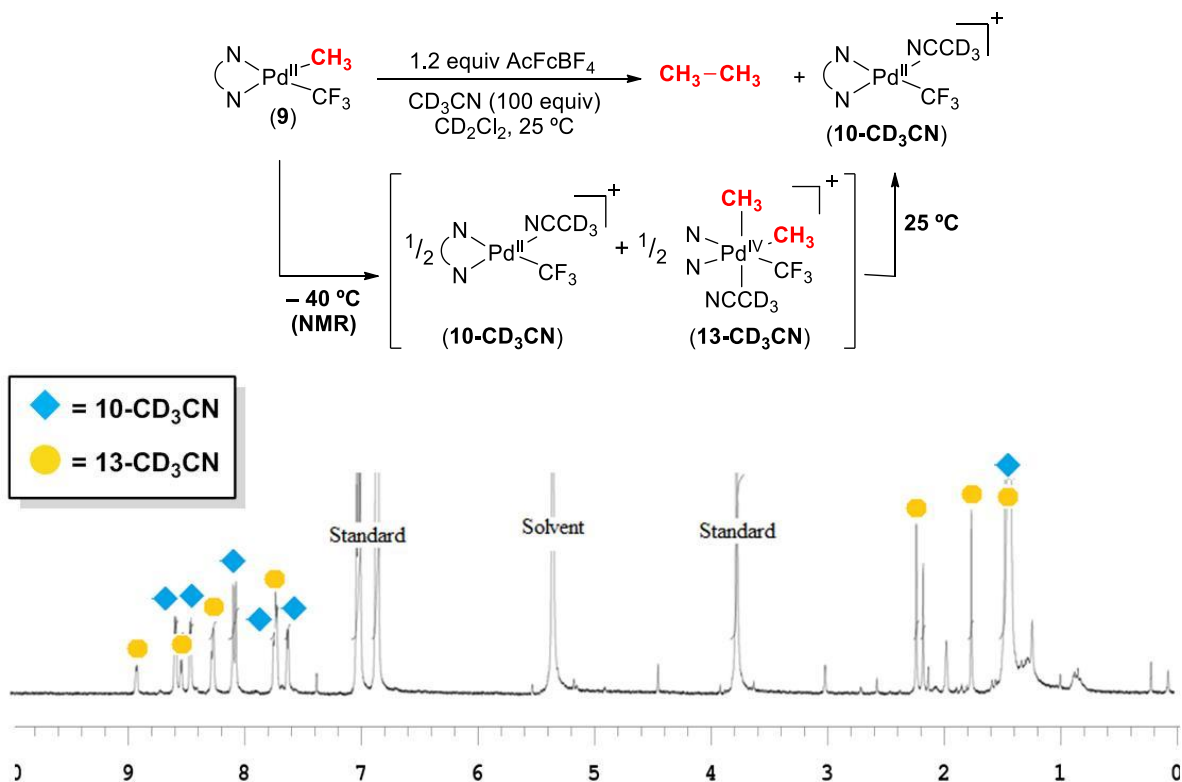
Based on DFT calculations, intermediates **11**, **12**, and **13** should not be detectable, since the oxidation step has the highest barrier. However, we hypothesized that the addition of a coordinating solvent might trap **11**, **12**, and/or **13** as 6-coordinate cationic species that could be detected at low temperature by NMR spectroscopy. The oxidation of **9** with NFTPT at $-40\text{ }^{\circ}\text{C}$ in CD_2Cl_2 in the presence of 100 equiv of CD_3CN resulted in a complex and uninterpretable mixture of ^1H and ^{19}F NMR signals. This is likely due to the coordination of several labile ligands present in solution (TP, F^- , OTf^-) to these cationic pentacoordinate intermediates **11**, **12** and **13**, shown in Scheme 2.8.

Scheme 2.8. Proposed Mechanism of Reaction of 9 with NFTPT



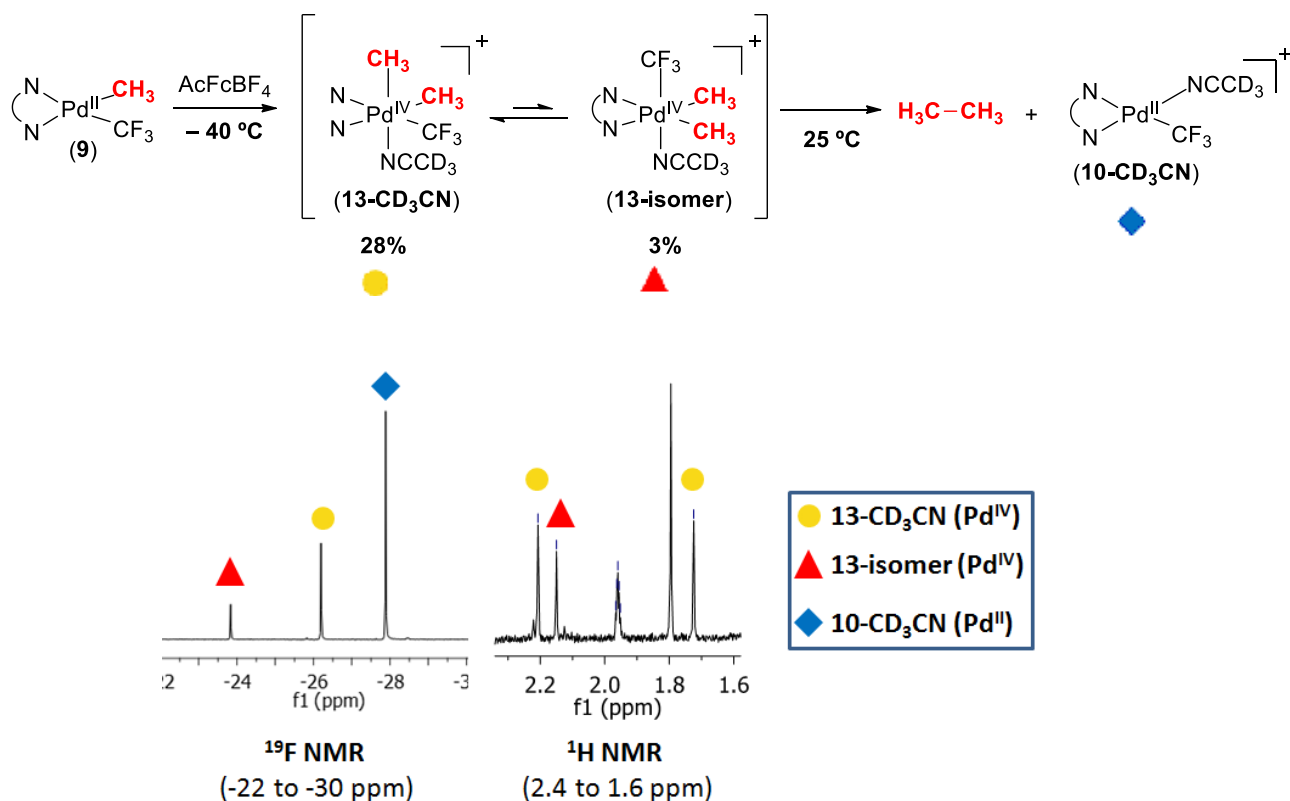
However, under otherwise identical conditions, the reaction of 1 equiv of **9** with 1.2 equiv of AcFcBF_4 cleanly afforded an intermediate with ^1H and ^{19}F NMR signals consistent with the formation of complex **13-CD}_3\text{CN} (Figure 2.7). This species was formed in 28% yield relative to an internal standard along with 38% of the Pd(II) product **10**. Warming the reaction mixture to $25\text{ }^{\circ}\text{C}$ over 24 h resulted in the disappearance of **13-CD}_3\text{CN}, with concomitant formation of ethane. The structure of **13-CD}_3\text{CN} was further characterized by $^1\text{H-}^1\text{H}$ HMBC, $^1\text{H-}^{13}\text{C}$ HSQC and $^1\text{H-}^1\text{H}$ ROESY.******

Figure 2.7. Oxidation of 9 with AcFcBF₄ Upon Addition of CD₃CN



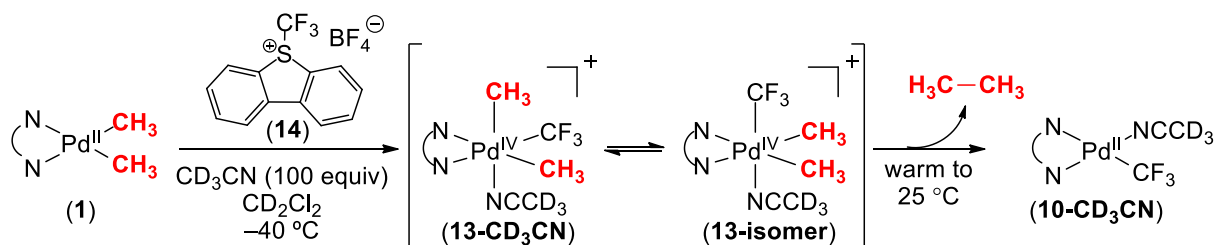
One additional intermediate (**13-isomer**) was also observed during the course of the reaction, albeit in much lower quantities as compared to **13-CD₃CN** (3% versus 28%, respectively, Figure 2.8). Based on the observance of two equivalent ^1H NMR shifts in the methyl region, we hypothesize this intermediate as **13-isomer**, shown in Figure 2.8. We hypothesize that **13-isomer** is formed upon isomerization of **13-CD₃CN**. Both **13-CD₃CN** and **13-isomer** are fully consumed upon warming the reaction to 25°C , generating ethane and Pd^{II} product **10-CD₃CN** as the sole products of this reaction. Liberation of ethane from **13-isomer** is less likely due to the poor orbital overlap of the two equatorial methyl ligands causing reductive elimination of $\text{H}_3\text{C-CH}_3$ to be energetically unfavorable.⁵⁴ Furthermore, the rate of appearance of $\text{H}_3\text{C-CH}_3$ was identical to the rate of decay of **13-CD₃CN**, supporting ethane generation from **13-CD₃CN** and not **13-isomer**. This suggests that **13-isomer** could be equilibrating with **13-CD₃CN**, which then reductively eliminates ethane.

Figure 2.8. New Pd^{IV} Intermediates Formed *In Situ* Upon Oxidation of **9 with AcFcBF₄**

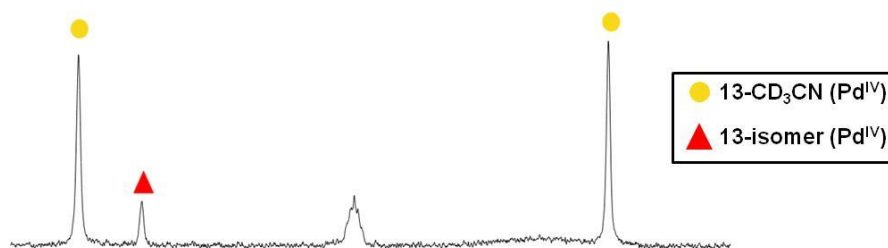


To further corroborate the structures of the observed intermediates in this transformation, **13-CD₃CN** and **13-isomer** were synthesized via an alternate route. The treatment of (dtbpy)Pd(CH₃)₂ (**1**) with Umemoto's oxidant (CF₃⁺) **14** at -40 °C afforded an intermediate with ¹H and ¹⁹F NMR resonances matching those of putative intermediates **13-CD₃CN** and **13-isomer** (Figure 2.9). Upon warming the reaction to 25 °C, ethane, **10-CD₃CN** and the byproduct of the CF₃⁺ oxidant, benzothiophene, were observed. This observation, along with the DFT calculations, strongly supports the involvement of Pd^{IV} intermediate **13-CD₃CN** and **13-isomer** in the oxidatively-induced generation of ethane from **9**.

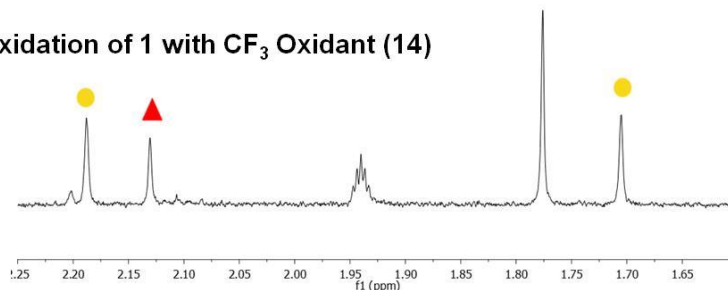
Figure 2.9. Authentic Synthesis of Pd^{IV} Intermediate 13-CD₃CN



Oxidation of 9 with AcFcBF₄



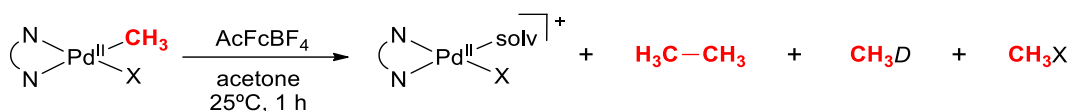
Oxidation of 1 with CF₃ Oxidant (14)



¹H NMR
(2.2 to 1.5 ppm)

Oxidation of Other Mono-Methyl Pd Complexes

To further investigate the scope of Pd^{II} complexes that can participate in this transformation, we examined the reactivity of several other mono-methyl Pd^{II} complexes bearing catalytically relevant X-type ligands. Analogous (tbpy)Pd^{II}(CH₃)(X) complexes, where X = OTFA, I, and Cl, were treated with AcFcBF₄ at 25 °C in acetone-*d*₆. Both the chloride and trifluoroacetate complex formed ethane in modest yields, with < 5% of products from competing pathways (ie. CH₃OTFA, CH₃Cl, and CH₃H), (Table 2.4). With the iodide complex, however, significant methyl iodide was observed, presumably due to competing H₃C–I reductive elimination. With the chloride complex, additional DFT calculations revealed a similar low energy pathway for the oxidation compared to both **3'** and **9'** (for results see p. 49-50). With these results, we have demonstrated ethane generation from several mono-methyl Pd^{II} for applications to future catalytic efforts to convert of methane to ethane.

Table 2.4. Reaction of Mono-methyl Complexes with AcFcBF₄^a

Entry	X =	% Yield Inorganic Pdt	% Yield C ₂ H ₆	% Yield CH ₃ D	% Yield CH ₃ X
1	Cl	71	23	<1	1 ^b
2 ^c	I	72	16	<1	52 ^d
3 ^c	OTFA	59	35	<1	1 ^e

^aConditions: **9** (4 μmol, 1 equiv), AcFcBF₄ (4.8 μmol, 1.2 equiv), 1,1,2-trichloroethane (4 μmol, 1 equiv, standard), acetone-*d*₆ (5 mM), 25 °C, 1 h. ^bMeCl observed. ^cYields based on previously reported calibration curve.⁷ ^dMeI observed as the major side product. ^eMeOTFA observed as the major side product.

Conclusions

Herein, we have demonstrated the generation of ethane from several catalytically relevant mono-methyl palladium complexes bearing a variety of X-type ligands (OAc, CF₃, I, Cl, OTFA).⁹ These transformations proceed upon treatment with oxidants AcFcBF₄ and NFTPT, resulting in high yielding, selective generation of ethane. Further studies with the acetate complex **3** and trifluoromethyl complex **9** demonstrate ethane formation likely does not involve CH₃• intermediates. DFT studies were conducted on the oxidation of the acetate and trifluoromethyl complexes with NFTPT. Based on this work, a low energy reaction pathway was proposed to involve: (a) initial oxidation as the highest energy step, (b) transmetalation of a methyl group from 1 equiv of a Pd^{IV} intermediate to 1 equiv of the starting Pd^{II} complex to provide a dimethyl Pd^{IV} intermediate, and (c) reductive elimination to liberate ethane from the resulting dimethyl Pd^{IV} intermediate. Efforts to experimentally observe intermediates upon oxidation of **3** or **9** with NFTPT resulted in a complex mixture of unstable intermediates, preventing any definitive identification of these intermediates. However, Pd^{IV} intermediates were observed by low temperature ¹H NMR upon oxidation of (dtbpy)Pd(CH₃(CF₃)) with AcFcBF₄. These results provide precedence for key steps of oxidative disproportionation and reductive coupling in our proposed catalytic cycle *en route* to the oxidative coupling of methane (Figure 2.2).

General Experimental Procedures and Characterization

General Instrumentation

NMR spectra were obtained on Varian vnmrs 700 (699.76 MHz for ^1H ; 175.95 MHz for ^{13}C), Varian vnmrs 500 (500.1 MHz for ^1H ; 125.75 MHz for ^{13}C ; 470.56 MHz for ^{19}F), Varian MR 400 (400.52 MHz for ^1H ; 125.70 MHz for ^{13}C ; 376.87 MHz for ^{19}F) or Varian Inova 500 (499.90 MHz for ^1H) spectrometers. ^1H , ^{13}C and ^{19}F chemical shifts are reported in parts per million (ppm) relative to the referenced solvent, and reported as singlet (s), doublet (d), triplet (t), quartet (q), doublet of doublets (dd) and multiplet (m).

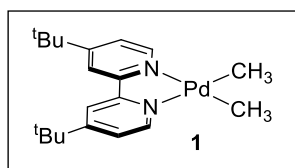
All solutions were prepared in the glove box under an atmosphere of nitrogen unless otherwise noted. J. Young NMR tubes for the oxidation reactions were obtained from Chemglass® and customized by our glassblower to minimize the total volume of the tube (0.8 mL total volume). The tubes were then filled to the top with solvent after addition of the oxidant to accurately measure the yield of gaseous product. Due to the large T_1 of ethane and the internal standard used, the following acquisition parameters were used for ^1H NMR spectroscopic analysis of ethane-forming reactions: scans = 2, acquisition time = 5 s, steady state scan = 0, and relaxation delay = 200 s.

Materials and Methods.

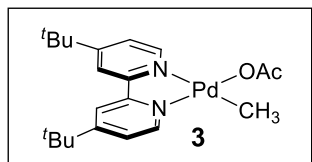
THF, CH_2Cl_2 , and pentanes were obtained from Fisher Scientific or VWR and dispensed from an Innovative Technologies solvent purification system using columns packed with activated alumina, copper catalyst, and molecular sieves. Acetone (Fisher) was refluxed over CaSO_4 , distilled, and then freeze-pump-thaw degassed. Benzene (Fisher) was refluxed over Na/benzophenone, distilled, and freeze-pump-thaw degassed. Acetonitrile- d_3 was obtained from Cambridge Isotope Laboratories, stored in a drybox, and used without further purification. Acetone- d_6 (“100%”) was purchased from Cambridge Isotope Laboratories in ampules and used in a dry box without further purification. CD_2Cl_2 (Cambridge) was dried over CaH_2 , distilled, and then freeze-pump-thaw degassed. 1,4-cyclohexadiene (Acros) was dried over CaCl_2 , distilled and then freeze-pump-thaw degassed. Palladium acetate (Pressure Chemical), palladium chloride (Pressure Chemical), TMSCF_3 (Ryan Scientific), CsF (Matrix Scientific), AgBF_4 (TCI), AgOAc (Aldrich), AgPF_6 (Alfa Aesar), benzoquinone (Aldrich), 4,4'-di-*tert*-butyl-2,2'-bipyridine

(Aldrich), ceric ammonium nitrate (Aldrich), iodine (Aldrich), iodobenzene diacetate (TCI), iodobenzene bis(trifluoroacetate) (Acros), *N*-fluoro-2,4,6-trimethylpyridinium triflate (TCI), potassium persulfate (Acros), 5-(trifluoromethyl)-dibenzothiophenium triflate (Aldrich), 1,1,2-trichloroethane (Aldrich), and methyl triflate (Aldrich) were obtained from commercial vendors and used without further purification. CsF (Matrix Scientific) was dried by heating to 200 °C overnight under vacuum and then stored in a glove box. Acetylferrocenium tetrafluoroborate was prepared using a literature procedure.⁵⁵

Characterization of Palladium (II) Mono-Methyl Complexes.

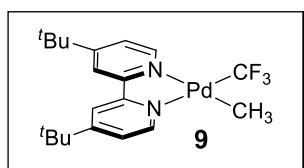


(dtbpy)Pd^{II}(CH₃)₂ (1). Complex **1** was prepared using a literature procedure. The ¹H NMR spectroscopic data for this complex matched that reported in the literature.⁵⁶

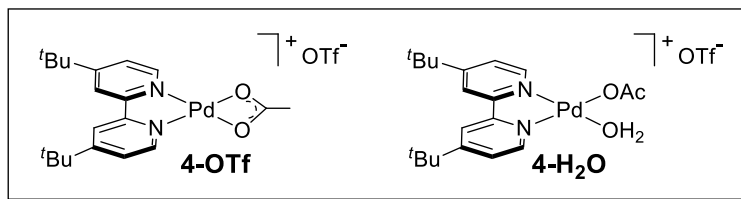


(dtbpy)Pd^{II}(CH₃)(OAc) (3). In an N₂-atmosphere dry box, (dtbpy)Pd(CH₃)(I)⁴² (316 mg, 0.62 mmol, 1 equiv) and AgOAc (115 mg, 0.69 mmol, 1.1 equiv) were combined in a 20 mL vial equipped with a Teflon stirbar. Dry acetone (10 mL) was added, the vial was wrapped in foil to exclude light, and the reaction mixture was stirred at 25 °C for 1 h. The resulting yellow-gray mixture was filtered through a plug of Celite®, the solvent was removed under vacuum, and the resulting yellow solids were dissolved in benzene (10 mL). The benzene solution was filtered through a plug of Celite®, and the volatiles were removed under vacuum to afford the product as a pale yellow powder (106 mg, 38% yield). ¹H NMR (699.76 MHz, 298 K, acetone-*d*₆): δ 8.54 (d,

$J = 2$ Hz, 1H), 8.52 (d, $J = 2$ Hz, 1H), 8.47 (d, $J = 6$ Hz, 1H), 8.35 (d, $J = 6$ Hz, 1H), 7.69-7.68 (multiple peaks, 2H), 1.92 (s, 3H), 1.44 (s, 9H), 1.43 (s, 9H), 0.65 (s, 3H). ^{13}C NMR (175.95 MHz, 298 K, acetone- d_6): δ 175.63, 164.34, 164.23, 157.94, 153.88, 150.32, 148.78, 124.61, 124.42, 121.53, 120.21, 36.37, 36.36, 30.61, 30.45, 24.43, -0.77 . Elemental Analysis: calculated for $\text{C}_{21}\text{H}_{30}\text{N}_2\text{O}_2\text{Pd}$, C: 56.19, H: 6.74, N: 6.24; Found: C: 56.41, H: 6.81, N: 6.21.



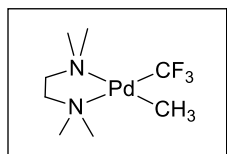
(dtbpy)Pd^{II}(CH₃)(CF₃) (9). In an N_2 -atmosphere dry box, (TMEDA)Pd(CH₃)(CF₃) (432 mg, 1.41 mmol, 1 equiv) and dtbpy (453 mg, 1.69 mmol, 1.2 equiv) were combined in a 20 mL scintillation vial equipped with a Teflon stirbar. Benzene (10 mL) was added, and the reaction mixture was stirred overnight at 25 °C. A pale yellow precipitate formed over the course of the reaction, and this precipitate was collected on a glass frit. The solids were then dissolved in acetone (5 mL). Pentanes (15 mL) were added, resulting in the precipitation of a pale yellow solid, which was collected by filtration. The solids were combined and dried under vacuum to afford the product as a pale yellow solid (502 mg, 78% yield). ^1H NMR (500.10 MHz, 298 K, CD_2Cl_2): δ 8.90 (dd, $J = 6$ Hz, 2 Hz, 1H), 8.54 (d, $J = 6$ Hz, 1H), 8.05 (d, $J = 2$ Hz, 1H), 8.05 (d, $J = 2$ Hz, 1H), 7.52 (dd, $J = 6$ Hz, 2 Hz, 1H), 7.51 (dd, $J = 6$ Hz, 2 Hz, 1H), 1.43 (s, 9H), 1.425 (s, 9H), 0.61 (s, 3H). ^{19}F NMR (470.56 MHz, 298 K, CD_2Cl_2): δ -21.14 (s, 3F). ^{13}C NMR (175.95 MHz, 298 K, CD_2Cl_2): 164.28, 163.64, 156.86, 154.62, 151.52 (q, $J = 4$ Hz), 148.44, 138.99 (q, $J = 366$ Hz), 124.12, 123.67, 119.38, 118.99, 35.94, 35.86, 30.61, 30.60, -2.41 (q, $J = 10$ Hz). Elemental Analysis: calculated for $\text{C}_{20}\text{H}_{27}\text{F}_3\text{N}_2\text{Pd}$, C: 52.35, H: 5.93, N: 6.11; Found: C: 52.31, H: 5.97, N: 6.11.



(dtbpy)Pd^{II}(OAc)⁺ (4-OTf) and (dtbpy)Pd^{II}(OAc)(H₂O)⁺ (4-H₂O). In an N₂-atmosphere dry box, (dtbpy)Pd^{II}(OAc)₂⁵⁷ (200 mg, 0.41 mmol, 1 equiv) was suspended in acetone (10 mL) in a 20 mL scintillation vial equipped with a Teflon stirbar. Methyl triflate (44.6 μL, 0.41 mmol, 1.0 equiv) was added, and the solution was stirred at 25 °C for 2 h. The filtrate was concentrated to dryness and dissolved in CH₂Cl₂ (5 mL). Pentanes (15 mL) were then added, resulting in the precipitation of a yellow solid. This precipitate was collected on a glass frit and dried under vacuum to afford an inseparable mixture of the κ²-acetate product (**4-OTf**) and the aquo complex (**4-H₂O**) as a yellow solid (164 mg, 92% overall yield).

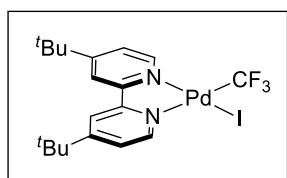
For 4-OTf: ¹H NMR (699.76 MHz, 298 K, acetone-*d*₆): 8.41 (d, *J* = 2 Hz, 2H), 8.30 (d, *J* = 6 Hz, 2H), 7.79 (dd, *J* = 6 Hz, 2 Hz, 2H), 2.42 (s, 3H), 1.32 (s, 18H). ¹³C NMR (175.95 MHz, 298 K, CD₂Cl₂): 188.61, 168.55, 156.86, 150.57, 126.09, 122.36, 36.66, 30.31, 24.44.

For 4-H₂O: ¹H NMR (699.76 MHz, 298 K, acetone-*d*₆): 8.83 (d, *J* = 6 Hz, 1H), 8.69 (d, *J* = 2 Hz, 1H), 8.68 (d, *J* = 2 Hz, 1H), 8.52 (d, *J* = 6 Hz, 1H), 8.09 (dd, *J* = 6 Hz, 2 Hz, 1H), 7.91 (dd, *J* = 6 Hz, 2 Hz, 1H), 2.77 (br. s, 2H), 2.51 (s, 3H), 1.44 (s, 18H). This complex was insufficiently soluble to obtain a fully resolved ¹³C NMR spectrum.

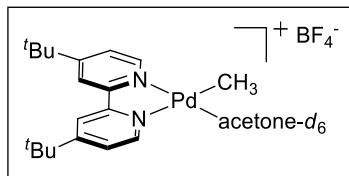


(TMEDA)Pd^{II}(CH₃)(CF₃). In an N₂-atmosphere dry box, CsF (539 mg, 3.37 mmol, 3 equiv), (TMEDA)Pd(CH₃)(I)⁵⁸ (364 mg, 1.12 mmol, 1 equiv), and TMSCF₃ (98 μL, 2.25 mmol, 2 equiv) were combined in a 50 mL Schlenk flask. THF (10 mL) was added, the flask was covered in foil, and the reaction mixture was stirred at 25 °C overnight. Additional TMSCF₃ (98 μL, 2.25 mmol, 2 equiv) and CsF (539 mg, 3.37 mmol, 3 equiv) were added, and the reaction was stirred for another

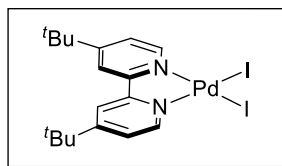
24 h. The reaction was then concentrated to dryness, CH_2Cl_2 (10 mL) was added, and the mixture was filtered through a plug of Celite®. The filtrate was concentrated to ~0.5 mL, and cold pentanes (10 mL) were added. The resulting mixture was stored at $-30\text{ }^\circ\text{C}$ for 1 h, during which time an off-white precipitate formed. The precipitate was collected on a fritted filter and dried under vacuum for 1 h to afford the product as an off-white powder (245 mg, 71% yield). ^1H NMR (699.76 MHz, 298 K, acetone- d_6): δ 2.72 (broad s, 2H), 2.62 (broad s, 2H), 2.58 (s, 6H), 2.46 (s, 6H), 0.10 (s, 3H). ^{19}F NMR (376.87 MHz, 298 K, acetone- d_6): δ -21.94 (s, 3F). ^{13}C NMR (175.95 MHz, 298 K, acetone- d_6): δ 138.28 (q, $J = 364$ Hz), 61.41, 59.98, 48.96, 48.69, -4.93 (q, $J = 11$ Hz). Elemental Analysis: calculated for $\text{C}_8\text{H}_{19}\text{F}_3\text{N}_2\text{Pd}$, C: 31.33, H: 6.24, N: 9.13; Found: C: 31.06, H: 6.12, N: 8.98.



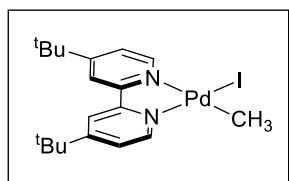
(dtbpy)Pd^{II}(I)(CF₃). (Bu_2bpy)Pd^{II}(CH₃)(CF₃) (160 mg, 0.35 mmol, 1 equiv) was suspended in a solution of I₂ (152 mg, 0.6 mmol, 1.7 equiv) and hexanes (10 mL) in a 20 mL scintillation vial equipped with a Teflon stirbar. A tan precipitate formed upon stirring for 4 h in the dark, and this precipitate was collected on a glass frit. The precipitate was dissolved in acetone (5 mL). Pentanes (15 mL) were then added, resulting in the precipitation of tan solid. The solid was collected by filtration and dried under vacuum to afford the product as a tan solid (74 mg, 37% yield). ^1H NMR (699.76 MHz, 298 K, acetone- d_6): δ 9.74 (d, $J = 6$ Hz, 1H), 8.84 (d, $J = 6$ Hz, 1H), 8.62 (d, $J = 2$ Hz, 1H), 8.58 (d, $J = 2$ Hz, 1H), 7.90 (dd, $J = 6$ Hz, 2 Hz, 1H), 7.73 (dd, $J = 6$ Hz, 2 Hz, 1H), 1.48 (s, 9H), 1.44 (s, 9H). ^{19}F NMR (376.87 MHz, 298 K, acetone- d_6): δ -10.53 (s, 3F). This complex was insufficiently soluble to obtain a fully resolved ^{13}C NMR spectrum. Elemental Analysis: calculated for $\text{C}_{19}\text{H}_{24}\text{F}_3\text{IN}_2\text{Pd}$, C: 39.98, H: 4.24, N: 4.91; Found: C: 40.07, H: 4.28, N: 4.82.



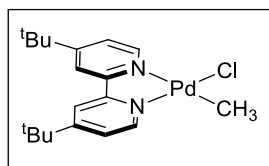
$(dtbpy)Pd^{II}(CH_3)(acetone-d_6)^+$. This complex was prepared using a literature procedure. The ¹H NMR spectroscopic data for this complex matched that reported in the literature.⁷



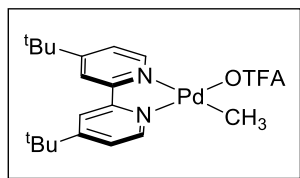
$(dtbpy)Pd^{II}(I)_2$. $(dtbpy)Pd(I)_2$ was prepared using a literature procedure. The ¹H NMR spectroscopic data for this complex matched that reported in the literature.⁵⁶



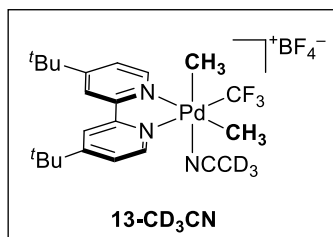
$(dtbpy)Pd^{II}(CH_3)(I)$. $(dtbpy)Pd(CH_3)(I)$ was prepared using a literature procedure. The ¹H NMR spectroscopic data for this complex matched that reported in the literature.⁵⁹



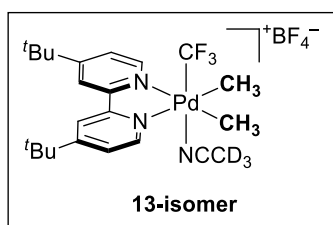
$(dtbpy)Pd^{II}(CH_3)(Cl)$. $(dtbpy)Pd(CH_3)(Cl)$ was prepared using a literature procedure. The ¹H NMR spectroscopic data for this complex matched that reported in the literature.³⁸



(dtbpy)Pd^{II}(CH₃)(OTFA). (dtbpy)Pd(CH₃)(OTFA) was prepared using a literature procedure. The ¹H and ¹⁹F NMR spectroscopic data for this complex matched that reported in the literature.³⁸

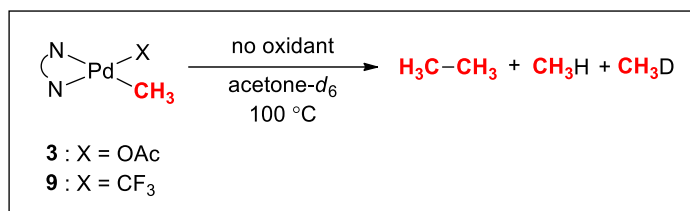


(dtbpy)Pd^{II}(CH₃)₂(CF₃)(CD₃CN)⁺ (13-CD₃CN). ¹H NMR (500.1 MHz, CD₂Cl₂, 233 K): δ 8.90 (d, *J* = 6 Hz, 1H), 8.54-8.52 (overlapping with other species, 1H), 8.28-8.26 (overlapping with other species, 2H), 7.76-7.73 (overlapping with other species, 1H), 7.70 (d, *J* = 6 Hz, 1H), 2.21 (s, 3H), 1.72 (s, 3H), 1.44-1.37 (overlapping with other species, 18H). ¹⁹F NMR (470.56 MHz, CD₂Cl₂, 233 K): δ -27.08 (s, 3F).



(dtbpy)Pd^{II}(CH₃)₂(CF₃)(CD₃CN)⁺ (13-isomer). ¹H NMR (500.1 MHz, CD₂Cl₂, 233 K): δ 8.58 (d, *J* = 6 Hz, 1H), 8.54-8.52 (overlapping with other species, 2H), 8.28-8.26 (overlapping with other species, 1H), 8.05-8.02 (overlapping with other species, 1H), 7.75-7.72 (overlapping with other species, 1H), 2.15 (s, 6H), 1.43-1.37 (overlapping with other species, 18H). ¹⁹F NMR (470.56 MHz, CD₂Cl₂, 233 K): δ -24.72 (s, 3F).

General Procedure for Thermolysis of Complexes 3 and 9



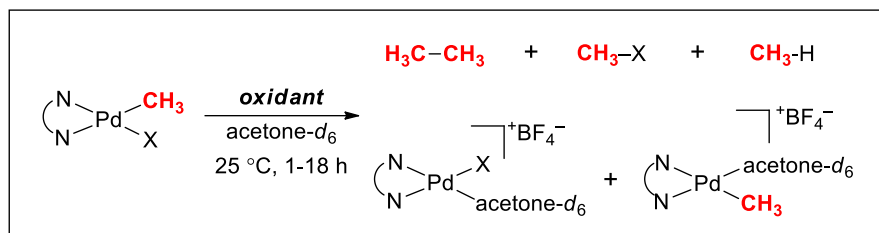
In an N₂-atmosphere dry box, the Pd^{II} complex (4 μmol), 1,1,2-trichloroethane (internal standard, 4 μmol, 20 μL of a 0.2 M solution in acetone-d₆, 1.1 equiv) and acetone-d₆ (0.8 mL) were added to a J. Young NMR tube, filling the NMR tube completely. A ¹H NMR spectrum was acquired at 25 °C to determine the initial integration ratio of the standard to the Pd^{II} starting material. The tube was completely submerged in a 100 °C oil bath and heated in ambient light for the appropriate time. The reaction was cooled to 25 °C and analyzed by ¹H NMR spectroscopy. For each complex, the yield of ethane, CH₄, and CH₃D were determined by integration of relevant peaks in the ¹H NMR spectra.

Table 2.5. Results from Thermolysis of 3 and 9

Complex	Reaction Time	% Yield C ₂ H ₆	% Yield CH ₄	% Yield CH ₃ D	% Yield starting material
3	21 h	7	7	83	nd
9	21 h	nd	nd	43	65
9	8 d	3	4	74	3

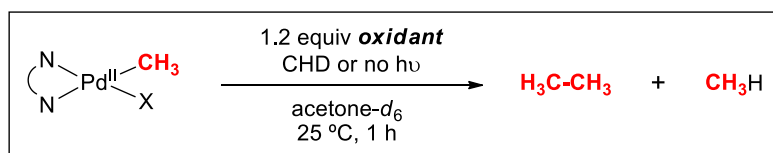
nd = not detected

General Procedure for Oxidation with Oxidants at 25 °C



In an N₂-atmosphere dry box, 0.3 mL (1 equiv, 4 μmol) of a stock solution of Pd^{II} complex (0.013 M in acetone-*d*₆) and 1,1,2-trichloroethane (internal standard, 60 μL of a 0.2 M solution in acetone-*d*₆, 1.1 equiv) were added to a J. Young NMR tube. A dry glass capillary was added to facilitate mixing of the complex with the oxidant. An initial ¹H NMR spectrum was acquired to determine the ratio of standard to complex. The tube was taken back into the dry box, where acetone-*d*₆ (0.1 mL) and a solution of the oxidant (0.2 mL of a 0.024 mM solution in acetone-*d*₆, 1.2 equiv) was added, filling the NMR tube to the top. The tube was quickly capped, was shaken vigorously, and analyzed after 1 h and 24 h at 25 °C by ¹H NMR spectroscopy. Yields were determined by integration of relevant peaks in the ¹H NMR spectra. To quantify the inorganic products, NaI (8 equiv) was added to the reaction mixture to generate the corresponding iodide complex. Yields were determined by integration of relevant peaks in the ¹H NMR spectra. The reported yields and standard deviations are based on three separate runs.

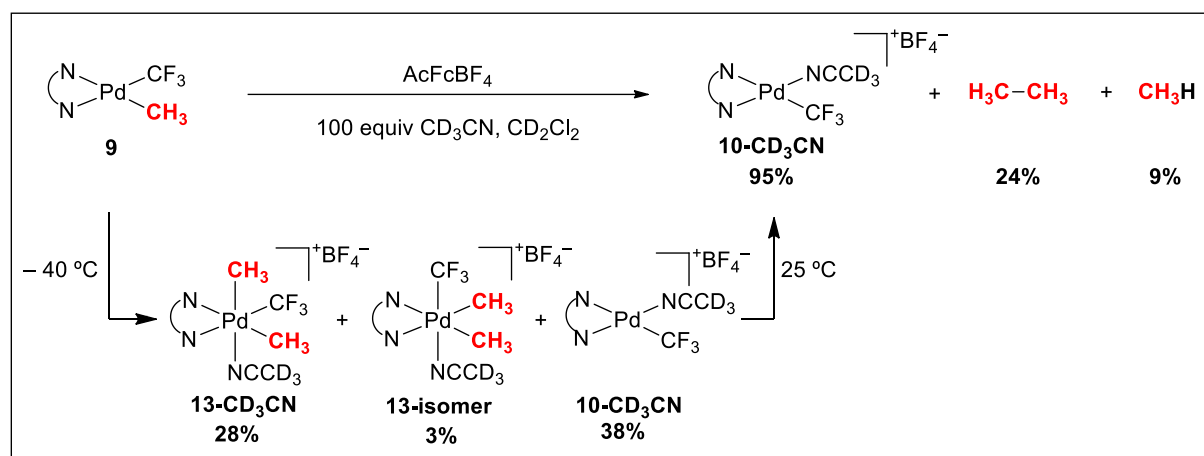
General Procedure for Radical Trap Experiments with Complex 3 or 9 at 25 °C



In an N₂-atmosphere dry box, 0.5 mL (1 equiv, 4 μmol) of a stock solution of complex **3** or **9** (0.008M in acetone-*d*₆), 1,4-cyclohexadiene (15.2 μL, 0.2 M, 40 eq), and 1,1,2-trichloroethane (internal standard, 20 μL of a 0.2 M solution in acetone-*d*₆, 1 equiv) were added to a J. Young NMR tube. A dry glass capillary was added to facilitate mixing of complex with the oxidant. An initial ¹H NMR spectrum was acquired to determine the ratio of standard to complex. The tube

was taken back into the dry box, where acetone-*d*₆ (0.2 mL) and a solution of acetylferrocenium tetrafluoroborate (0.1 mL of a 0.048 M solution in acetone-*d*₆, 1.2 equiv) or a solution of N-fluoro-2,4,6-trimethylpyridinium triflate (0.1 mL of a 0.2 M solution in acetone-*d*₆, 5.0 equiv) was added, filling the NMR tube completely. The tube was quickly capped, shaken vigorously, and was allowed to stand for ~1 h at 25 °C. The reaction was then analyzed by ¹H NMR spectroscopy, which showed complete consumption of the mono-methyl complex. Yields were determined by integration of relevant peaks in the ¹H NMR spectra. The reported yields and standard deviations are based on three separate runs.

Representative Procedure for Oxidation of Complex **9** with AcFcBF₄ at -40 °C



In an N₂-atmosphere dry box, Pd complex **9** (1.8 mg, 4 μmol), 1,1,2-trichloroethane (internal standard, 20 μL of a 0.22 mM solution in CD₃CN), and CD₂Cl₂ (0.5 mL) were combined in a J. Young NMR tube. An initial ¹H NMR spectrum was acquired to determine the ratio of standard to complex **9**. The tube was taken back into the dry box and was placed in a cold well at -181 °C until completely frozen (required ~30 min). With the tube still in the cold bath, AcFcBF₄ (0.1 mL of 0.048 M solution in CD₂Cl₂, 1.2 equiv) was added, and the resulting mixture was allowed to stand in the cold bath until it was completely frozen (required ~15 min). The NMR tube was sealed, removed from the drybox, and immediately placed in a -78 °C cold bath. After 30 min at -78 °C, the tube was shaken vigorously. The tube was then inserted into an NMR spectrometer with the probe pre-cooled to -40 °C. The initial spectrum (after 15 min) showed partial consumption of

starting material **3** (28% remaining) and the formation of three inorganic complexes (proposed to be **13-CD₃CN**, **13-isomer** and **10-CD₃CN**), seen in Figure 2.10 and Figure 2.11. No ethane was detected at this temperature. After 1 h at $-40\text{ }^{\circ}\text{C}$, the sample was warmed to $25\text{ }^{\circ}\text{C}$ over 30 min. At this point, the ^1H NMR spectrum showed the generation of ethane (24% yield) and complex **10-CD₃CN** (95% yield) along with traces of unreacted starting material (7%) and methane (9%). The mixture of intermediates at low temperatures was further characterized by ^1H - ^1H gradient COSY, ^1H - ^1H ROESY, ^1H - ^{13}C HSQC and ^1H - ^{13}C HMBC NMR spectroscopy at $-20\text{ }^{\circ}\text{C}$, using pyridine-*d*₅ as the trapping ligand due to increased stability of the intermediates. Yields were determined by integration of relevant peaks in the ^1H NMR spectra.

Figure 2.10. ^1H NMR Spectra for Low Temperature Oxidation of **9** with AcFcBF

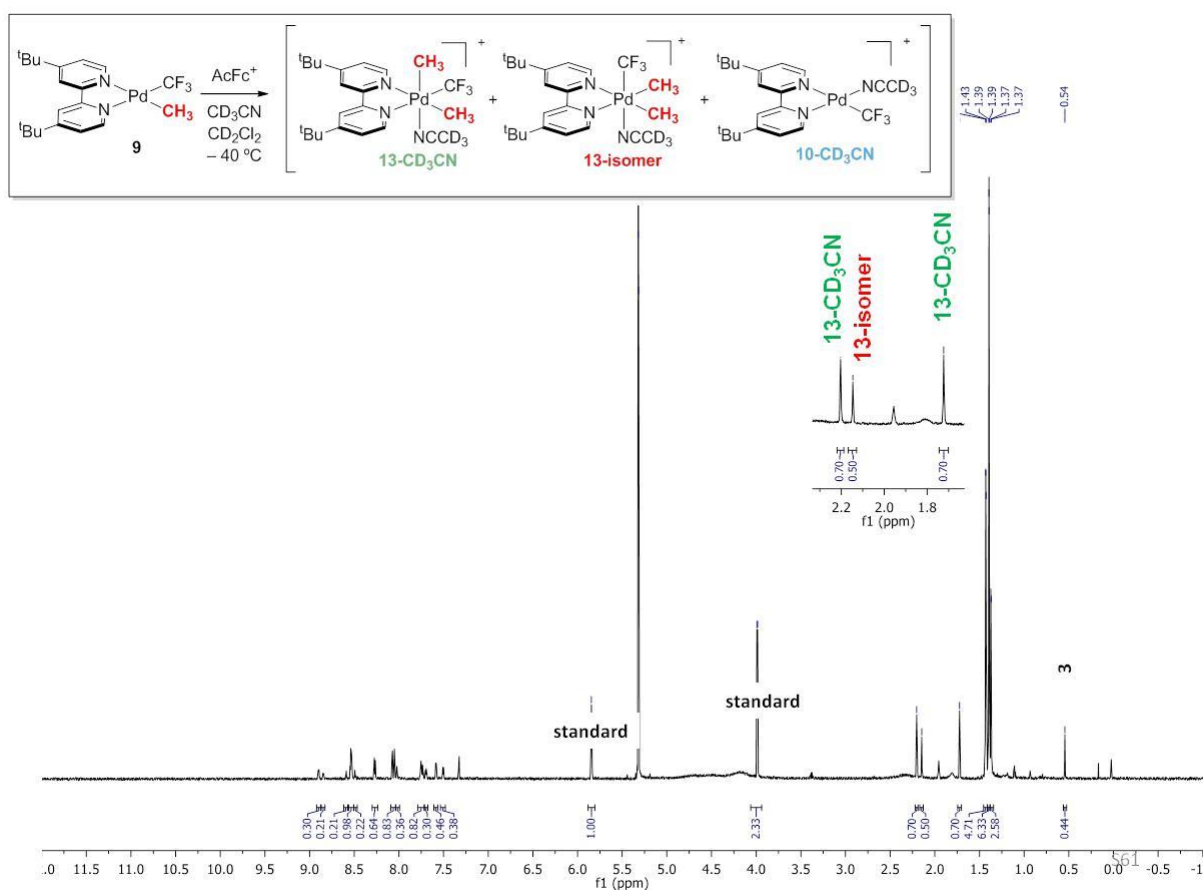
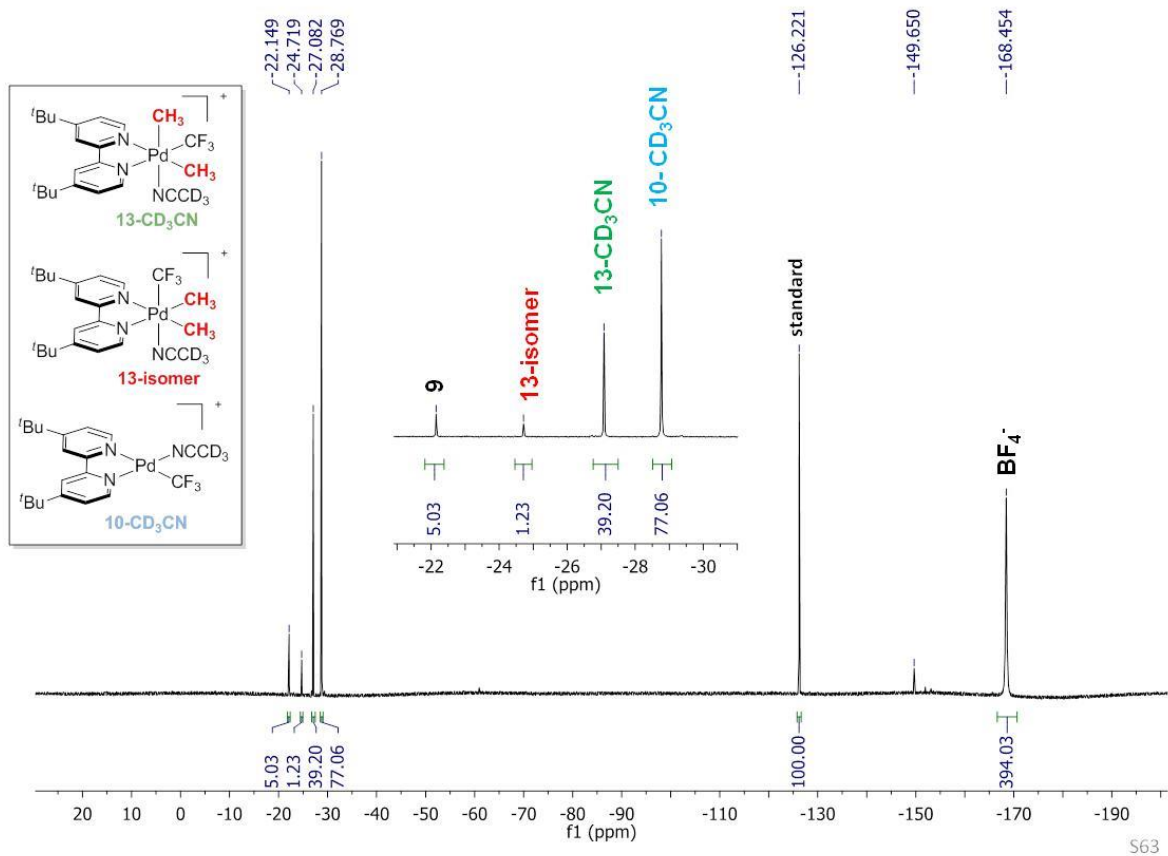


Figure 2.11. ^{19}F NMR Spectra for Low Temperature Oxidation of **9** with AcFcBF_4



S63

Characterization of Pd^{IV} Intermediates

The previous procedure for low temperature oxidation of **9** with AcFcBF₄, was followed with the exception of the 100 equiv of CD₃CN which was replaced with 100 equiv of pyridine-*d*₅ for enhanced stability of the intermediates, and thus ease of characterization (Figure 2.12 and 2.13).

Figure 2.12. ¹H-¹H ROESY NMR Spectra

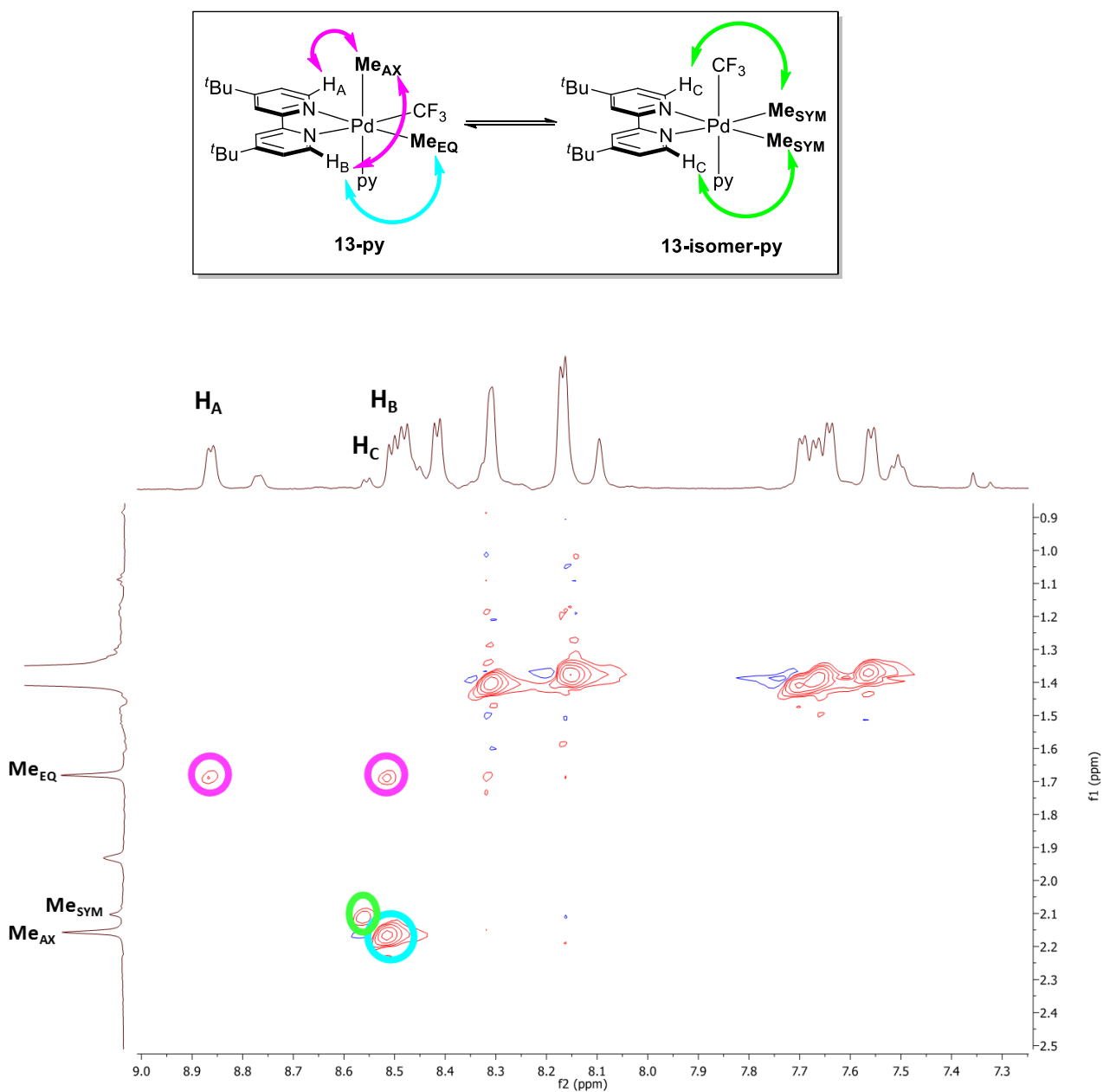
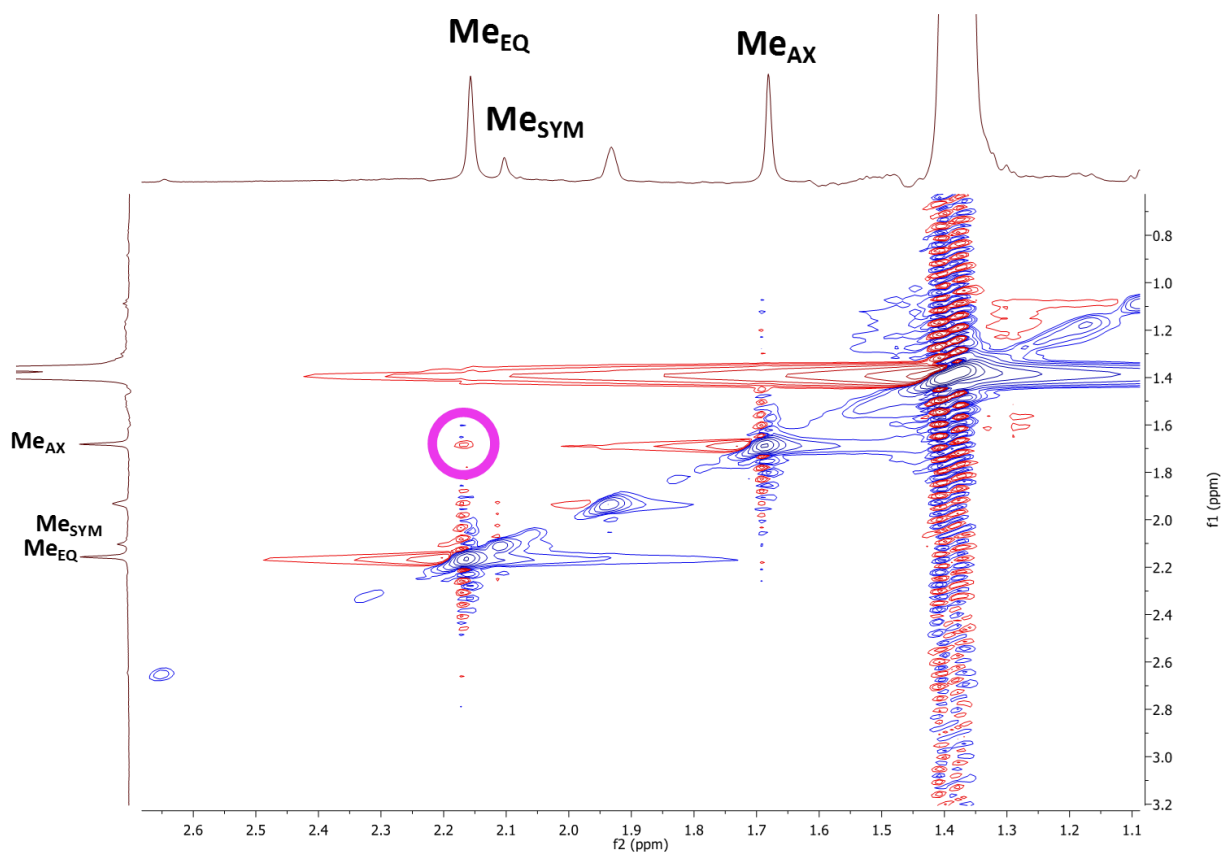
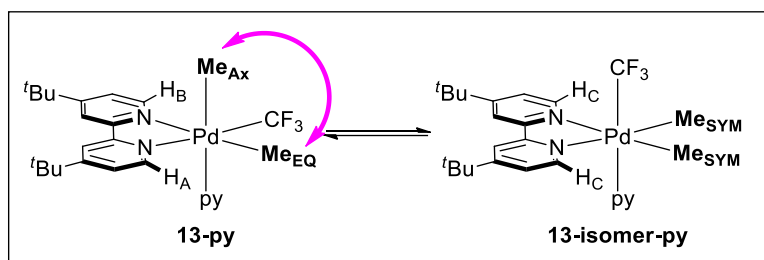
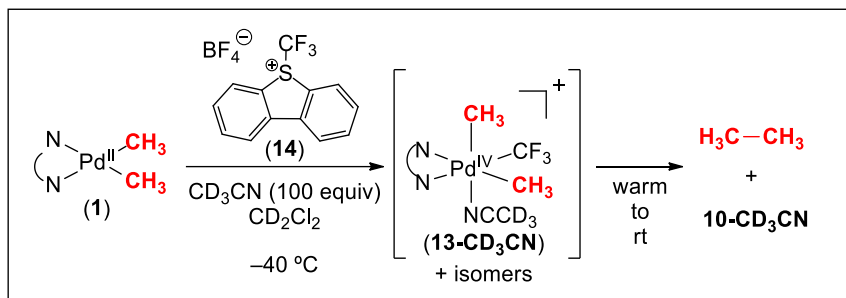


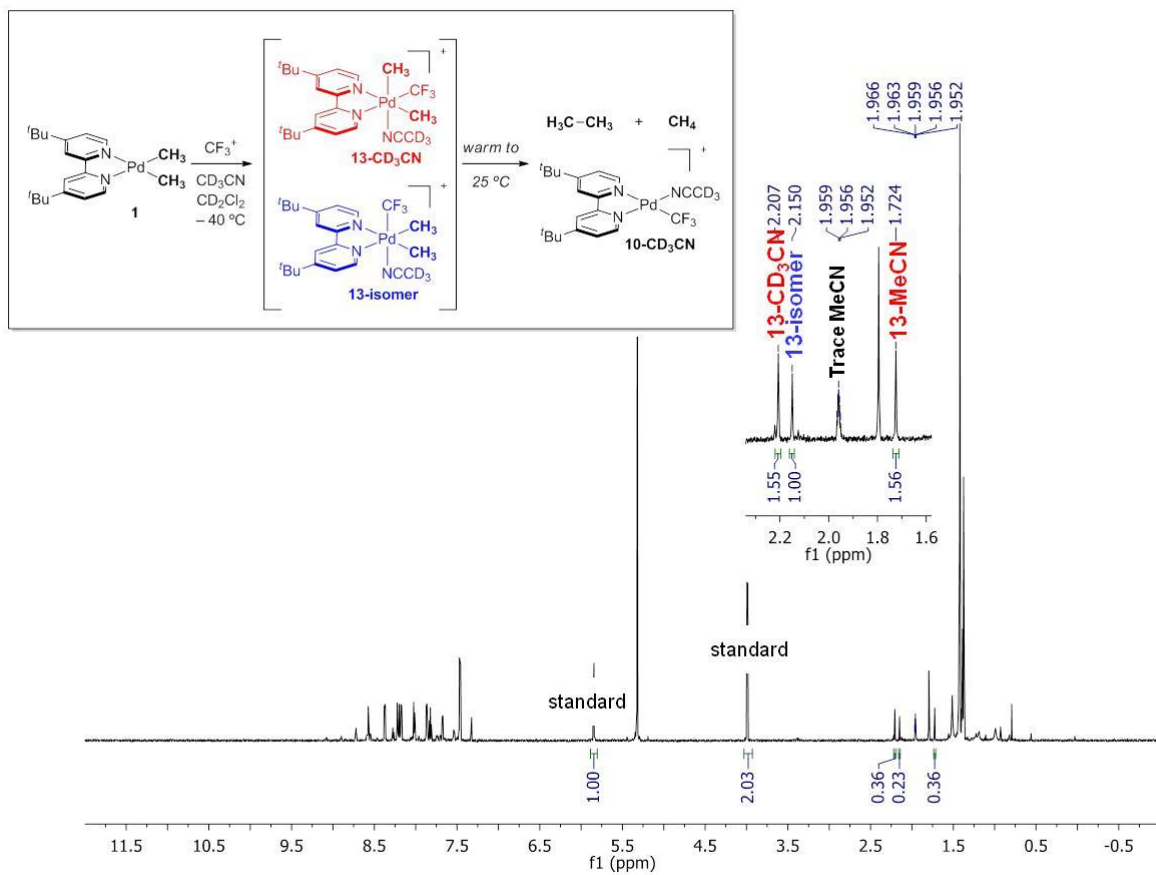
Figure 2.13. ^1H - ^1H ROESY NMR Spectra





Independent Synthesis of Proposed Intermediates 13-CD₃CN and 13-isomer. In an N₂-atmosphere dry box, (dtbpy)Pd(CH₃)₂ (**1**) (1.6 mg, 4 μmol), 1,1,2-trichloroethane (internal standard, 20 μL of a 0.22 mM solution in CD₃CN), and CD₂Cl₂ (0.5 mL) were combined in a J. Young NMR tube. An initial ¹H NMR spectrum was acquired to determine the ratio of standard to complex **1**. The tube was taken back into the dry box and was placed in a cold well at -181 °C until completely frozen (required ~30 min). With the tube still in the cold bath, trifluoromethyl dibenzothiophenium tetrafluoroborate **14** (0.1 mL of 0.048 M solution in CD₂Cl₂, 1.2 equiv) was added, and the resulting mixture was allowed to stand in the cold bath until it was completely frozen (required ~15 min). The NMR tube was sealed, removed from the dry box, and immediately placed in a -78 °C cold bath. After 30 min at -78 °C, the tube was shaken vigorously. The tube was then inserted into an NMR spectrometer with the probe pre-cooled to -40 °C. The initial ¹H and ¹⁹F NMR spectra showed complete consumption of the starting material (dtbpy)Pd(CH₃)₂ (**1**). A complex mixture of Pd-containing products was formed (Figure 2.14). Importantly, two of the major species showed ¹H and ¹⁹F NMR resonances identical to those of proposed intermediates **13-CD₃CN** and **13-isomer**. These complexes were formed in 18% and 5% yield, respectively. After 1 h at -40 °C, the sample was warmed to 25 °C over 15 min. At this point, the ¹H NMR spectrum showed the generation of ethane (12% yield) along with **10-CD₃CN** (21%). Yields were determined by integration of relevant peaks in the ¹H NMR spectra.

Figure 2.14. ^1H NMR Spectra for Independent Synthesis of Proposed Intermediates 13- CD_3CN and 13-isomer.



Computational Details

Gaussian 09 was used at the B3LYP⁶⁰⁻⁶² level of density functional theory (DFT) for geometry optimization. Other computational details have been reported.⁹

Figure 2.15. DFT Calculations for the Low Energy Pathway for Oxidation of (dtbpy)Pd(CH₃)(Cl).

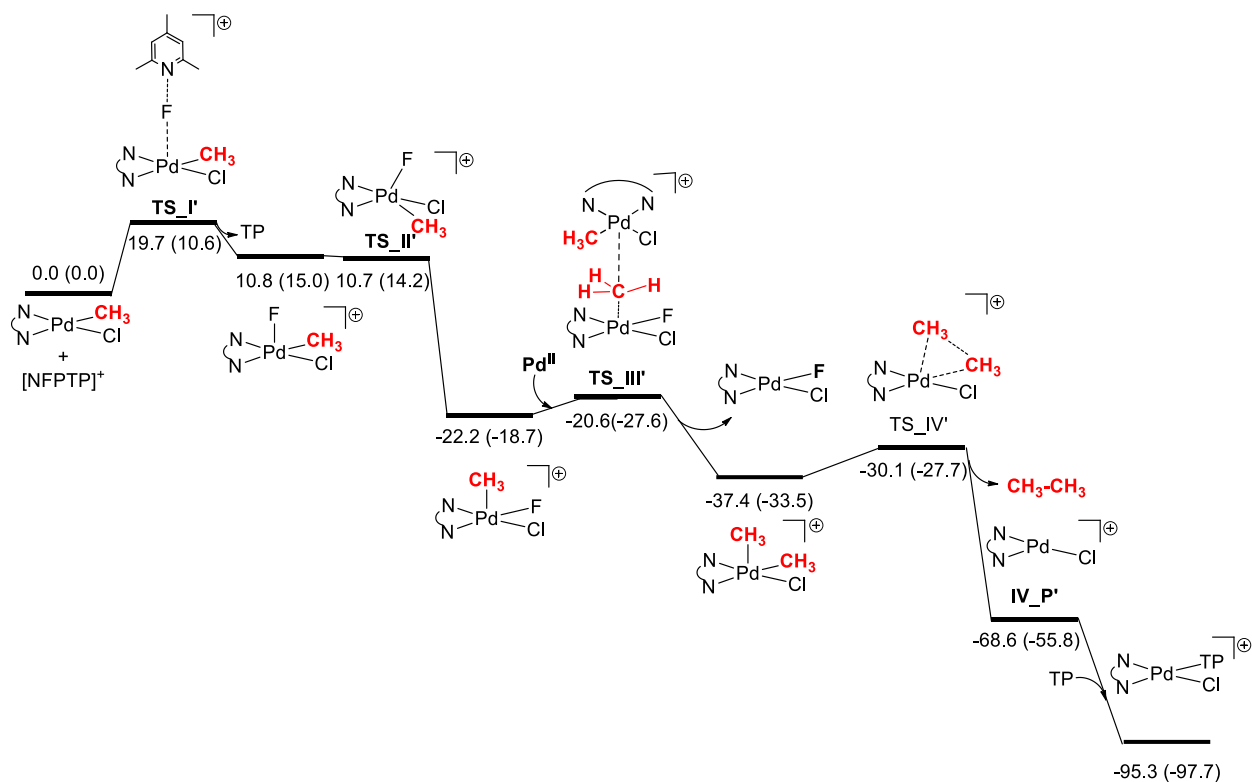
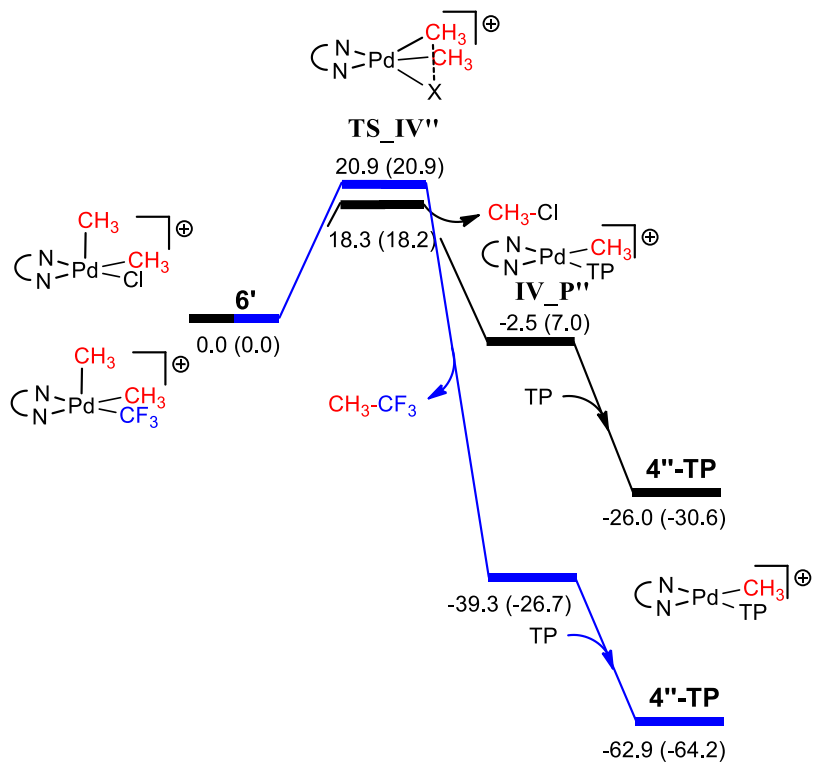


Figure 2.16. DFT Calculations for the Low Energy Pathway for Competing Reductive Elimination with the Chloride Complex.



References

- (1) Holmen, A. *Catal. Today* **2009**, *142*, 2.
- (2) Crabtree, R. H. *Chem. Rev.* **1995**, *95*, 987.
- (3) Hammond, C.; Conrad, S.; Hermans, I. *ChemSusChem* **2012**, *5*, 1668.
- (4) Lunsford, J. H. *Catal. Today* **2000**, *63*, 165.
- (5) Shilov, A. E.; Shul, G. B. *Chem. Rev.* **1997**, *97*, 2879.
- (6) Alvarez-Galvan, M. C. C.; Mota, N.; Ojeda, M.; Rojas, S.; Navarro, R. M. M.; Fierro, J. L. G. *Catal. Today* **2011**, *171*, 15.
- (7) Lanci, M. P.; Remy, M. S.; Kaminsky, W.; Mayer, J. M.; Sanford, M. S. *J. Am. Chem. Soc.* **2009**, *131*, 15618.
- (8) Lanci, M. P.; Remy, M. S.; Lao, D. B.; Sanford, M. S.; Mayer, J. M. *Organometallics* **2011**, *30*, 3704.
- (9) Lotz, M. D.; Remy, M. S.; Lao, D. B.; Ariaifard, A.; Yates, B. F.; Canty, A. J.; Mayer, J. M.; Sanford, M. S. *J. Am. Chem. Soc.* **2014**, *136*, 8237.
- (10) Li, Z.; Li, C.-J. *J. Am. Chem. Soc.* **2005**, *127*, 3672.
- (11) Li, Z.; Li, C.-J. *J. Am. Chem. Soc.* **2006**, *128*, 56.
- (12) Xie, J.; Li, H.; Zhou, J.; Cheng, Y.; Zhu, C. *Angew. Chem. Int. Ed. Engl.* **2012**, *51*, 1252.
- (13) Nobuta, T.; Tada, N.; Fujiya, A.; Kariya, A.; Miura, T.; Itoh, A. *Org. Lett.* **2013**, *15*, 574.
- (14) Yeung, C. S.; Dong, V. M. *Chem. Rev.* **2011**, *111*, 1215.
- (15) Shiotani, A.; Itatani, H.; Inagaki, T. *J. Mol. Catal.* **1986**, *34*, 57.
- (16) Itatani, H.; Yoshimoto, H.; Shiotani, A.; Yokota, A.; Yoshikiyo, M. Biphenyl compounds by dehydration dimerization of aromatic monocyclic compounds., March 13, 1980.
- (17) Periana, R. A.; Mironov, O.; Taube, D.; Bhalla, G.; Jones, C. J. *Science* **2003**, *301*, 814.
- (18) Kao, L. C.; Hutson, A. C.; Sen, A. *J. Am. Chem. Soc.* **1991**, *113*, 700.
- (19) Muehlhofer, M.; Strassner, T.; Herrmann, W. A. *Angew. Chem. Int. Ed.* **2002**, *41*, 1745.
- (20) Stahl, S. S.; Labinger, J. A.; Bercaw, J. E. *Angew. Chem. Int. Ed.* **1998**, *37*, 2180.
- (21) Crabtree, R. H. *J. Chem. Soc. Dalt. Trans.* **2001**, *17*, 2437.
- (22) Labinger, J. A.; Bercaw, J. E. *Nature* **2002**, *417*, 507.

- (23) Shul'pin, G. B. *Dalton Trans.* **2013**, 42, 12794.
- (24) Khusnutdinova, J. R.; Rath, N. P.; Mirica, L. M. *J. Am. Chem. Soc.* **2010**, 132, 7303.
- (25) Luo, J.; Rath, N. P.; Mirica, L. M. *Organometallics* **2013**, 32, 3343.
- (26) Remy, M. S.; Cundari, T. R.; Sanford, M. S. *Organometallics* **2010**, 29, 1522.
- (27) Byers, P. K.; Canty, A. J.; Skelton, B. W.; White, A. H. *J. Chem. Soc. Chem. Commun.* **1986**, 23, 1722.
- (28) Byers, P. K.; Canty, A. J.; Crespo, M.; Puddephatt, R. J.; Scott, J. D. *Organometallics* **1988**, 7, 1363.
- (29) Duecker-Benfer, C.; van Eldik, R.; Canty, A. J. *Organometallics* **1994**, 13, 2412.
- (30) Canty, A. J. *Dalt. Trans.* **2009**, 47, 10409.
- (31) Khusnutdinova, J. R.; Qu, F.; Zhang, Y.; Rath, N. P.; Mirica, L. M. *Organometallics* **2012**, 31, 4627.
- (32) Tang, F.; Zhang, Y.; Rath, N. P.; Mirica, L. M. *Organometallics* **2012**, 31, 6690.
- (33) Holtcamp, M. W.; Henling, L. M.; Day, M. W.; Labinger, J. A.; Bercaw, J. E. *Inorg. Chim. Acta* **1998**, 270, 467.
- (34) Lin, M.; Hogan, T.; Sen, A. *J. Am. Chem. Soc.* **1997**, 119, 6048.
- (35) An, Z.; Pan, X.; Liu, X.; Han, X.; Bao, X. *J. Am. Chem. Soc.* **2006**, 128, 16028.
- (36) Yuan, J.; Wang, L.; Wang, Y. *Ind. Eng. Chem. Res.* **2011**, 50, 6513.
- (37) Munz, D.; Meyer, D.; Strassner, T. *Organometallics* **2013**, 32, 3469.
- (38) Remy, M. S. *Group 10 Methyl Transfer Reactions Toward Catalyst Development for Oxidative Oligomerization of Methane* **2011**.
- (39) Markies, B. A.; Canty, A. J.; Boersma, J.; van Koten, G. *Organometallics* **1994**, 13, 2053.
- (40) Crumpton, D. M.; Goldberg, K. I. *J. Am. Chem. Soc.* **2000**, 122, 962.
- (41) Hull, K. L.; Anani, W. Q.; Sanford, M. S. *J. Am. Chem. Soc.* **2006**, 128, 7134.
- (42) Ball, N. D.; Kampf, J. W.; Sanford, M. S. *J. Am. Chem. Soc.* **2010**, 132, 2878.
- (43) Racowski, J. M.; Ball, N. D.; Sanford, M. S. *J. Am. Chem. Soc.* **2011**, 133, 18022.
- (44) Racowski, J. M.; Gary, J. B.; Sanford, M. S. *Angew. Chem., Int. Ed.* **2012**, 51, 3414.
- (45) Maleckis, A.; Sanford, M. S. *Organometallics* **2011**, 30, 6617.
- (46) Ye, Y.; Ball, N. D.; Kampf, J. W.; Sanford, M. S. *J. Am. Chem. Soc.* **2010**, 132, 14682.

- (47) Powers, D. C.; Lee, E.; Ariaifard, A.; Sanford, M. S.; Yates, B. F.; Canty, A. J.; Ritter, T. *J. Am. Chem. Soc.* **2012**, *134*, 12002.
- (48) Kruis, D.; Markies, B. A.; Canty, A. J.; Boersma, J.; van Koten, G. *J. Organomet. Chem.* **1997**, *532*, 235.
- (49) Canty, A. J.; Denney, M. C.; Skelton, B. W.; White, A. H. *Organometallics* **2004**, *23*, 1122.
- (50) Canty, A. J.; Patel, J.; Rodemann, T.; Ryan, J. H.; Skelton, B. W.; White, A. H. *Organometallics* **2004**, *23*, 3466.
- (51) Wang, L.; Stahl, S. S.; Labinger, J. A.; Bercaw, J. E. *J. Mol. Catal. A Chem.* **1997**, *116*, 269.
- (52) Johansson, L.; Ryan, O. B.; Rømming, C.; Tilset, M.; Romming, C.; Tilset, M. *Organometallics* **1998**, *17*, 3957.
- (53) Aye K.-T.; Canty, A. J.; Crespo, M.; Puddephatt, R. J.; Scott, J. D.; Watson, A. A. *Organometallics* **1989**, *8*, 1518.
- (54) Bartlett, K. L.; Goldberg, K. I.; Borden, W. T. *J. Am. Chem. Soc.* **2000**, *122*, 1456.
- (55) Connelly, N. G.; Geiger, W. E. *Chem. Rev.* **1996**, *96*, 877.
- (56) Engelter, C.; Thornton, D. A. *Transit. Met. Chem.* **1990**, *15*, 212.
- (57) Milani, B.; Alessio, E.; Mestroni, G.; Sommazzi, A.; Garbassi, F.; Zangrando, E.; Bresciani-Pahor, N.; Randaccio, L. *J. Chem. Soc. Dalton Trans.* **1994**, *13*, 1903.
- (58) De Graaf, W.; Boersma, J.; Smeets, W. J. J.; Spek, A. L.; Van Koten, G. *Organometallics* **1989**, *8*, 2907.
- (59) Byers, P. K.; Canty, A. J.; Crespo, M.; Puddephatt, R. J.; Scott, J. D. *Organometallics* **1988**, *7*, 1363.
- (60) Lee, C.; Yang, W.; Parr, R. G. *Phys. Rev. B* **1988**, *37*, 785.
- (61) Miehlisch, B.; Savin, A.; Stoll, H.; Preuss, H. *Chemical Physics Letters* **1989**, *157*, 200.
- (62) Becke, A.; Becke, A. *J. Chem. Phys.* **1993**, *98*, 5648.

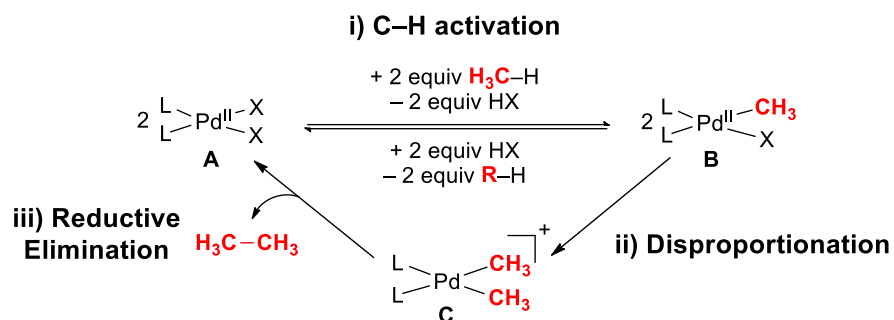
CHAPTER 3

Investigating C–H Activation at Palladium: Studies with Arene Model Substrates

Background

The oxidative coupling of abundant methane to form higher alkanes would be an attractive route to fuels and commodity chemicals.¹ In our pursuits of a system to achieve this transformation, we sought to further explore one key step in this process, C–H activation (Scheme 3.1, step *i*). In the previous chapter, we demonstrated the selective and high yielding generation of ethane from mono-methyl palladium (II) complexes such as **B** (steps *ii* and *iii*). Thus, further investigation of C–H activation at Pd^{II} species of the general structure **A**, would better inform our proposed catalytic cycle.

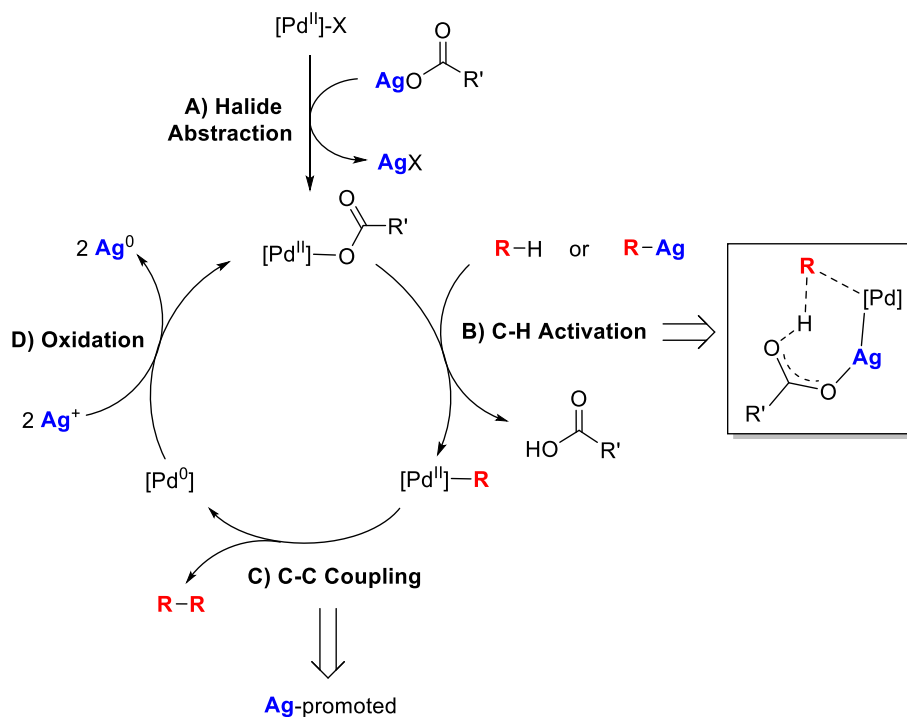
Scheme 3.1. Proposed Catalytic Cycle for Methane Functionalization



Palladium (II) species have been utilized in a wide variety of C–H functionalization reactions, often in conjunction with additives, such as silver salts.^{2–6} Silver additives have been shown to enhance yields in C–H functionalization reactions;^{6–8} however, the role of these additives is often not well established. Thus, to better understand the mechanism of C–H activation, we sought to explore the role of silver in these transformations with a Pd^{II} species.

Some of the commonly proposed roles of silver additives include: (1) the AgX provides an X-type ligand for the Pd center, assisting in C–H activation at Pd (Scheme 3.2, step A);^{9–16} (2) the AgX reacts with Pd to form a bimetallic Pd–Ag intermediate that facilitates C–H activation (step B);^{20–22} (3) the Ag⁺ salt promotes the initial C–H cleavage to form a Ag–R intermediate (step B);^{20–24} (4) the Ag⁺ salt facilitates C–C reductive elimination at Pd (step C);²⁵ or (5) the Ag⁺ salt serves as a terminal oxidant to regenerate the Pd catalyst (step D).^{19,21,22,26–42} However, experimental evidence to definitively establish the role of silver salts remains relatively rare.^{15,19–21,27,41} Thus, our initial work focused on the use of a model system to experimentally elucidate the role of silver salts in C–H activation using Pd complexes analogous to A (Scheme 3.1).

Scheme 3.2. Proposed Catalytic Cycle for Methane Functionalization



Development of a Model System

In this model system, the choice of substrate was crucial in order to investigate both the mechanism of C–H activation with palladium and the role of silver salts in this step. Although ultimately methane is our desired substrate for C–H activation studies with Pd, significant challenges arise in studies with this substrate. One major challenge associated with the activation of methane is the potential instability of the resulting Pd^{II} -Me products at the elevated temperatures required for methane activation.^{45,46} Thus, we sought to develop a model system to gain a better mechanistic understanding of the C–H activation step with palladium complexes based on two key criteria. First, we targeted substrates that would yield stable, isolable Pd products from C–H activation, in order to selectively investigate the C–H activation step. Second, we focused on a substrate that has been utilized in C–H functionalization catalysis, in order to gain mechanistic insight directly relevant to catalytic applications. On the basis of these criteria, our initial studies were conducted with pentafluorobenzene (C_6F_5H) as the substrate for our model system. C_6F_5H is a particularly convenient choice because it is a liquid and contains a spectroscopic ^{19}F handle, both of which simplify reaction procedures and analysis. Initial studies of C_6F_5H activation were

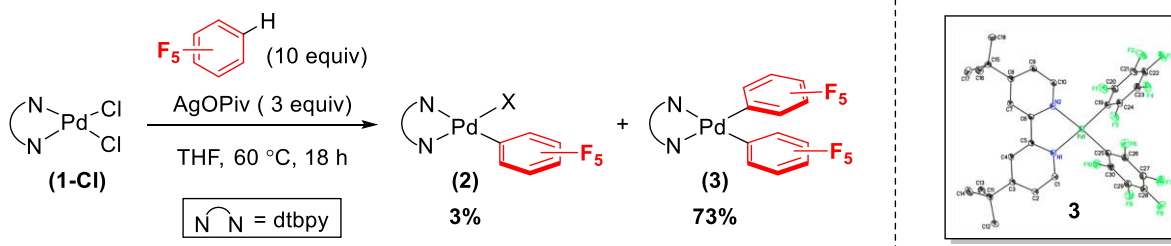
conducted with the model complex, (4,4'-di-*tert*-butyl-2,2'-bipyridyl)Pd(Cl)₂ (**1-Cl**), as analogous Pd complexes have been generated in the reductive elimination of ethane shown in Chapter 2 (Scheme 3.1, steps *ii* and *iii*).

Results and Discussion

Probing the Reactivity of the Model System with C₆F₅H

We established initial conditions for the activation of C₆F₅H with **1-Cl** and a silver salt. Treatment of **1-Cl** with AgOPiv and C₆F₅H afforded predominantly the pentafluorophenyl palladium product **3**, along with trace amounts of **2** (Scheme 3.3). To confirm the structure of the major product **3**, this complex was synthesized independently by reaction of the previously reported (1,5-cyclooctadiene)Pd(C₆F₅)₂⁴⁷ with 4,4'-di-*tert*-butyl-2,2'-bipyridine. Complex **3** was also characterized by ¹H, ¹³C, and ¹⁹F NMR spectroscopy, as well as an X-ray crystal structure. Gratifyingly, complex **3** is remarkably stable, as heating to 100 °C for up to 5 d did not lead to reductive elimination or other decomposition pathways. Furthermore, C₆F₅H has been utilized in a variety of catalytic transformations,^{10,29,30,48–51} fulfilling our two requirements for a model system. The establishment of a simple model system allowed us next to investigate the role of silver additives in the mechanism of C–H activation.

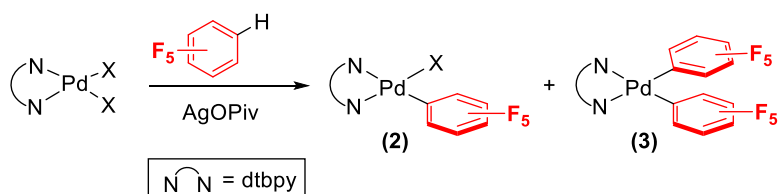
Scheme 3.3. Activation of C₆F₅H with 1-Cl to Generate 2 and 3



Under these conditions, we found that **2** and **3** were not observed in the absence of silver salts (Table 3.1, entry 5). Ag salts have been shown to participate in halide abstraction, generating a more active Pd species.^{9,14,52} Thus, we envisioned silver salts to perform a similar halide abstraction under our conditions to access the bis-pivalate complex **1-OPiv**. To probe this theory, **1-OPiv** was synthesized and subsequently subjected to the reaction conditions with AgOPiv, affording similar yields of **2** and **3** as **1-Cl** (Table 3.1, entry 2). However, only trace amounts of **2**

and **3** were detected with **1-O_{Piv}** in the absence of AgOPiv (entry 6), suggesting that the role of AgOPiv is not solely to perform halide abstraction and form **1-O_{Piv}** under these conditions. Notably, similar trends in reactivity were observed with other carboxylate complexes, **1-OAc** and **1-OTFA**. Treatment of **1-OAc** and **1-OTFA** with AgOPiv and C₆F₅H resulted in mixtures of **2** and **3** (Table 3.1, entries 3-4), albeit in lower yields with **1-OTFA**. However, upon exclusion of silver salts, **1-OAc** afforded only trace amounts of **2** and **3** (entry 7). For further studies, we chose to investigate Ag-mediated C–H activation at Pd carboxylate complexes. These reactions are less likely to proceed through a halide abstraction step, which should simplify mechanistic studies.

Table 3.1. Probing Carboxylate Complexes in C₆F₅H Activation^a

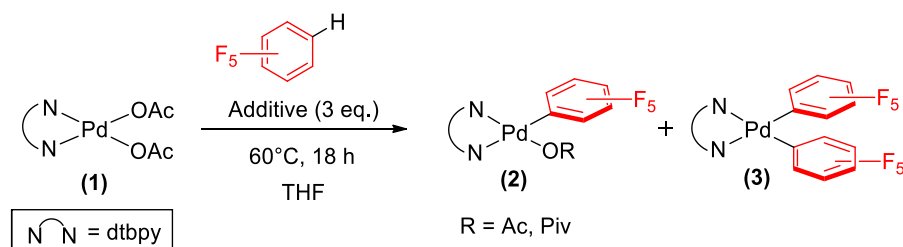


Entry	X =	Equiv of AgOPiv	% Yield of 2	% Yield of 3
1	Cl	3	3	73
2	O _{Piv}	3	4	74
3	OAc	3	11	68
4	OTFA	3	19	38
5	Cl	None	< 1	< 1
6	O _{Piv}	None	1	<1
7	OAc	None	1	<1

^aConditions: Pd complex (25 μmol, 1 equiv), AgOPiv (75 μmol, 3 equiv), C₆F₅H (28 μL, 250 μmol, 10 equiv), tetrahydrofuran (25 mM), 60 °C, 18 h.

We began our investigation with **1-OAc**, as it generated modest yields of **2** and **3** and could be easily synthesized from more readily available starting materials. Further optimization of the reaction conditions afforded an 88% yield of **3** from **1-OAc**, AgOPiv and C₆F₅H (Table 3.2, entry 1). However, in the absence of AgOPiv, <1% conversion to organometallic products **2** and **3** was observed under otherwise analogous conditions (Table 3.2, entry 2). As consistently poor reactivity was observed in the absence of silver, we sought to further explore the role of silver salts in C₆F₅H activation.

Table 3.2. Developing a Model System to Investigate C–H Activation



Entry	Additive	% Yield 2	% Yield 3
1 ^a	AgOPiv	<1	88
2 ^b	none	<1	<1
3 ^c	Ag ₂ O	<1	85
4 ^c	Ag ₂ CO ₃	21	39
5 ^a	AgOAc	12	30
6 ^a	AgOTFA	60	19
7 ^a	AgBF ₄	<1	1
8 ^a	AgPF ₆	<1	<1
9 ^a	MOPiv ^d	<1	<1
10 ^a	M ₂ CO ₃ ^e	<9	<2

^aConditions: **1-OAc** (12.2 mg, 25 μmol , 1 equiv), additive (75 μmol , 3 equiv), C₆F₅H (0.2 mL, 1.8 mmol, 72 equiv), THF (0.025 M, 1 mL).; ^bConditions: **1-OAc** (12.2 mg, 25 μmol , 1 equiv), C₆F₅H (0.2 mL, 1.8 mmol, 72 equiv), THF (0.025 M, 1 mL).; ^cConditions: **1-OAc** (12.2 mg, 25 μmol , 1 equiv), Ag additive (37.5 μmol , 1.5 equiv), C₆F₅H (0.2 mL, 1.8 mmol, 72 equiv), THF (0.025 M, 1 mL); ^dM = Na, Li, Cs, Me₄N. ^eM = Na, Li, Cs

We probed the reactivity of other Ag salts in the activation of C₆F₅H with **1-OAc**. Other basic silver salts, Ag₂CO₃, AgOAc and AgOTFA, generated mixtures of products **2** and **3**, potentially as a result of decreased solubility compared to AgOPiv under these conditions. Interestingly, Ag₂O afforded comparable yields to that of AgOPiv despite its low solubility. Silver salts bearing less basic ligands (tetrafluoroborate and hexafluorophosphate) performed poorly in these reactions. Additionally, notable fluctuations in yield were observed from reactions conducted under ambient light, likely due to decomposition of Ag species formed during the reaction. Therefore, all reactions were conducted in the exclusion of light.

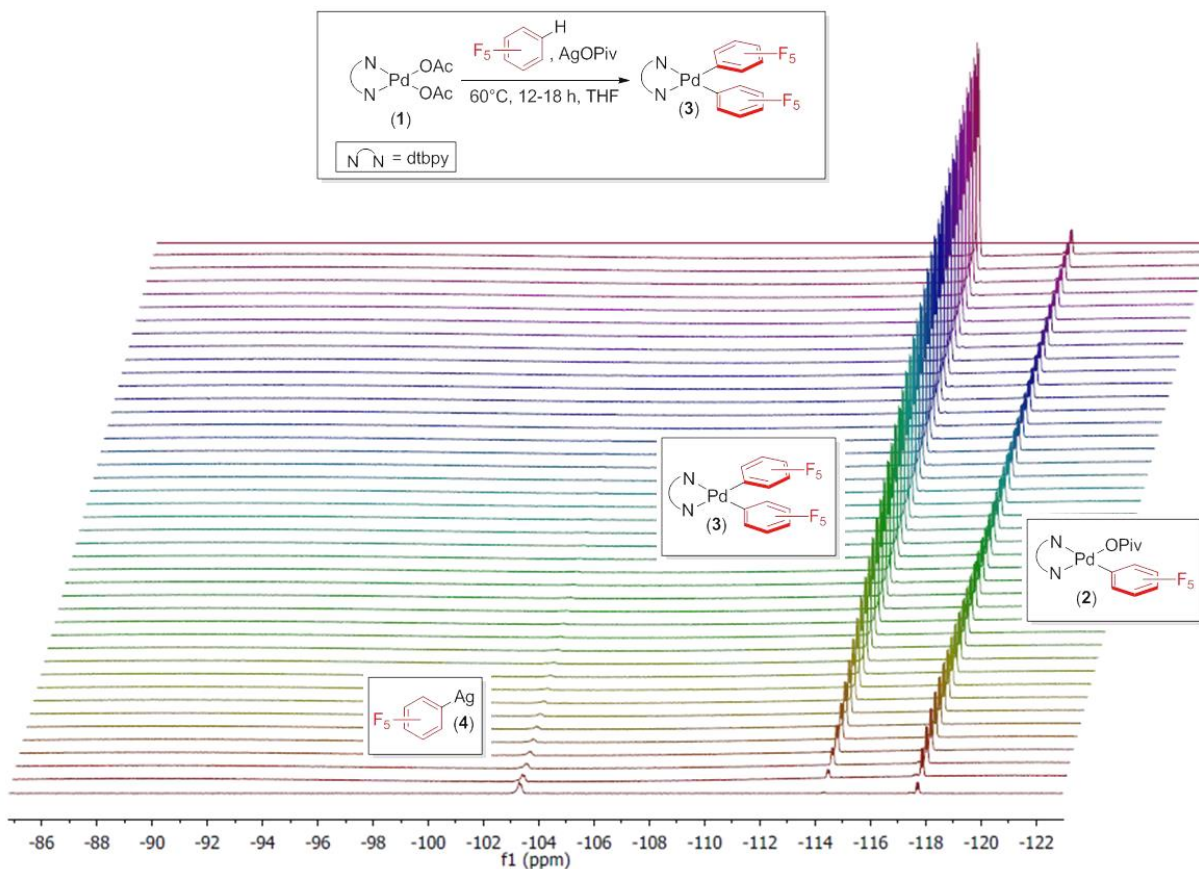
To examine the effect of bases in this reaction, the silver additive was replaced with pivalate and carbonate bases with varying solubilities. NaOPiv, LiOPiv, CsOPiv and Me₄NOPiv all afforded <1% of products **2** and **3** under otherwise similar conditions (Table 3.2, entry 9). Carbonate bases (Na₂CO₃, Li₂CO₃ and Cs₂CO₃) performed similarly, generating ≤2% of **3**. Collectively, these data suggest silver salts are required to form substantial yields of **3** from C₆F₅H and **1-OAc**.

Other Ag-promoted pathways shown in Scheme 3.2 (C–C coupling and reoxidation) can be ruled out, as the formation of **3** is a redox neutral process and reductive elimination does not occur under these conditions. Therefore, the silver additives are likely participating in the C–H activation step through either a bimetallic Pd-Ag intermediate or through Ag-arene formation. To distinguish between these two pathways, we focused on efforts to detect intermediates formed during the reaction.

Investigating the Intermediates in the Reaction

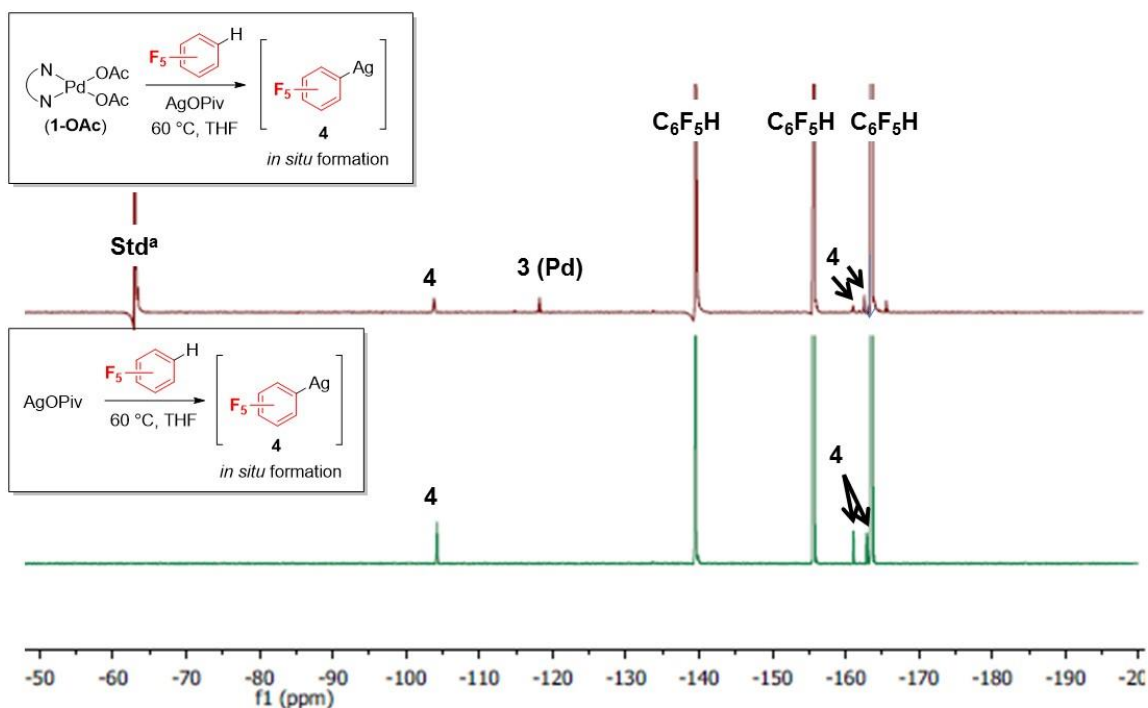
To detect the presence of transient intermediates, the reaction between **1-OAc**, C₆F₅H, and AgOPiv was monitored by ¹⁹F NMR spectroscopy. Formation of **2** was initially observed, followed by rapid formation of **3**. Over 18 h, **2** was completely consumed, presumably to form **3**. Interestingly, an intermediate (**4**) was observed at -103 ppm at the beginning of the reaction. Intermediate **4** was quickly consumed, with concomitant generation of palladium products **2** and **3** (Figure 3.1).

Figure 3.1. Monitoring the Reaction by ^{19}F NMR Spectroscopy



Based on prior reports of a Ag-aryl complex,^{21,22,24} we hypothesized **4** to be a Ag-arene species, generated by the activation of $\text{C}_6\text{F}_5\text{H}$ with AgOPiv . To probe the formation of this intermediate (**4**) via Ag-mediated activation, we also monitored the reaction in the absence of Pd. In the absence of light, the combination of $\text{C}_6\text{F}_5\text{H}$ and AgOPiv resulted in formation of intermediate **4**, with the diagnostic resonance at -103 ppm (Figure 3.2, bottom). When $\text{C}_6\text{F}_5\text{H}$ and CsOPiv were combined under analogous conditions, no new peaks were observed. These results suggest that **4** is not a Pd-containing intermediate.

Figure 3.2. Overlapping ^{19}F NMR Spectra for *In Situ* Observation of 4

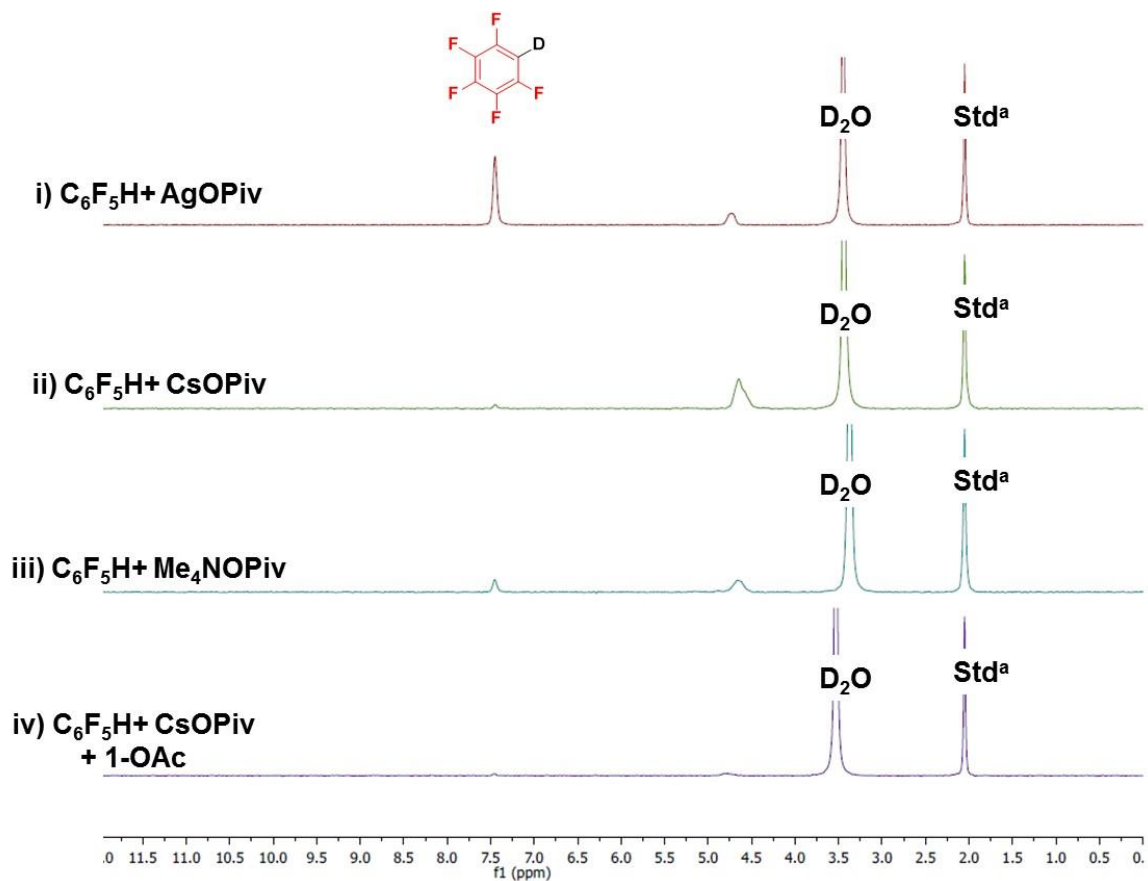


^aStd = α,α,α -trifluorotoluene

H/D Exchange Studies with $\text{C}_6\text{F}_5\text{H}$

Additional H/D exchange studies with $\text{C}_6\text{F}_5\text{H}$ and MOPiv were conducted to further study the mechanism of this transformation. To probe the activity of MOPiv in H/D exchange, palladium was excluded from the reaction. Excess D_2O was added to react with Ag-aryl intermediates, incorporating deuterium in pentafluorobenzene to allow the quantification of C–H activation by ^2H NMR spectroscopy. Treatment of a solution of $\text{C}_6\text{F}_5\text{H}$ (1 equiv) and 5 equiv of D_2O in THF with AgOPiv (0.04 equiv) resulted in 83% deuterium incorporation after 18 h at 60 °C (Figure 3.3, *i*). However, the analogous reactions with CsOPiv and Me_4NOpiv afforded only 3 and 11% deuterium incorporation, respectively (Figure 3.3, *ii* and *iii*). Shown in Figure 3.3 (*iv*), the addition of **1-OAc** to reactions with CsOPiv resulted in <2% deuterium incorporation, providing further evidence to suggest Pd does not directly participate in the C–H activation step. Collectively, these data support the key role of AgOPiv in activation of $\text{C}_6\text{F}_5\text{H}$, rather than base- or palladium-mediated pathways.

Figure 3.3. H/D Exchange Studies with C₆F₅H and Various MOPIV Sources

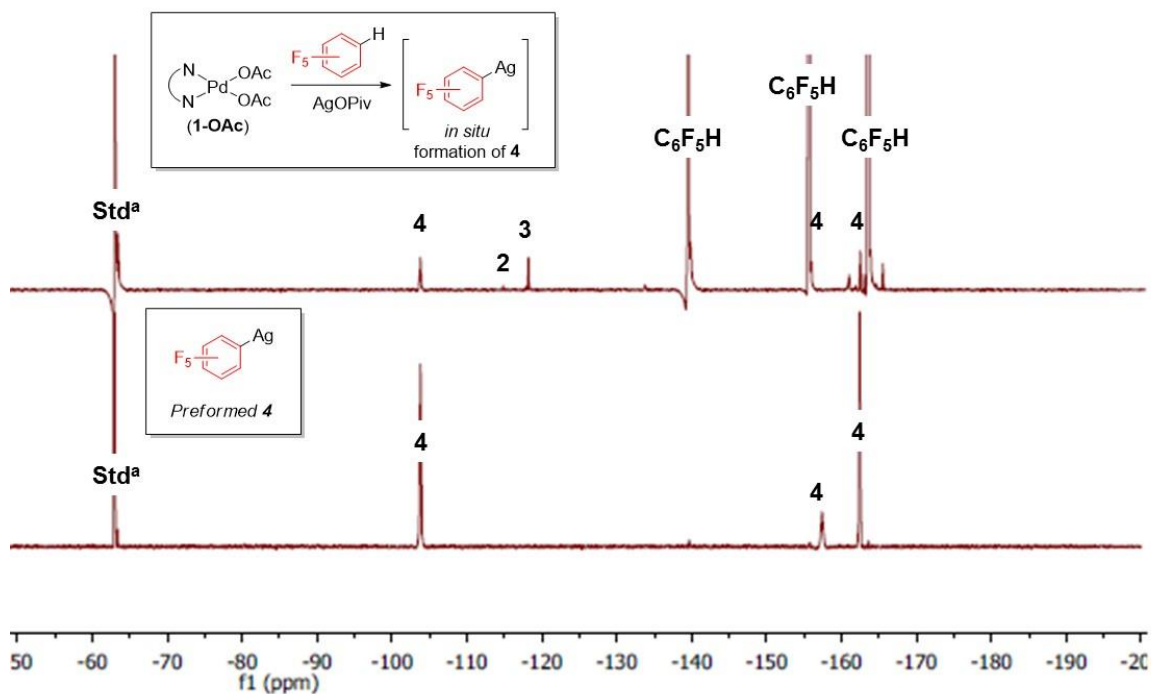


^aStd = *d*₆-acetone

Synthesis of an Authentic Ag-C₆F₅ (**4**)

To confirm the structure of **4**, Ag-C₆F₅ was independently synthesized and isolated from LiC₆F₅ and AgTFA according to a literature procedure.⁵³ As shown in Figure 3.4, the ¹⁹F NMR spectrum of the isolated Ag-C₆F₅ correlates to that of intermediate **4**. After 24 h in solution at 25 °C, **4** decomposes to a silver mirror and C₆F₅H, presumably due to protonation by adventitious water.

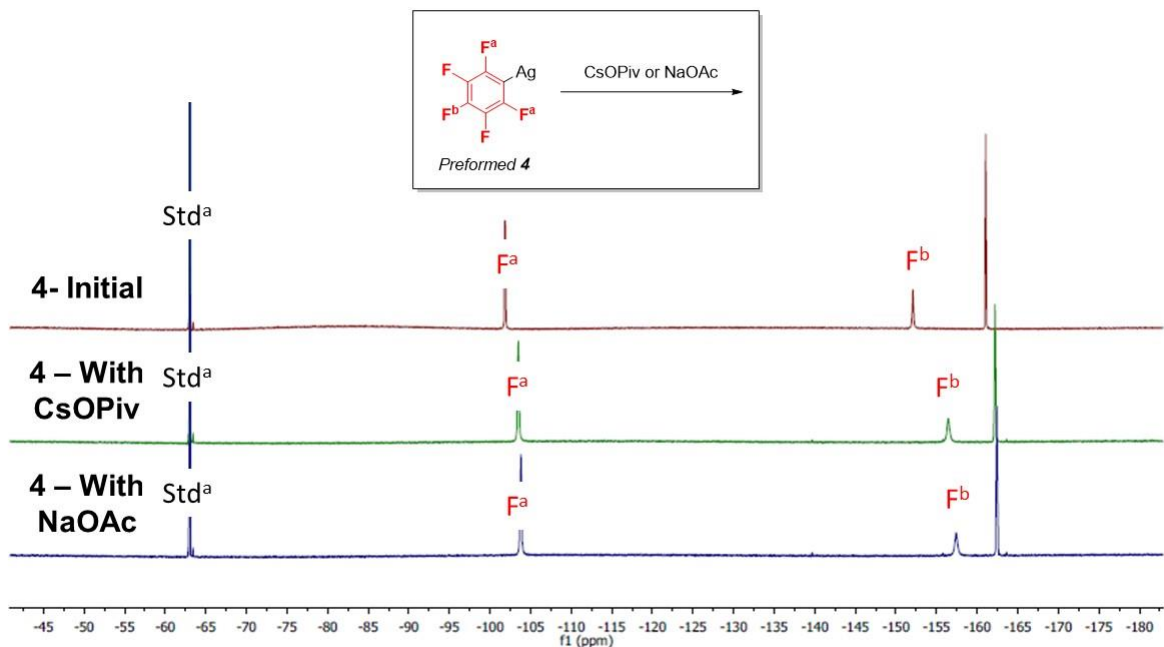
Figure 3.4. Comparison of *In Situ* Formation of **4 with Authentically Synthesized **4****



$^a\text{Std} = \alpha,\alpha,\alpha$ -trifluorotoluene

Notably, significant shifting of the resonances of **4** was observed by ^{19}F NMR spectroscopy, likely due to the presence of different ligands in solution. As the isolated $\text{Ag-C}_6\text{F}_5$ (**4**) was synthesized in acetonitrile, we proposed that weakly coordinated acetonitrile ligands are likely being displaced with pivalate or acetate anions during the reaction, resulting in shifts of the ^{19}F resonances for complex **4**. To probe our hypothesis, spectral data for authentic samples of complex **4** were collected upon addition of CsOPiv and NaOAc . Shifts in the ortho- and para- fluorine resonances from -101.83 and -152.09 ppm to -103.80 and -157.42 ppm were observed upon addition of these salts, shown in Figure 3.5. This fluxional ligand exchange accounts for slight differences in ^{19}F resonances for **4**, shown later in this chapter.

Figure 3.5. Observance of Shifting ^{19}F NMR Resonances in Isolated Ag Species (4) With Acetate and Pivalate Anions

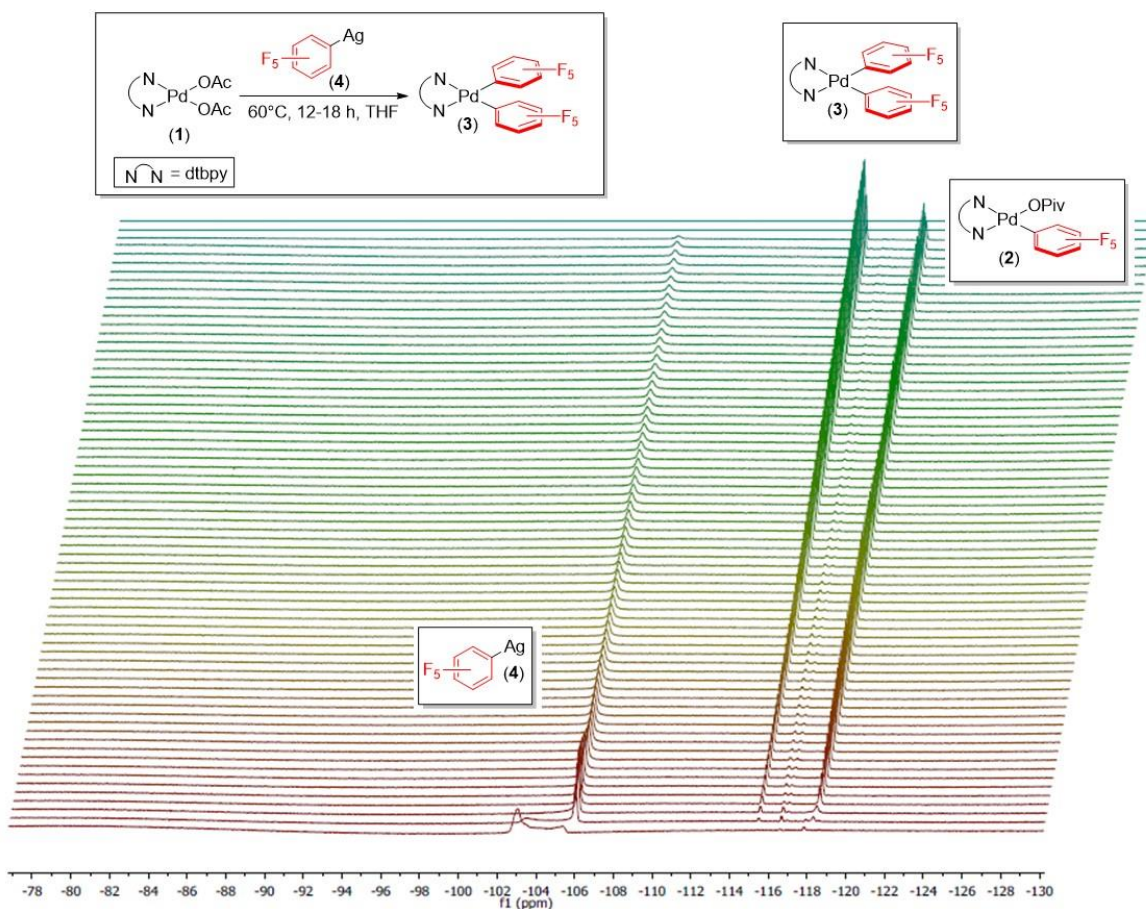


$^a\text{Std} = \alpha, \alpha, \alpha$ -trifluorotoluene

Reactivity of **1-OAc** with **4**

We next examined the reactivity of isolated **4** with palladium complex **1-OAc**. Upon treatment of **1-OAc** with 3 equiv of $\text{Ag-C}_6\text{F}_5$ (**4**), complex **3** was generated in 91% yield. Monitoring the reaction by ^{19}F NMR spectroscopy, we observed similar overall reactivity to that with $\text{AgOPiv}/\text{C}_6\text{F}_5\text{H}$, albeit much faster than the latter due to higher initial concentrations of **4** (Figure 3.6). Also, the broad signal between -102 and -107 ppm represents complex **4**, likely resulting from ligand exchange in the presence of acetate anions. This fluxional ligand exchange was further demonstrated in the previous section (Figure 3.5).

Figure 3.6. Monitoring the Reaction of 1-OAc with Preformed **4 by ^{19}F NMR**



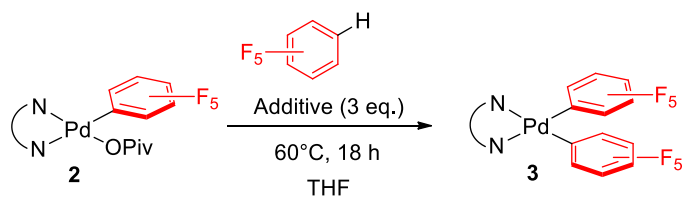
Collectively, these results provide strong evidence to support the role of AgOPiv in the activation of $\text{C}_6\text{F}_5\text{H}$, forming the Ag- C_6F_5 species **4**. We propose that the short-lived species **4** then undergoes transmetalation to Pd to generate **2** and **3**. A similar mechanism has been proposed by Nolan and coworkers in the Au-catalyzed carboxylation of 1,3,5-trifluorobenzene, proceeding through a similar Ag-arene intermediate followed by transmetalation to Au.²³ In addition, prior reports demonstrating Pd-catalyzed $\text{C}_6\text{F}_5\text{H}$ /arene cross-coupling reactions have suggested formation of a Ag- C_6F_5 intermediate.²² However, this is the first reported example of the direct observation of a Ag- C_6F_5 intermediate via C-H cleavage at Ag. This insight into the role of silver in arene activation could inform future studies in the catalytic arene C-H functionalization reactions.

Reactivity of Mono-aryl Complex **2**

As transmetalation between Ag-C₆F₅ (**4**) and palladium species **1-OAc** likely proceeds through mono-aryl intermediate **2**, further stoichiometric studies were conducted with palladium species **2**. We chose to conduct studies with the mono-aryl pivalate complex **2**, (dtbpy)Pd(C₆F₅)(OPiv), due to its enhanced solubility relative to the analogous acetate complex. Complex **2** was synthesized from (dtbpy)Pd(C₆F₅)(I) and AgOPiv, and it was characterized by ¹H, ¹³C, and ¹⁹F NMR spectroscopy. Modest decomposition was observed with **2** after 18 h in THF at 60°C, resulting in 60% of **2** and detectable amounts of palladium black and C₆F₅H. Despite the decreased stability, we proposed that the rate of conversion of **2** to **3** under the reactions conditions likely outcompetes alternate decomposition pathways to attain high yields of **3**.

Treatment of **2** with AgOPiv and C₆F₅H afforded **3** in 87% yield (Table 3.3, entry 1), comparable to overall conversion of **1-OAc** to **3** under analogous conditions. In the absence of AgOPiv, <1% of **3** was observed. Replacing AgOPiv with other pivalate bases, such as CsOPiv, resulted in trace amounts (<1%) of **3** (entry 3). Thus, we propose that a similar transmetalation with Ag-C₆F₅ occurs at **2**.

Table 3.3. Reactivity of Mono-Aryl Palladium Complex **2**

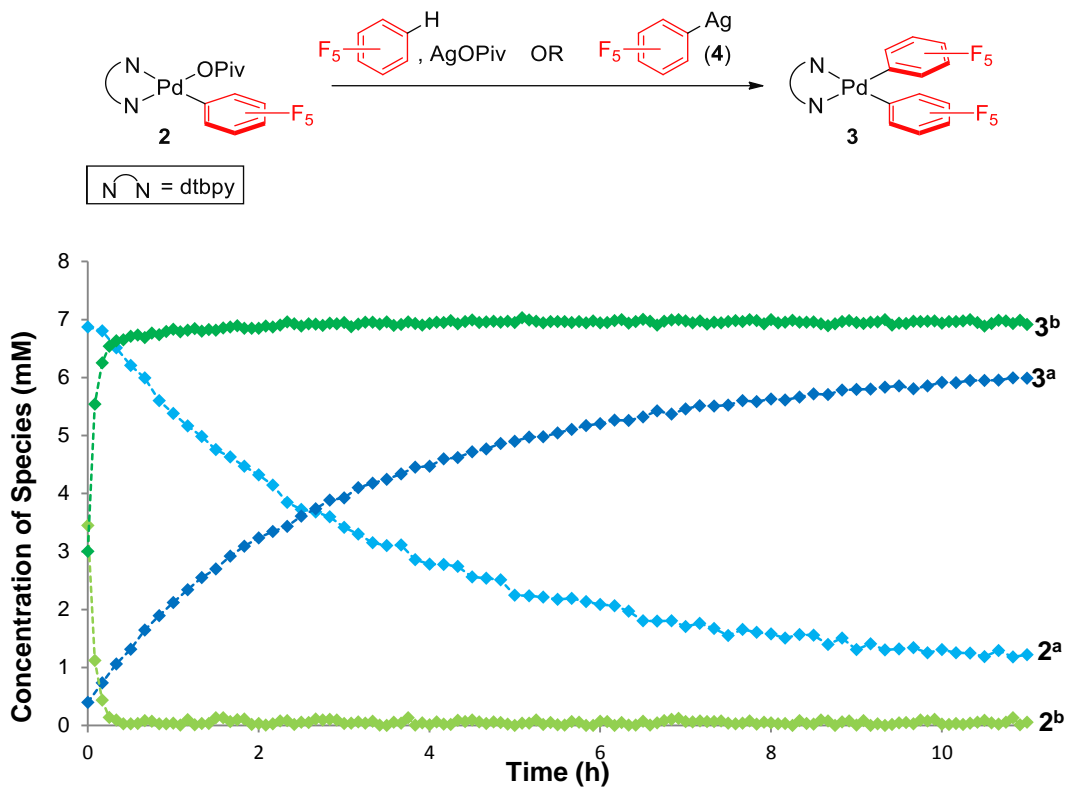


Entry	Additive	Equiv of C ₆ F ₅ H	% Yield of 3	% Remaining 2
1	AgOPiv	36 equiv	87	< 1
2	none	36 equiv	<1	77
3	CsOPiv	36 equiv	< 1	78
4	AgOPiv	none	5	70

To probe our hypothesis of transmetalation at mono-aryl species **2**, the reaction was monitored by ¹⁹F NMR spectroscopy to observe the formation of intermediate **4**. Intermediate **4** is detected upon treatment of **2** with C₆F₅H and AgOPiv, albeit in lower concentrations and with faster

consumption than reactions with **1-OAc**. Furthermore, the initial rates of formation of **3** (5.3×10^{-5} mM/sec) and consumption of **2** (-5.4×10^{-5} mM/sec) were similar, further supporting the conversion of **2** to **3**. To gain additional insight into the involvement of intermediate **4**, complex **2** was treated with 2 equiv of isolated Ag-C₆F₅ (**4**). This reaction rapidly formed **3** within 2 h. (Figure 3.7). Collectively, our studies support a pathway proceeding via initial formation of **2**, by a Ag-promoted activation of C₆F₅H, followed by a second Ag-C₆F₅ (**4**) transmetalation at **2** to generate **3**.

Figure 3.7. Reactivity of 4 with AgOPiv/C₆F₅H or Preformed Ag-Arene 5

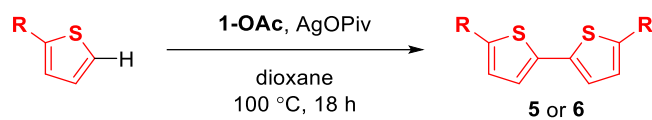


Stoichiometric studies of well-defined Pd^{II} complexes have provided evidence to support a non-oxidative role for Ag in C–H activation of C₆F₅H. This mechanistic insight for the role of silver in C–H activation reactions could have important implications for catalytic C–H functionalization reactions with Pd. However, using this model system, catalytic studies are not feasible due to the high stability of the resulting palladium complex **3**. Thus, we chose to study a more catalytically relevant system using thiophenes as substrates. We specifically chose 2-substituted thiophenes in order to block one site from C–H activation, hindering the formation of higher oligomers and

simplifying product analysis. Thiophenes have been widely demonstrated as substrates for Pd-catalyzed C–H functionalization reactions, and these transformations are generally proposed to proceed through Pd-mediated C-H activation.^{21,27,28,30,40,54–58} In addition, many of these reports require silver salts to enhance reactivity.^{21,27,28,30,40,54–58} Thus, we chose to study the catalytic dimerization of 2-substituted thiophenes to better understand the role of silver carboxylates in catalysis.

Moving Towards Catalysis: Stoichiometric Thiophene Coupling

Initial studies with 2-substituted thiophenes (2-methyl and 2-trifluoromethyl Thiophene) were conducted using conditions analogous to those used in the stoichiometric studies with C₆F₅H (see on p. 87). In these studies, we observed similar trends in reactivity as stoichiometric studies with C₆F₅H, suggesting a similar dependence on AgOPiv. We next sought to demonstrate the catalytic application with thiophene substrates. Thus, we optimized our reaction using conditions resembling previously published catalytic conditions,^{27,28,57} by decreasing the catalyst loadings and increasing the reaction temperature. Treatment of 2-methyl thiophene with AgOPiv and **1-OAc** (10 mol%) in dioxane at 100 °C afforded **5** in 53% yield after 18 h (Table 3.4, entry 1). Other silver salts yielded diminished amounts of **5** under otherwise analogous conditions (entries 2-5). In the presence of other pivalate bases, no coupled product was detected, shown in Table 3.4 (entry 6). Under identical conditions, 60% of the dimer **6** was generated from 2-trifluoromethyl thiophene (entry 8), with no product **6** formed using CsOPiv (entry 10). We also probed the dimerization of 2-substituted thiophenes using the commercially available Pd(OAc)₂ trimer as the catalysts, since this is commonly utilized in C-H functionalization reactions with thiophene substrates.^{21,29,49} Interestingly, diminished yields of dimerized products **5** and **6** were observed with Pd(OAc)₂ under otherwise analogous conditions, demonstrating the utility of **1-OAc** in these transformations (Table 3.4, entries 7,11). Since the trends in reactivity are similar to that of our studies with C₆F₅H, we propose a similar mechanism involving activation of thiophene via Ag-mediated activation.

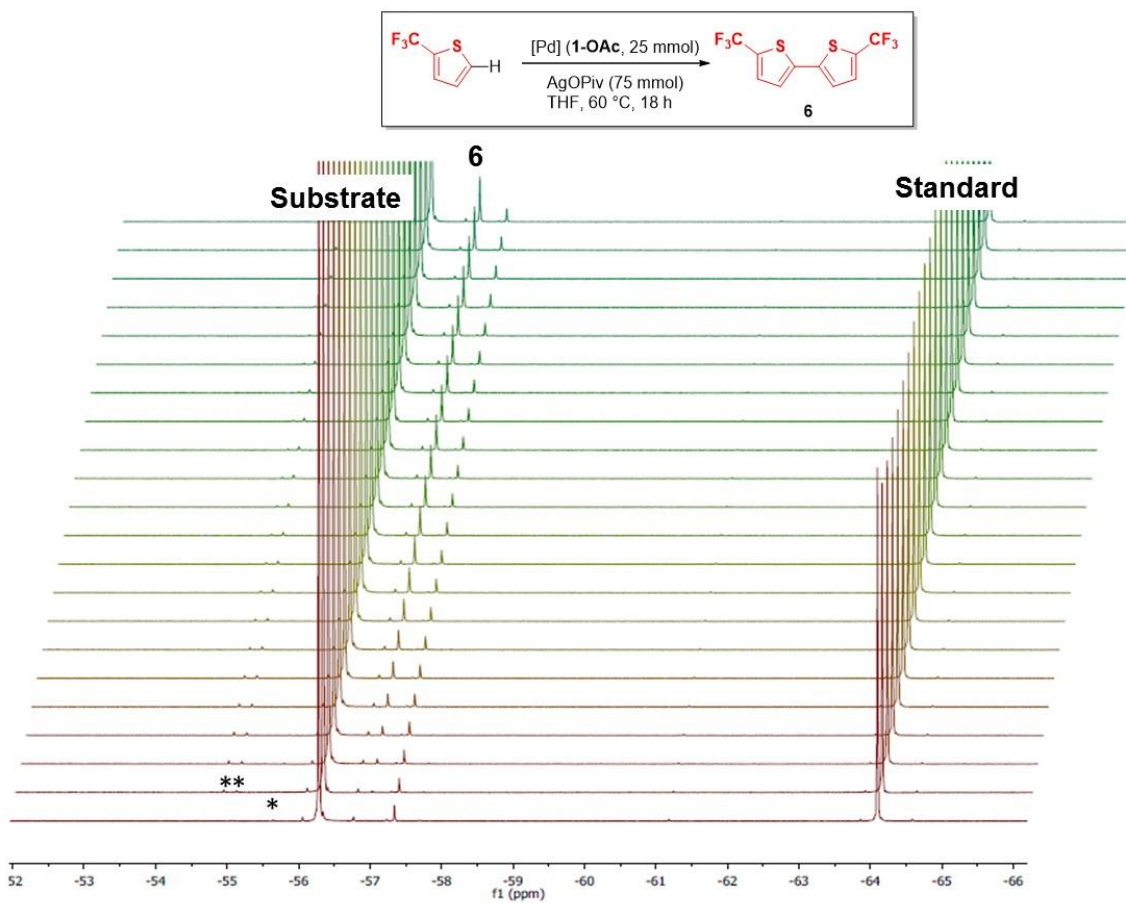
Table 3.4. Dimerization of Thiophenes Under Optimized Conditions^a

Entry	R =	Additive	% Yield of Dimer 5 or 6
1	CH ₃	AgOPiv	53
2	CH ₃	AgOAc	8
3	CH ₃	Ag ₂ CO ₃	12
4	CH ₃	Ag ₂ O	16
5	CH ₃	AgPF ₆	<1
6	CH ₃	MOPiv ^b	<1
7	CH ₃	AgOPiv, Pd(OAc) ₂ ^c	28
8	CF ₃	AgOPiv	60
9	CF ₃	CsOPiv	<1
10	CF ₃	AgOPiv, Pd(OAc) ₂ ^c	38

^aConditions: thiophene (1 mmol, 3.3 equiv based on oxidant), additive (300 mmol, 1 equiv), **1-OAc** (15 μ mol, 10 mol%), dioxane (1 M), 100 $^\circ$ C, 18h; ^bM = Na, Li, Cs, Me₄N; ^cWith Pd(OAc)₂ instead of **1-OAc**.

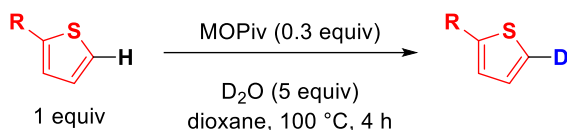
To further probe our mechanistic hypothesis, *in situ* NMR experiments were performed with 2-trifluoromethyl thiophene using ¹⁹F NMR spectroscopy to facilitate the detection of small concentrations of transient intermediates. At 60 $^\circ$ C, several unknown intermediates were observed by ¹⁹F NMR spectroscopy, denoted by asterisks in Figure 3.8, along with rapid product formation. However, attempts to further characterize these intermediates by *in situ* NMR experiments proved unsuccessful. Additionally, we were unable to synthesize a Ag-thiophene intermediate in a similar route as Ag-C₆F₅, likely due to the instability of the more electron-rich thiophene-Ag species.

Figure 3.8. ^{19}F NMR Experiment of Dimerization of 2-Trifluoromethyl Thiophene



Std = α,α,α -trifluorotoluene

To further probe the mechanism of the C–H activation step, we performed a series of H/D exchange experiments with both 2-methyl thiophene and 2-trifluoromethyl thiophene. Addition of D_2O (5 equiv) to the reaction of the thiophene substrate (1 equiv) and AgOPiv resulted in 26 and 13% deuterium incorporation for 2-methyl thiophene and 2-trifluoromethylthiophene, respectively. The analogous reaction with other MOPiv sources resulted in only trace amounts of deuterium incorporation for both substrates, seen in Table 3.7 (entries 2, 3, 6). Interestingly, using a pivalate base in the presence of our palladium complex (**1-OAc**) also resulted in <1% deuterium incorporation in 2-methyl thiophene. Collectively, these data suggest C–H activation is occurring at Ag, potentially through a Ag intermediate similar to **4**.

Table 3.5. Deuterium Incorporation of 2-substituted Thiophenes

Entry	X =	MOPiv	Pd Source	% Yield of Dimer
1	CH ₃	Ag	none	20
2	CH ₃	Cs	none	<1
3	CH ₃	Me ₄ N	none	6
4	CH ₃	Cs	1-OAc ^a	1
5	CF ₃	Ag	none	13
6	CF ₃	Cs	none	<1

^aWith addition of **1-OAc** (7.4 mgs, 10 mol%) to the reactions conditions.

Conclusions

Herein, we have demonstrated the role of silver in the activation of pentafluorobenzene with Pd^{II} complexes. Based on our *in situ* NMR experiments and rate studies, we propose this transformation proceeds via: (1) activation of C₆F₅H by AgOPiv followed by (2) transmetalation at **1-OAc** to generate organometallic intermediate **2**, and finally (3) a second transmetalation at **2** to generate **3**. Furthermore, we have been able to demonstrate the first example of *in situ* formation of Ag-C₆F₅ upon C–H activation of C₆F₅H.

We have extended these stoichiometric studies with C₆F₅H to a catalytic studies with thiophenes. Interestingly, activation of similar substrates has been widely proposed to occur at the Pd center, employing silver salts as a terminal oxidant.^{27,30,57} Under our conditions, silver salts are also likely to facilitate the reoxidation of Pd, as substoichiometric amounts of palladium were used in our catalytic studies. However, we provide evidence to support an additional non-oxidative role of Ag. Based on H/D exchange experiments with thiophenes and analogous work with the C₆F₅H system, we propose a similar mechanism involving Ag-mediated activation of thiophene and subsequent transmetalation at Pd.

Although C₆F₅H and thiophene are much more reactive towards C–H activation than CH₄, we envision applying these conditions with analogous Ag and Pd complexes to future catalytic

reactions with CH₄. Interestingly, a number of different homogeneous metal species have been employed in the activation and/or functionalization of methane. As mentioned in Chapter 1, Pd and Pt have been utilized in the partial oxidation of methane to afford methanol.⁵⁹⁻⁶¹ However, this reactivity is not limited to group 10 metals. For example, methane functionalization has also been demonstrated with group 11 and 12 metals Au,⁶² Hg,⁶⁰ and Tl.⁶³ Future studies aimed at determining the viability of this approach will be pursued in our efforts to oligomerize methane.

General Experimental Procedures and Characterization of Data

General Instrumentation.

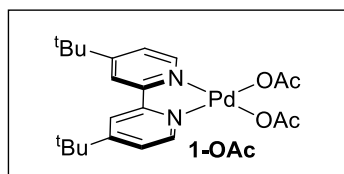
NMR spectra were obtained on Varian vnmrs 700 (699.76 MHz for ¹H; 175.95 MHz for ¹³C), Varian vnmrs 500 (500.1 MHz for ¹H; 125.75 MHz for ¹³C; 470.56 MHz for ¹⁹F), Varian MR 400 (400.52 MHz for ¹H; 125.70 MHz for ¹³C; 376.87 MHz for ¹⁹F) or Varian Inova 500 (499.90 MHz for ¹H) spectrometers. ¹H, ¹³C and ¹⁹F chemical shifts are reported in parts per million (ppm) relative to the referenced solvent peak. Multiplicities are reported as singlet (s), doublet (d), triplet (t), quartet (q), doublet of doublets (dd) and multiplet (m). ¹⁹F NMR yields were reported based on the internal standard α,α,α -trifluorotoluene using the following acquisition parameters for NMR spectroscopic analysis: scans = 8, acquisition time = 5 s, steady state scan = 0, and relaxation delay = 10 s. ²H NMR yields were reported based on the internal standard acetone-*d*₆, using a 10 s relaxation delay. Gas chromatography was carried out on a Shimadzu 17A using a Restek Rtx®-5 (Crossbond 5% diphenyl/95% dimethyl polysiloxane; 15 m, 0.25 mm ID, 0.25 μ m df) column. GC calibrated yields are reported relative to neopentyl benzene as an internal standard. All stock solutions were made using volumetric glassware. All reactions and synthesis of metal complexes were run in air, except the synthesis of the Ag-C₆F₅ species (**4**) and any NMR array reactions with **4**, which were conducted in a glove box under an atmosphere of N₂.

Materials and Methods

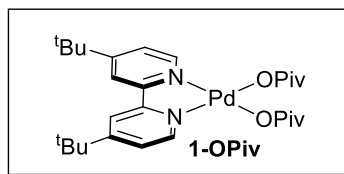
THF, CH₂Cl₂, diethyl ether and pentanes were obtained from Fisher Scientific or VWR. Dry THF was dispensed from an Innovative Technologies solvent purification system using columns packed with activated alumina, copper catalyst, and molecular sieves. Anhydrous acetonitrile and 1,4-dioxane were obtained from Alfa Aesar. All deuterated solvents were obtained from Cambridge Isotope Laboratories and used without further purification. Cesium carbonate

(Aldrich), cesium pivalate (Aldrich), 5,5'-dimethyl-2,2'-dithiophene (Acros), 4,4'-di-*tert*-butyl-2,2'-bipyridine (Aldrich), lithium carbonate (Aldrich), 2-methyl thiophene (Acros), *n*-butyl lithium (Acros), neopentyl benzene (Alfa Aesar), Palladium acetate (Pressure Chemical), palladium chloride (Pressure), palladium pivalate (Aldrich), palladium trifluoroacetate (Strem), pentafluorobenzene (Oakwood), pentafluorophenyl iodide (Matrix), silver tetrafluoroborate (TCI), silver oxide (Acros), silver acetate (Aldrich), silver trifluoroacetate (Acros), sodium carbonate (Alfa Aesar), sodium pivalate (Acros), 2-trifluoromethyl thiophene (Oakwood), α,α,α -trifluorotoluene (TCI), tris(dibenzylideneacetone) dipalladium (Oakwood) were obtained from commercial vendors and used without further purification. (dtbpy)PdCl₂⁶⁴, silver pivalate⁶⁵, tetramethylammonium pivalate⁶⁶, lithium pivalate⁶⁷ and silver carbonate⁶⁸ were prepared based on literature procedure.

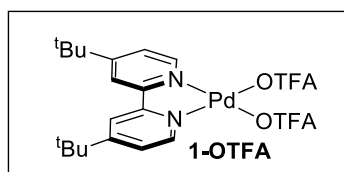
Synthesis and Characterization of Palladium Complexes and Other Compounds



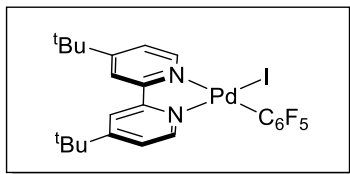
(dtbpy)Pd^{II}(OAc)₂ (1). Combined commercially available palladium acetate (500 mgs, 2.22 mmol, 1 equiv), 4,4'-di-*tert*-butyl-2,2'-bipyridine (708 mgs, 2.64 mmol, 1.2 equiv), acetic acid (2 drops) in acetone (10 mL) and stirred with a Teflon stirbar for 18 h at 25 °C. A yellow precipitate formed over the course of the reaction. Pentanes were added and the pale yellow precipitate was collected on a glass frit. The solid was dried under vacuum to afford the product as a pale yellow powder (897 mg, 82% yield). ¹H NMR (500.10 MHz, 298 K, DMSO-*d*₆): δ 8.58 (d, *J* = 2 Hz, 2 H), 8.02 (d, *J* = 6 Hz, 2 H), 7.76 (dd, *J* = 6, 2 Hz, 2 H), 1.89 (s, 6 H), 1.40 (s, 18 H). ¹³C NMR (175.95 MHz, 298 K, DMSO-*d*₆): 175.51, 165.27, 155.09, 148.99, 124.00, 120.94, 35.85, 29.86, 23.58. Elemental Analysis: calculated for C₂₂H₃₀N₂O₄Pd, C: 53.61, H: 6.13, N: 5.68; Found: C: 53.42, H: 6.04, N: 5.77.



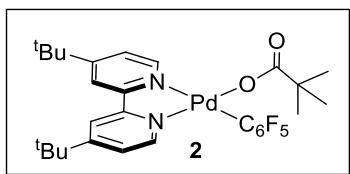
(dtbpy)Pd^{II}(OPiv)₂ (1-OPiv). Dissolved commercially available palladium pivalate (350 mgs, 1.1 mmol, 1 equiv) and 4,4'-di-*tert*-butyl-2,2'-bipyridine (307 mgs, 1.14 mmol, 1.01 equiv) in acetone (10 mL) and stirred with a Teflon stirbar for 18 h at 25 °C. The yellow solution was concentrated to 0.5 mL. Pentanes (15 mL) were added and to yellow solution and yellow crystals formed over 24 h at 25 °C. The yellow crystalline solid was collected on a glass frit. The solid was dried under vacuum to afford the product as a pale yellow powder (461 mg, 73% yield). ¹H NMR (400.53 MHz, 298 K, acetone-*d*₆): δ 8.59 (d, J = 2 Hz, 2 H), 8.09 (d, J = 6 Hz, 2 H), 7.76 (dd, J = 6, 2 Hz, 2 H), 1.45 (s, 18 H), 1.14 (s, 18 H). ¹³C NMR (175.95 MHz, 298 K, DMSO-*d*₆): 182.59, 165.17, 154.99, 148.62, 124.18, 120.88, 38.49, 35.88, 29.87, 28.37.



(dtbpy)Pd^{II}(OTFA)₂ (1-OTFA). Dissolved commercially available palladium trifluoroacetate (200 mgs, 0.6 mmol, 1 equiv) and 4,4'-di-*tert*-butyl-2,2'-bipyridine (177 mgs, 0.66 mmol, 1.1 equiv) in acetone (10 mL) and stirred with a Teflon stirbar for 18 h at 25 °C. Decolorizing charcoal was added, stirred for 1 h, and filtered over Celite® to remove Pd⁰. The filtrate was concentrated to 0.5 mL. Pentanes (15 mL) were added at 25 °C and a solid precipitated. The solid was collected on a glass frit and dried under vacuum for 2 h to afford the product as a pale yellow powder (422 mg, quantitative conversion). ¹H NMR (500.10 MHz, 298 K, acetone-*d*₆): δ 8.69 (d, J = 2 Hz, 2 H), 7.98 (d, J = 6 Hz, 2 H), 7.87 (dd, J = 6, 2 Hz, 2 H), 1.46 (s, 18 H). ¹³C NMR (175.95 MHz, 298 K, acetone-*d*₆): 167.27, 162.65 (q, J = 36 Hz), 157.62, 150.16, 126.05, 122.91, 116.45 (q, 290 Hz), 37.39, 30.85. ¹⁹F NMR (470.51 MHz, 298K, acetone-*d*₆): δ -74.93 (s, 6 F).

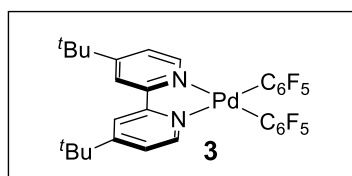


(dtbpy)Pd^{II}(C₆F₅)(I) (1). Combined commercially available tris(dibenzylideneacetone) dipalladium(0) (150 mgs, 0.45 mmol, 1 equiv) and 4,4'-di-*tert*-butyl-2,2'-bipyridine (180 mgs, 0.67 mmol, 3 equiv) in tetrahydrofuran (10 mL) and stirred with a Teflon stirbar for 30 m at 60 °C in foil-wrapped vial. Pentafluorophenyl iodide (120 μL, 0.9 mmol, 4 equiv) was then added and the reaction was stirred at 60 °C for 12 h. The reaction was then filtered through a plug of Celite® and the solvent was removed under vacuum. The resulting red-orange residue was recrystallized by vapor diffusion in dichloromethane: pentanes (1:10) to yield red-orange needles. ¹H NMR (400.52 MHz, 298 K, acetone-*d*₆): δ 9.58 (d, *J* = 6 Hz, 1H), 8.65 (d, *J* = 2 Hz, 2H), 7.82 (dd, *J* = 6 Hz, 2 Hz, 1H), 7.78 (d, *J* = 6 Hz, 1H), 7.64 (dd, *J* = 6 Hz, 2 Hz, 1H), 1.47 (s, 9H), 1.43 (s, 9H). ¹³C NMR (175.95 MHz, 298 K, acetone-*d*₆): 165.87, 165.70, 157.35, 156.12, 153.77, 150.80, 125.47, 125.23, 121.82, 121.37, 36.54, 36.51, 30.40, 30.26 (note: the pentafluorophenyl carbons are not reports as these were not fully relaxed after 12 h). ¹⁹F NMR (376.84 MHz, 298K, acetone-*d*₆): δ -116.27 (m, 2 F), -162.94 (t, *J* = 19 Hz, 1 F), -165.60 (m, 2 F).

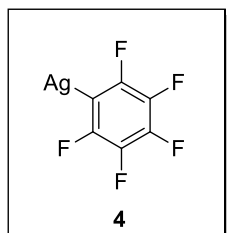


(dtbpy)Pd^{II}(C₆F₅)(OPiv) (2). (dtbpy)Pd^{II}(C₆F₅)(I) (135 mgs, 0.2 mmol, 1 equiv) was dissolved in acetone (10 mL) and AgOPiv (42 mgs, 0.2 mmol, 1 equiv) and a Teflon stirbar were added to the reaction vial. The reaction was wrapped in foil and stirred at 25 °C for 1-2 h. The resulting yellow-gray solution was filtered through a plug of Celite® and concentrated under reduced pressure. The pale yellow residue was dissolved in dichloromethane (5 mL) and stirred with decolorizing charcoal, filtered over Celite® and the filtrate was again concentrated under reduced pressure. The solid was then dissolved in dichloromethane (2 mL) and pentanes were added to

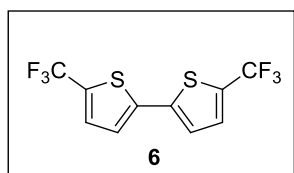
precipitate out the product. A pale yellow solid was collected on a glass frit, (157 mg, 50.6% yield). ^1H NMR (699.76 MHz, 298 K, acetone- d_6): δ 8.63 (d, $J = 2$ Hz, 1H), 8.62 (d, $J = 2$ Hz, 1H), 8.37 (d, $J = 6$ Hz, 1H), 8.03 (d, $J = 6$ Hz, 1H), 7.88 (dd, $J = 6, 2$ Hz, 1H), 7.57 (dd, $J = 6, 2$ Hz, 1H), 1.47 (s, 9H), 1.42 (s, 9H), 1.01 (s, 9H). ^{13}C NMR (175.95 MHz, 298 K, acetone- d_6): δ 183.34, 166.65, 166.21, 158.04, 155.79, 154.21, 149.11, 125.73, 125.41, 122.34, 121.47, 40.34, 37.16, 37.04, 31.00, 30.81, 29.49 (pentafluorophenyl carbons not fully relaxed after 18h). ^{19}F NMR (376.84 MHz, 298K, acetone- d_6): δ -118.96 (m, 2F), -163.92 (t, $J = 19$ Hz, 1F), -166.19 (m, 2F).



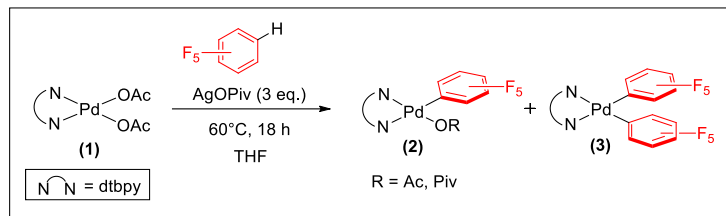
(dtbpy)Pd^{II}(C₆F₅)₂ (3). The (cyclooctadiene)Pd^{II}(C₆F₅)₂ complex (200 mgs, 0.42 mmol, 1 equiv) was dissolved in dichloromethane (10 mL) and 4,4'-di-*tert*-butyl-2,2'-bipyridine (134 mgs, 0.5 mmol, 1.2 equiv) and a Teflon stirbar were added. The reaction was stirred at 25 °C for 1 h, and then pentanes (10 mL) were added and the reaction was cooled to -30 °C for 18h to precipitate out the product. Recrystallization in dichloromethane: pentanes yielded 149 mgs of a white, crystalline solid (50 % conversion). ^1H NMR (699.76 MHz, 298 K, acetone- d_6): δ 8.69 (d, $J = 2$ Hz, 2H), 7.99 (d, $J = 6$ Hz, 2H), 7.66 (dd, $J = 6, 2$ Hz, 2H), 1.44 (s, 18H). ^{13}C NMR (175.95 MHz, 298 K, acetone- d_6): δ 165.96, 156.57, 151.30, 148.50 (dd, $J = 227, 22$ Hz), 137.44 (m), 125.27, 121.62, 118.83 (t, $J = 53$ Hz), 36.61, 30.47. ^{19}F NMR (376.84 MHz, 298K, acetone- d_6): δ -115.74 (m, 4 F), -163.21 (t, $J = 20$ Hz, 2 F), -165.32 (m, 4 F).



Silver-pentafluorophenyl species (4). Complex **4** was prepared using a literature procedure.⁵³ The ¹H NMR spectroscopic data for this complex matched that reported in the literature. ¹³C NMR (175.95 MHz, 298 K, acetone-*d*₆): δ 152.75 (dd, *J* = 230, 27 Hz), 142.86 (d, *J* = 251 Hz), 138.70 – 135.76 (m), 109.27 (t, *J* = 73 Hz). ¹⁹F NMR (376.84 MHz, 298K, acetone- *d*₆): δ -102.16 – -102.58 (m), -152.16 (t, *J* = 19 Hz), -161.82 – -162.19 (m).

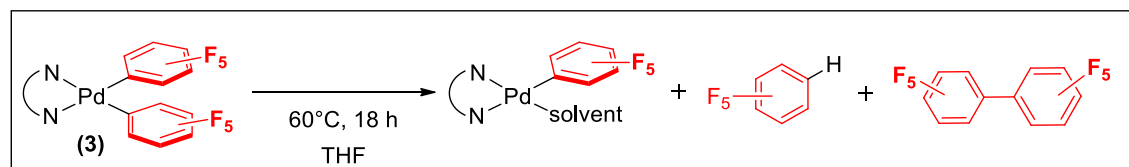


5,5'-bis(trifluoromethyl)-2,2'-bithiophene (6). Combined previously reported (PhCN)₂PdCl₂ (29 mg, 0.075 mmol)⁶⁹, potassium fluoride (145.5 mg, 2.5 mmol, 2 equiv) and silver nitrate (424.5 mg, 2.5 mmol, 2 equiv) and added 2-trifluoromethyl thiophene (141 μL, 1.25 mmol, 1 equiv), dimethyl sulfoxide (8 mL) and a Teflon stirbar. Stirred the reaction at 25 °C for 20 h and then added more potassium fluoride (145.5 mg, 2.5 mmol, 2 equiv), (PhCN)₂PdCl₂ (29 mg, 0.075 mmol), and silver nitrate (424.5 mg, 2.5 mmol, 2 equiv). Continued stirring at 25 °C for 24 h and then filtered over a plug of Celite® and washed plug with diethyl ether (2 x 20 mL). Washed the filtrate with distilled water (2 x 20 mL), dried with Mg₂SO₄ and evaporated solvent under reduced pressure. Obtained pale yellow crystals (125.2 mgs, 66.4 %) upon evaporation. ¹H NMR (699.76 MHz, 298 K, acetone-*d*₆): δ 7.67 (d, *J* = 4 Hz, 2H), 7.53 (d, *J* = 4 Hz, 2H). ¹³C NMR (175.95 MHz, 298 K, acetone-*d*₆): δ 140.27, 131.76, 131.12 (q, *J* = 39 Hz), 126.91, 123.42 (q, *J* = 268 Hz). ¹⁹F NMR (376.84 MHz, 298K, acetone- *d*₆): δ -56.19 (s, 6 F).



Representative Procedure for Stoichiometric $\text{C}_6\text{F}_5\text{H}$ Activation with **1-OAc**

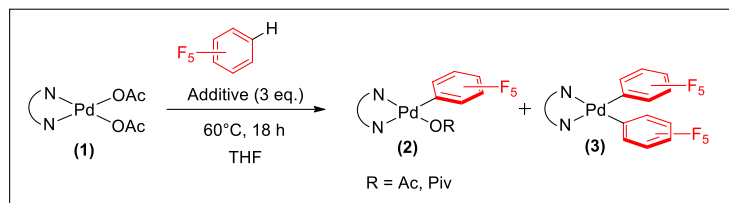
In air, Pd^{II} complex **1-OAc** (12.3 mg, 25 μmol , 1 equiv) and AgOPiv (15.6 mg, 75 μmol , 3 equiv) were weighed into a 4 mL vial. THF (1 mL, 0.025 M), $\text{C}_6\text{F}_5\text{H}$ (0.2 mL, 1.8 mmol, 72 equiv), and a Teflon stirbar were added to the vial. The reaction was stirred at 60°C for 18h, in the exclusion of light. The slurry was cooled and filtered over Celite® to remove solids. The filtrate was concentrated under reduced pressure to remove unreacted substrate. The residue was then dissolved in THF (0.5 mL) and α,α,α -trifluorotoluene (20 μL of a 0.41 mM solution in THF) was added as an internal standard. ^{19}F NMR spectrum was acquired at 25°C to determine the integration ratio of the standard to Pd^{II} product.



Thermolysis Studies of **3**

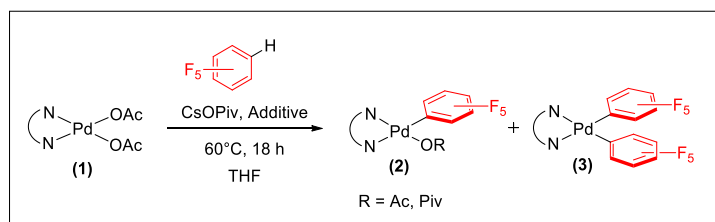
In air, the bis-aryl Pd^{II} complex **3** (15 mg, 21 μmol , 1 equiv) was added to a screw-cap NMR tube with $\text{C}_6\text{F}_5\text{H}$ (0.2 mL, 1.8 mmol, 72 equiv), α,α,α -trifluorotoluene (20 μL of a 0.41 mM solution in THF) as a standard, and THF (1 mL, 0.021 M). The tube was kept at 25°C for 24 h and a ^{19}F NMR spectrum was acquired at 25°C to determine the integration ratio of the standard to **3**. The tube remained at 25°C for an additional 16 h and a second ^{19}F NMR spectrum was acquired at 25°C . No decomposition was observed. The tube was then heated at 100°C for 3 d and another ^{19}F NMR spectrum was acquired at 25°C . No decomposition was observed and the integration ratios between **3** and standard remained the same. The tube was heated an additional 2

d at 100 °C and a final ^{19}F NMR spectrum was acquired at 25 °C. Similar ratios between standard and **3** were observed.



General Procedure for Experiments with Various Silver Salts or Pivalate Bases

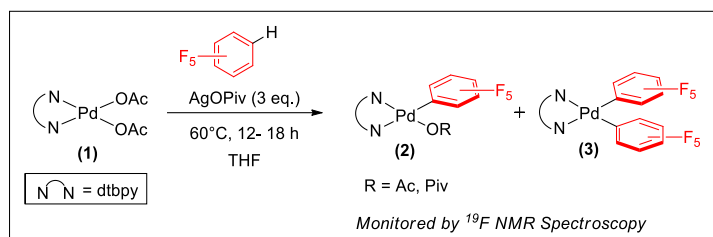
In air, the Pd^{II} complex **1-OAc** (12.3 mg, 25 μmol , 1 equiv) and additive (75 μmol , 3 equiv) were weighed into a 4 mL vial. THF (1 mL, 0.025 M), C₆F₅H (0.2 mL, 1.8 mmol, 72 equiv), and a Teflon stirbar were added to the vial. The reaction was stirred at 60 °C for 18h, in the exclusion of light. The slurry was cooled and filtered over Celite® to remove solids. The filtrate was concentrated under reduced pressure to remove excess substrate. The residue was then dissolved in THF (0.5 mL) and α,α,α -trifluorotoluene (20 μL of a 0.41 mM solution in THF) was added as an internal standard. ^{19}F NMR spectrum was acquired at 25 °C to determine the integration ratio of the standard to the Pd^{II} product. All reactions were performed in triplicate.



General Procedure for Experiments with Lewis Acids

In air, the Pd^{II} complex **1-OAc** (12.3 mg, 25 μmol , 1 equiv), CsOPiv (17.5 mg, 75 μmol , 3 equiv), and lewis acid additive (50 μmol , 2 equiv) were weighed into a 4 mL vial. THF (1 mL, 0.025 M), C₆F₅H (0.2 mL, 1.8 mmol, 72 equiv), and a Teflon stirbar were added to the vial. The reaction was covered with aluminum foil and stirred at 60 °C for 18h, in the exclusion of light. The slurry was cooled and filtered over Celite® to remove solids. The filtrate was concentrated

under reduced pressure to remove excess substrate. The residue was then dissolved in THF (0.5 mL) and α,α,α -trifluorotoluene (20 μL of a 0.41 mM solution in THF) was added as an internal standard. ^{19}F NMR spectrum was acquired at 25 $^{\circ}\text{C}$ to determine the integration ratio of the standard to the Pd^{II} product. All reactions were performed in duplicate.

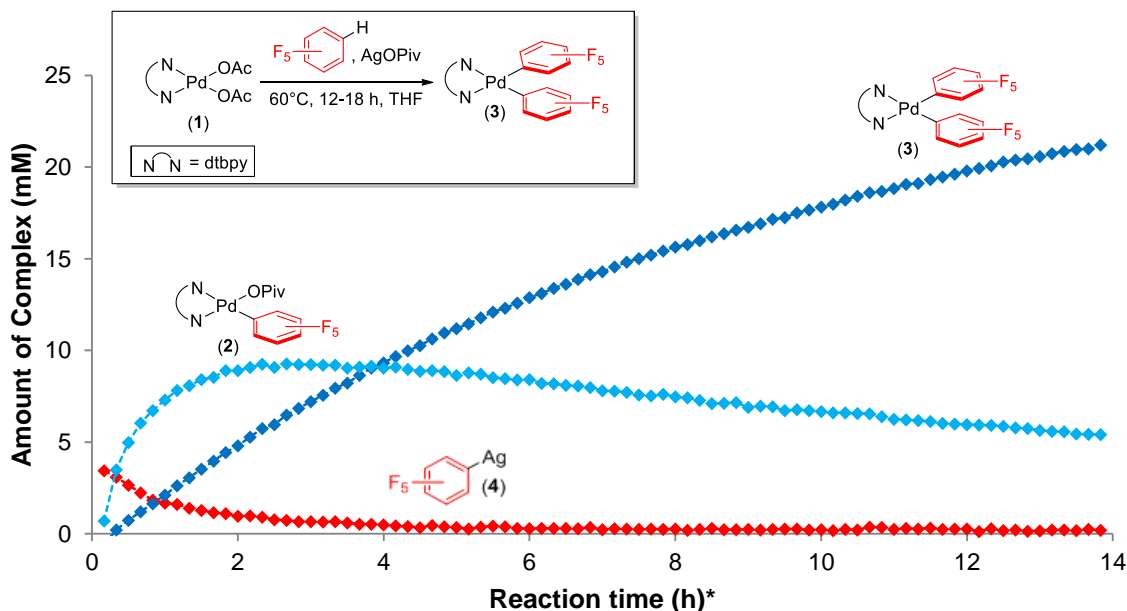


General Procedure for *in situ* NMR Experiments with AgOPiv and $\text{C}_6\text{F}_5\text{H}$.

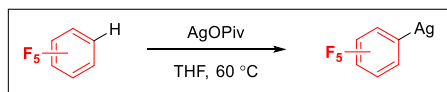
On comparable scale to vial reactions: In air, the Pd^{II} complex **1-OAc** (25 μmol , 1 equiv) and AgOPiv (15.6 mg, 75 μmol , 3 equiv) were weighed into a screw cap NMR tube. THF (1 mL, 0.025 M), $\text{C}_6\text{F}_5\text{H}$ (28 μL , 252 μmol , 10 equiv), and an internal standard, α,α,α -trifluorotoluene (10 μL) were added to the vial. The tube was covered with aluminum foil until inserting into the NMR spectrometer, preheated to 60 $^{\circ}\text{C}$. The reaction was monitored by ^{19}F NMR for 12 - 18h at 60 $^{\circ}\text{C}$.

On a Reduced Scale: In air, the Pd^{II} complex **1-OAc** (10 μmol , 1 equiv) and AgOPiv (30 μmol , 6.2 mg, 3 equiv) were weighed into a screw cap NMR tube. THF (1 mL), $\text{C}_6\text{F}_5\text{H}$ (11 μL , 100 μmol , 10 equiv), and an internal standard, α,α,α -trifluorotoluene (2 μL) were added to the vial. The tube was covered with aluminum foil until inserting into the NMR spectrometer, preheated to 60 $^{\circ}\text{C}$. The reaction was monitored by ^{19}F NMR for 12 - 18h at 60 $^{\circ}\text{C}$.

Figure 3.9. Plot of the Reaction of 1-OAc with C₆F₅H Upon Addition of AgOPiv



Procedure for *in situ* Generation of Ag-arene without Pd.



In air, AgOPiv (90 μmol , 15.6 mg, 1 equiv) was weighed into a 4 mL vial. THF (1 mL), C₆F₅H (0.2 mL, 1.8 mmol, 24 equiv), and a Teflon stirbar were added to the vial. The reaction was stirred at 60 °C for 1 - 2 h, in the exclusion of light. The slurry was cooled and a ¹⁹F NMR spectrum was taken at 25 °C to observe **4**.

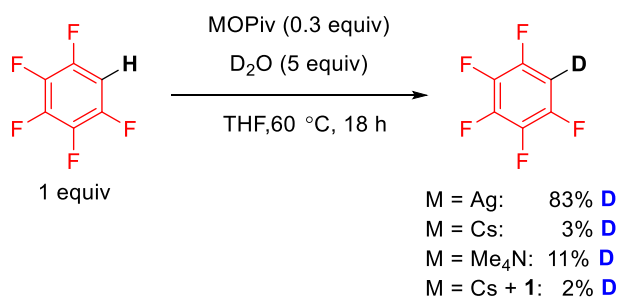
Procedure for H/D Exchange Experiments with C₆F₅H

For Reactions without Palladium Complex: In air, MOPiv (75 μmol , 0.4 equiv) was weighed into a 4 mL vial. THF (1 mL, 0.025 M), C₆F₅H (0.2 mL, 1.8 mmol, 1 equiv), D₂O (163 μL , 9 mmol, 5 equiv) and a Teflon stirbar were added to the vial. The reaction was stirred at 60 °C for

18h, in the exclusion of light. The slurry was cooled and filtered over Celite® to remove solids. Acetone-*d*₆ (20 μL, 272 μmol) was added as an internal standard. ²H NMR spectra were acquired at 25 °C to determine the amount of deuterium incorporation using a relaxation delay of 10 s.

For reactions with Palladium Complex: In air, **1-OAc** (12.3 mg, 25 μmol, 0.01 equiv) and CsOPiv (17.6 mg, 75 μmol, 0.4 equiv) were weighed in a 4 mL vial. THF (1 mL, 0.025 M), C₆F₅H (0.2 mL, 1.8 mmol, 1 equiv), D₂O (163 μL, 9 mmol, 5 equiv) and a Teflon stirbar were added to the vial. The reaction was stirred at 60 °C for 18h in the exclusion of light. The slurry was cooled and filtered over Celite® to remove solids. Acetone-*d*₆ (20 μL, 272 μmol) was added as an internal standard. ²H NMR spectra were acquired at 25 °C to determine the amount of deuterium incorporation using a relaxation delay of 10 s.

Scheme 3.4. H/D Exchange with C₆F₅H and Various MOPiv Sources

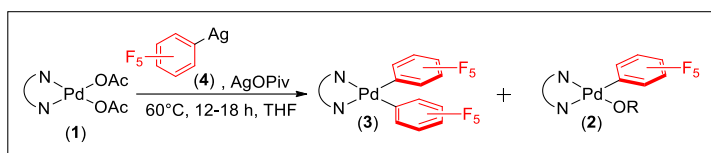


Synthesis of Authentic Sample of **4**.

Complex **4** was prepared using a literature procedure.⁵³ The ¹H NMR spectroscopic data for this complex matched that reported in the literature. ¹³C NMR (175.95 MHz, 298 K, acetone-*d*₆): δ 152.75 (dd, J = 229.6, 27.3 Hz), 142.86 (d, J = 250.6 Hz), 138.70 – 135.76 (m), 109.27 (t, J = 72.7 Hz). ¹⁹F NMR (376.84 MHz, 298K, acetone-*d*₆): δ -102.16 – -102.58 (m), -152.16 (t, J = 19.2 Hz), -161.82 – -162.19 (m).

General Procedure for Observing Shifting Peaks of **4** by ^{19}F NMR.

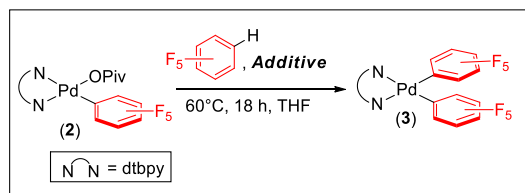
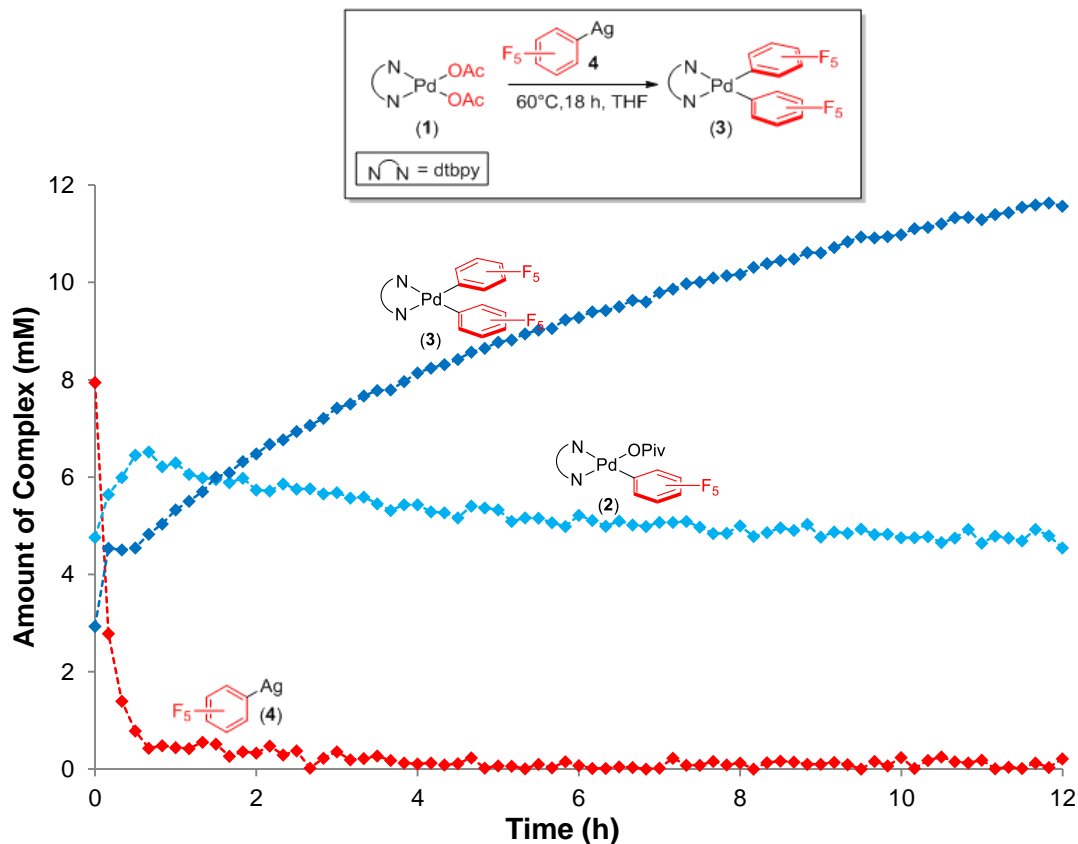
In a N_2 -filled glovebox, **4** (7 mg, 26 μmol , 1 equiv) was dissolved in dry THF (0.5 mL) in an amber NMR tube. An initial ^{19}F NMR spectrum was taken at 25 $^\circ\text{C}$. A solution of CsOPiv (6 mg, 26 μmol , 1 equiv) in dry THF (0.2 mL) was added to the NMR tube, the tube was shaken, and a second ^{19}F NMR spectrum was taken at 25 $^\circ\text{C}$. A solution of NaOAc (4 mg, 26 μmol , 1 equiv) in dry THF (1 mL) was added to the NMR tube, the tube was shaken, and a third ^{19}F NMR spectrum was taken at 25 $^\circ\text{C}$.



General Procedure for in situ NMR reaction of **1-OAc** with AgC_6F_5 .

In a N_2 -filled glovebox, the Pd^{II} complex **1-OAc** (10 μmol) and isolated **4** (30 μmol , 8.25 mg, 3 equiv) were weighed into a screw cap NMR tube. THF (1 mL) and an internal standard, α,α,α -trifluorotoluene (2 μL) were added to the vial. The tube was covered with aluminum foil until inserting into an NMR, preheated to 60 $^\circ\text{C}$. The reaction was monitored by ^{19}F NMR for 12 - 18h at 60 $^\circ\text{C}$.

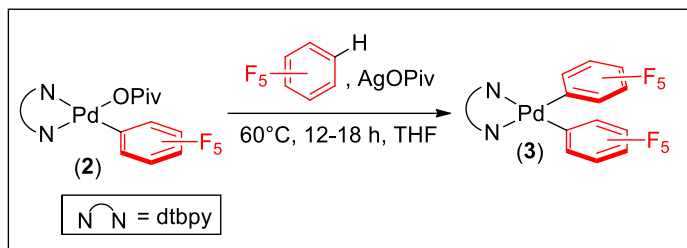
Figure 3.10. Plot of the Reaction of 1-OAc with 4.



General Procedure for Reactivity of 2 with Additives

In air, Pd^{II} complex **2** (16.1 mg, 25 μ mol, 1 equiv) and the respective additive (75 μ mol, 3 equiv) were weighed into a 4 mL vial. THF (1 mL), C₆F₅H (0.1 mL, 0.9 mmol, 36 equiv), and a Teflon stirbar were added to the vial. The reaction was stirred at 60 °C for 18h, in the exclusion of light. The slurry was cooled and filtered over Celite® to remove solids. The filtrate was concentrated under reduced pressure to remove excess substrate. The residue was then dissolved in THF (0.5 mL) and α,α,α -trifluorotoluene (20 μ L of a 0.41 mM solution in THF) was added as

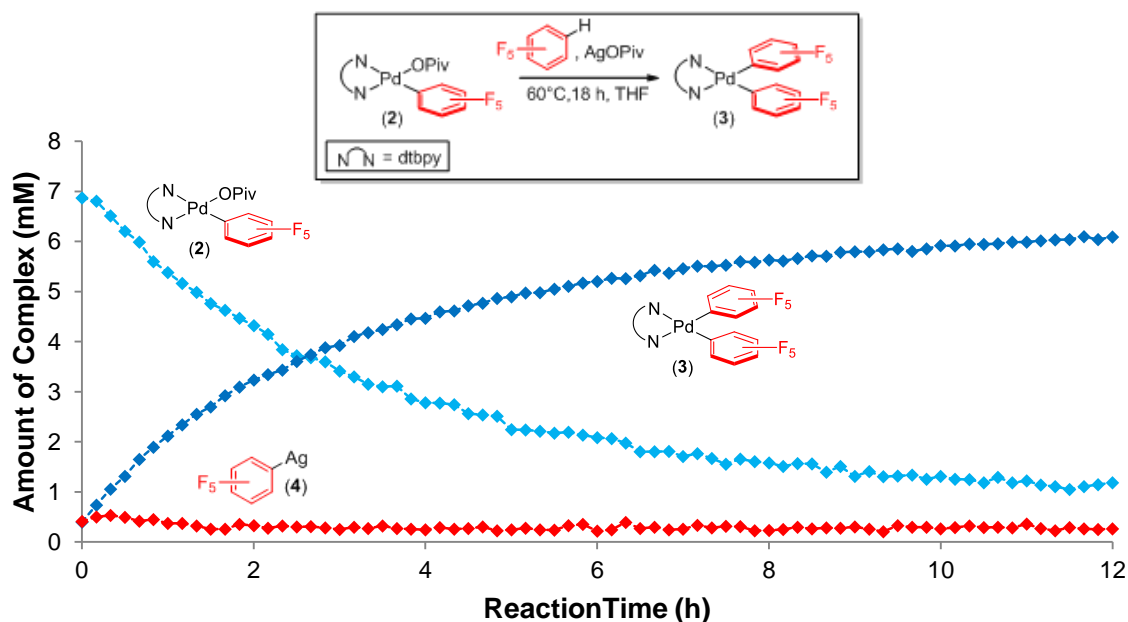
an internal standard. ^{19}F NMR spectra were acquired at 25 °C to determine the integration ratio of the standard to the Pd^{II} product. All reactions were performed in triplicate.



General Procedure for NMR Experiments with 2 and AgOPiv.

In air, the Pd^{II} complex **2** (10 μmol) and AgOPiv (10 μmol , 6.4 mg, 1 equiv) were weighed into a screw cap NMR tube. THF (1 mL), $\text{C}_6\text{F}_5\text{H}$ (11 μL , 100 μmol , 10 equiv), and an internal standard, α,α,α -trifluorotoluene (2 μL) were added to the vial. The tube was covered with aluminum foil until inserting into an NMR, preheated to 60 °C. The reaction was monitored by ^{19}F NMR for 12 - 18h at 60 °C.

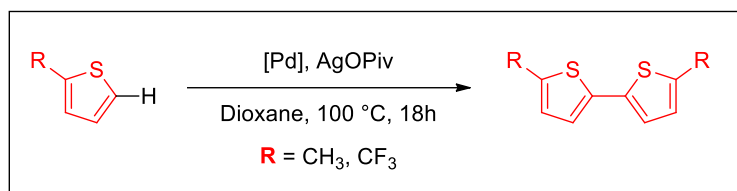
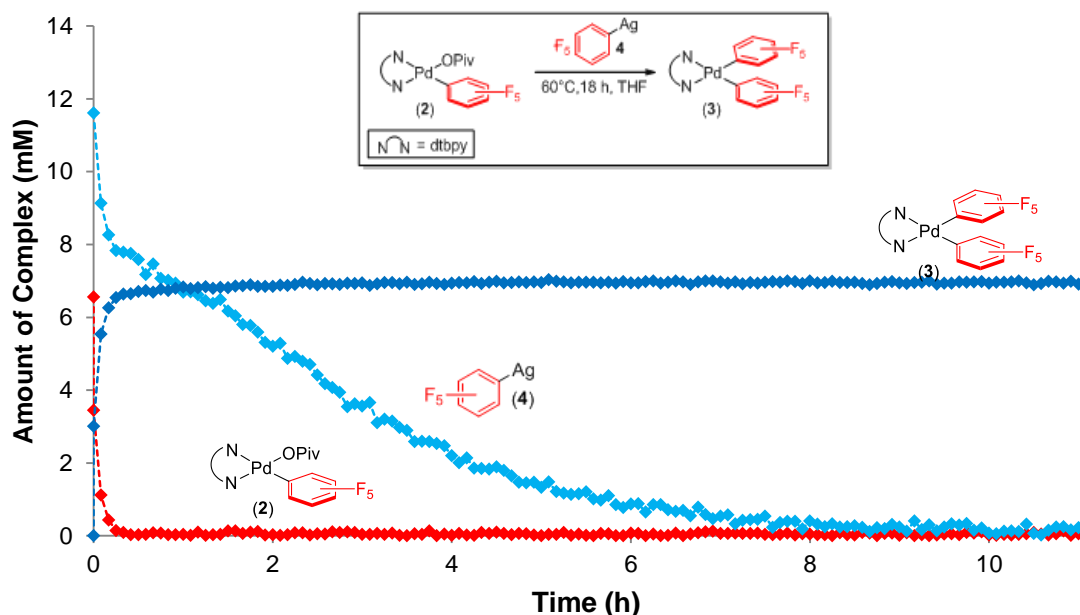
Figure 3.11. Plot of the Reaction Progress Upon Treatment of 2 with $\text{C}_6\text{F}_5\text{H}/\text{AgOPiv}$.



General Procedure for reactions of 2 with 4.

In a N₂-filled glovebox, the Pd^{II} complex 2 (6.4 mg, 10 μmol, 1 equiv) and 4 (20 μmol, 5.5 mg, 2 equiv) were weighed into a screw cap NMR tube. THF (1 mL) and an internal standard, α,α,α-trifluorotoluene (2 μL) were added to the vial. The tube was covered with aluminum foil until inserting into an NMR, preheated to 60 °C. The reaction was monitored by ¹⁹F NMR for 12 - 18h at 60 °C.

Figure 3.12. Plot for the Reaction Upon Treatment of 2 with AgC₆F₅ (4).



General Procedure for Stoichiometric Reactions with 2-substituted thiophenes.

In air, the Pd^{II} complex 1-OAc (12.3 mgs, 25 μmol, 1 equiv) and the respective additive (75 μmol, 3 equiv) were weighed into a 4 mL vial. THF (1 mL, 0.25 M), thiophene (250 mmol, 10 equiv), and a Teflon stirbar were added to the vial. The reaction was stirred at 60 °C for 18h, in the exclusion of light. The slurry was cooled and filtered over Celite® to remove solids. The filtrate was then diluted with dichloromethane, an internal standard was added (neopentyl benzene, 20

μL , 1.3 mM in THF), and samples were analyzed by GC. Yields were reported based on calibrated GC yields, based on Ag as a $2 e^-$ oxidant (moles pdt/(moles of Ag/2)*100 = % yield). All reactions were performed in at least duplicate.

Table 3.6. Dimerization of 2-R-Thiophene with 1-OAc Under Stoichiometric Conditions

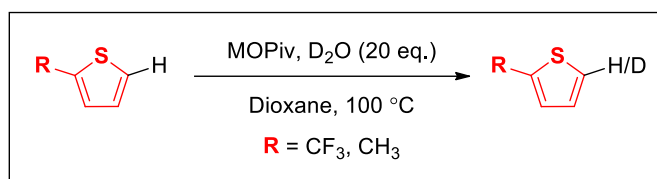
Reaction scheme: 2-R-thiophene (10 equiv) reacts with [Pd] (1-OAc, 25 mmol), AgOPiv (3 equiv) in THF at 60 °C for 18h to form dimer 5 or 6.

Entry	R =	Additive	% Yield of 5 or 6
1	CH ₃	AgOPiv	16
2	CH ₃	none	<1
3 ^b	CH ₃	Ag Salts ^c	< 1
4	CH ₃	MOPiv ^c	< 1
5 ^d	CH ₃	Lewis Acid ^e	< 1
6	CF ₃	AgOPiv	41
7	CF ₃	none	< 1
8	CF ₃	Ag ₂ O	29
9	CF ₃	Other Ag Salts ^f	<1
10	CF ₃	MOPiv ^c	<1
11 ^d	CF ₃	Lewis Acid ^e	<1

^aConditions: 2-CH₃-thiophene (25 μL , 250 μmol , 10 equiv), additive (75 mmol, 3 equiv), **1** (25 μmol , 1 equiv), THF (0.025 M), 60 °C, 18h; ^bAg Salts = AgOAc, Ag₂CO₃ (37.5 mmol), Ag₂O (37.5 mmol), AgBF₄; ^cM = Na, Cs, Me₄N.; ^dWith 2 equiv of additive (50 mmol); ^eLewis acid = AlCl₃, BF₃OEt₂, Cr(CO)₆, InCl₃, (Me₂S)AuCl, Sc(OTf)₂, SnCl₂, W(CO)₆, Zn(OAc)₂; ^fAg = AgOAc, Ag₂CO₃ (37.5 mmol), AgBF₄.

General Procedure for Catalytic Reactions with 2-substituted thiophenes.

In air, the Pd^{II} complex **1-OAc** (7.4 mg, 15 μmol) and AgOPiv (62.4 mg, 300 μmol, 1 equiv) were weighed into a 4 mL vial. Dioxane (1 mL, 1M), thiophene substrate (1 mmol, 3.3 equiv), and a Teflon stirbar were added to the vial. The reaction was stirred at 100 °C for 18h, in the exclusion of light. The reaction was cooled and filtered over Celite® to remove solids. The filtrate was then diluted with dichloromethane, an internal standard was added (neopentyl benzene, 20 μL, 1.3 mM in THF), and samples were analyzed by GC. Yields were reported based on calibrated GC yields, based on Ag as a 2 e⁻ oxidant (moles pdt/(moles of Ag/2)*100 = % yield). All reactions were performed in at least duplicate.

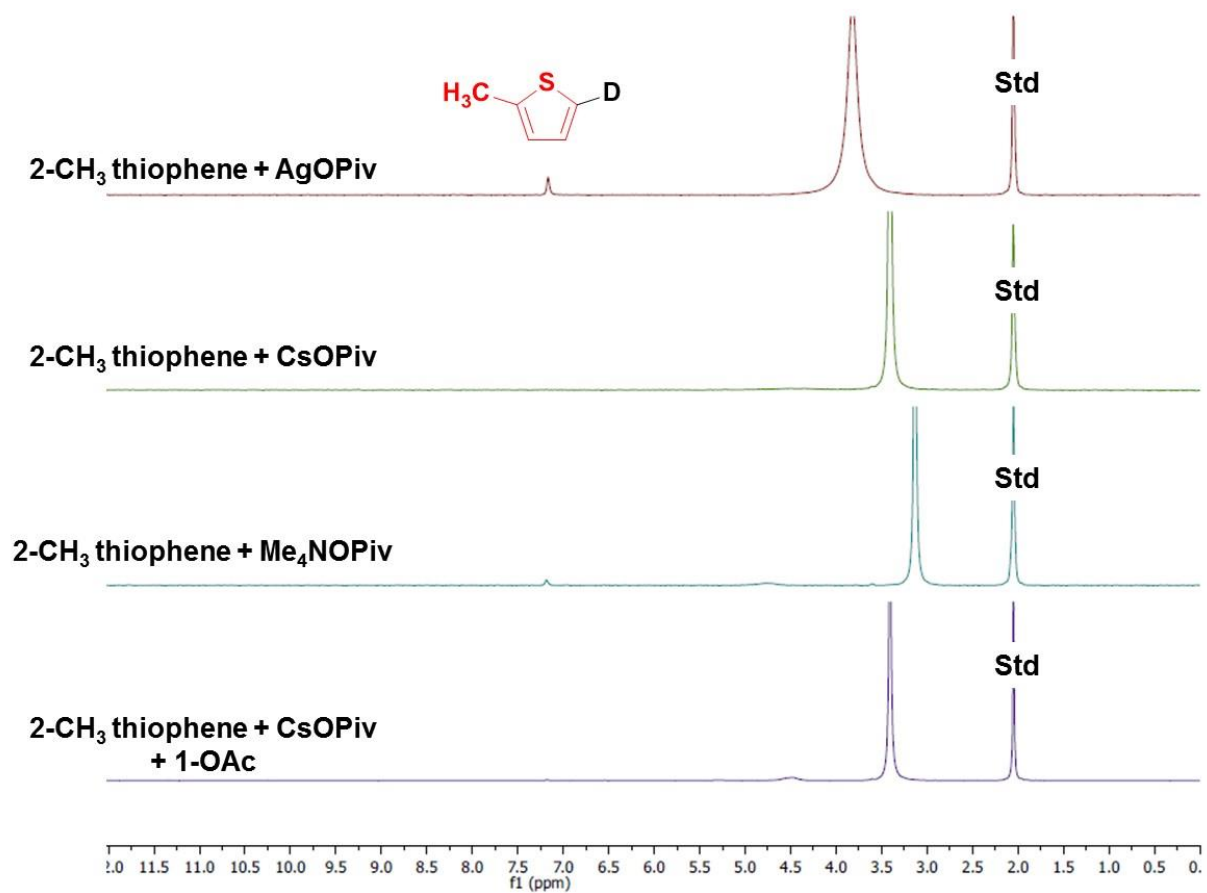


General Procedure for H/D Exchange Reactions of Thiophene Substrates with MOPiv.

Without Pd: In air, MOPiv (300 μmol, 0.3 equiv) was weighed into a 4 mL vial. Dioxane (1M, 1 mL), thiophene substrate (1 mmol, 1 equiv), D₂O (90 μL, 5 mmol, 5 equiv) and a Teflon stirbar were added to the vial. The reaction was stirred at 100 °C for 4 h, in the exclusion of light. The reaction was cooled and 20 μL of acetone-*d*₆ was added to the reaction vial as an internal deuterium standard. A portion of the solution was then transferred into an NMR tube and analyzed by ²H NMR Spectroscopy. Yields of deuterium incorporation are reported based on the internal standard.

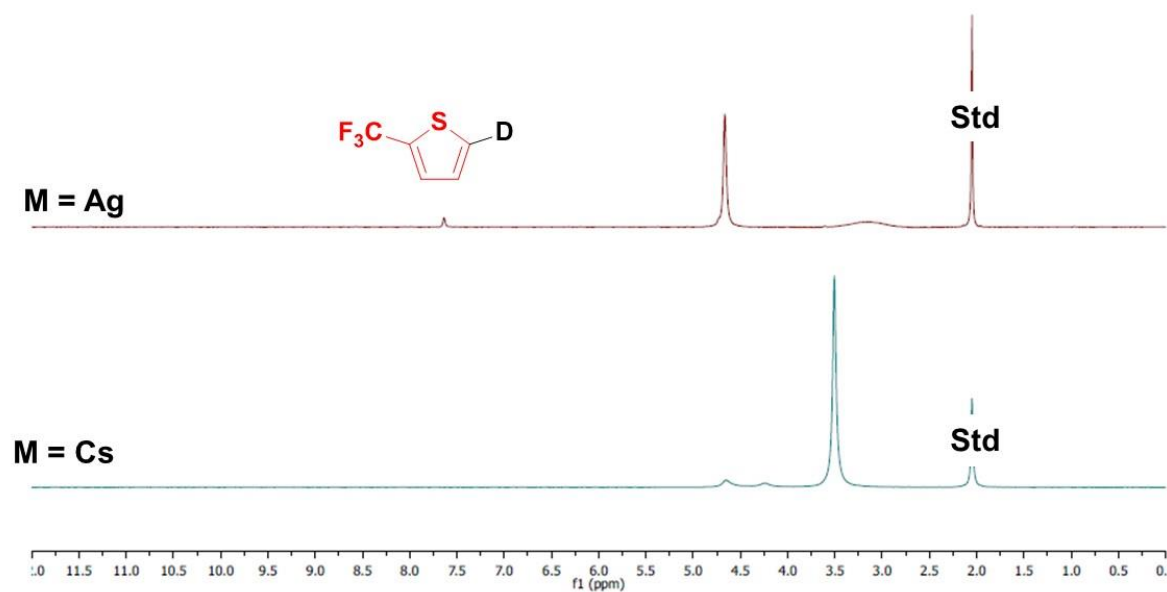
With Pd: In air, **1-OAc** (7.4 mg, 15 μmol) and CsOPiv (300 μmol, 0.3 equiv) were weighed into a 4 mL vial. Dioxane (1M, 1 mL), thiophene substrate (1 mmol, 1 equiv), D₂O (90 μL, 5 mmol, 5 equiv) and a Teflon stirbar were added to the vial. The reaction was stirred at 100 °C for 4 h, in the exclusion of light. The reaction was cooled and 20 μL of acetone-*d*₆ was added to the reaction vial as an internal deuterium standard. A portion of the solution was then transferred into an NMR tube and analyzed by ²H NMR Spectroscopy. Yields of deuterium incorporation are reported based on the internal standard.

Figure 3.13. Overlaped Spectra for H/D Exchange of 2-methyl thiophene and MOPiv.

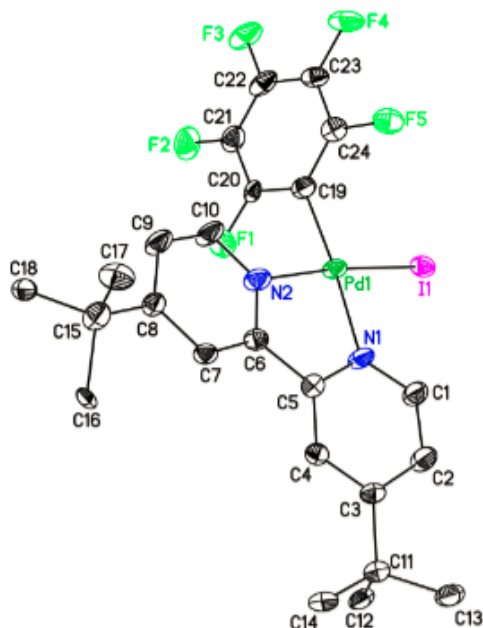


*Std = acetone-*d*₆

Figure 3.14. Overlaped Spectra for H/D Exchange of 2-trifluoromethyl thiophene and MOPiv.



*Std = acetone- d_6



Structure Determination of (dtbpy)Pd^{II}(C₆F₅)(I) via Single Crystal X-ray Crystallography.³

In air, X-ray quality crystals were grown by dissolving (dtbpy)Pd^{II}(C₆F₅)(I) in a small amount of dichloromethane and crystallized by diffusion in pentanes at 25 °C. Yellow plates were obtained after 3 d. A crystal of dimensions 0.06 x 0.04 x 0.04 mm was mounted on a Rigaku AFC10K Saturn 944+ CCD-based X-ray diffractometer equipped with a low temperature device and Micromax-007HF Cu-target micro-focus rotating anode ($\lambda = 1.54187 \text{ \AA}$) operated at 1.2 kW power (40 kV, 30 mA). The X-ray intensities were measured at 85(1) K with the detector placed at a distance 42.00 mm from the crystal. A total of 2159 images were collected with an oscillation width of 1.0° in ω . The exposure time was 5 sec. for the low angle images, 30 sec. for high angle. The integration of the data yielded a total of 70288 reflections to a maximum 2θ value of 136.44° of which 4306 were independent and 4195 were greater than $2\sigma(I)$. The final cell constants (Table 3.7) were based on the xyz centroids 44179 reflections above $10\sigma(I)$. Analysis of the data showed negligible decay during data collection; the data were processed with CrystalClear 2.0 and corrected for absorption. The structure was solved and refined with the Bruker SHELXTL (version 2008/4) software package, using the space group Pbca with $Z = 8$ for the formula C₂₄H₂₄N₂F₅PdI.

³ All crystal structures were resolved by Dr. Jeff Kampf

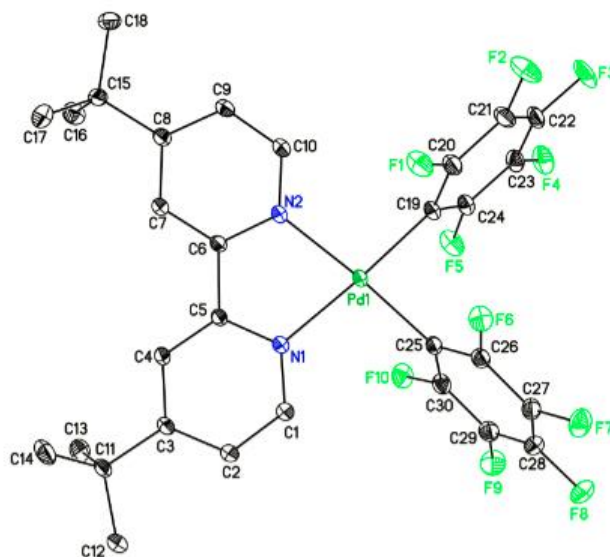
All non-hydrogen atoms were refined anisotropically with the hydrogen atoms placed in idealized positions. Full matrix least-squares refinement based on F^2 converged at $R_1 = 0.0419$ and $wR_2 = 0.0975$ [based on $I > 2\sigma(I)$], $R_1 = 0.0429$ and $wR_2 = 0.0983$ for all data. Additional details are presented in Table 1 and are given as Supporting Information in a CIF file. Acknowledgement is made for funding from NSF grant CHE-0840456 for X-ray instrumentation.

Sheldrick, G.M. SHELXTL, v. 2008/4; Bruker Analytical X-ray, Madison, WI, 2008.

CrystalClear Expert 2.0 r12, Rigaku Americas and Rigaku Corporation (2011), Rigaku Americas, 9009, TX, USA 77381-5209, Rigaku Tokyo, 196-8666, Japan.

Table 3.7. Crystal Data and Structure Refinement for (dtbpy)Pd^{II}(C₆F₅)(I).

Empirical formula	C ₂₄ H ₂₄ F ₅ IN ₂ Pd
Formula weight	668.75
Temperature	85(2) K
Wavelength	1.54178 Å
Crystal system	Orthorhombic
Space group	Pbca
Unit cell dimensions	a = 12.3979(2) Å alpha = 90° b = 17.5191(3) Å beta = 90° c = 21.6820(15) Å gamma = 90°
Volume	4709.3(3) Å ³
Z	8
Calculated density	1.886 mg/mm ³
Absorption coefficient	17.142 mm ⁻¹
F(000)	2608
Crystal size	0.06 x 0.04 x 0.04 mm ³
Theta range for data collection	4.08 to 68.22°
Limiting indices	-14<=h<=14, -21<=k<=21, -25<=l<=26
Reflections collected / unique	70288
Unique Refelctions	4306 [R(int) = 0.0801]
Completeness to $\theta = 35.01$	100 %
Absorption correction	Semi-empirical from equivalents
Max. and min. transmission	0.5472 and 0.4261
Refinement method	Full-matrix least-squares on F ²
Data / restraints / parameters	4306 / 48 / 336
Goodness-of-fit on F ²	1.003
Final R indices [$I > 2\sigma(I)$]	R ₁ = 0.0419, wR ₂ = 0.0975
R indices (all data)	R ₁ = 0.0429, wR ₂ = 0.0983
Largest diff. peak and hole	1.291 and -0.923 e.Å ⁻³



Structure Determination of **3** via Single Crystal X-ray Crystallography.

In air, X-ray quality crystals of **3** were grown by dissolving **3** in a small amount of dichloromethane and crystallized by diffusion in pentanes at $-33\text{ }^{\circ}\text{C}$. Colorless prisms of **3** were obtained after 24 h. A crystal of dimensions $0.31 \times 0.28 \times 0.17\text{ mm}$ was mounted on a Bruker SMART APEX-I CCD-based X-ray diffractometer equipped with a low temperature device and fine focus Mo-target X-ray tube ($\lambda = 0.71073\text{ \AA}$) operated at 1500 W power (50 kV, 30 mA). The X-ray intensities were measured at $85(1)\text{ K}$; the detector was placed at a distance 5.070 cm from the crystal. A total of 4055 frames were collected with a scan width of 0.5° in ω and 0.45° in ϕ with an exposure time of 10 s/frame . The integration of the data yielded a total of 65510 reflections to a maximum 2θ value of 70.02° of which 12093 were independent and 11239 were greater than $2\sigma(I)$. The final cell constants (Table 3.8) were based on the xyz centroids of 9695 reflections above $10\sigma(I)$. Analysis of the data showed negligible decay during data collection; the data were processed with SADABS and corrected for absorption. The structure was solved and refined with the Bruker SHELXTL (version 2008/4) software package, using the space group $P1\bar{1}$ with $Z = 2$ for the formula $\text{C}_{30}\text{H}_{24}\text{N}_2\text{F}_{10}\text{Pd}$. All non-hydrogen atoms were refined anisotropically with the hydrogen atoms placed in idealized positions. Full matrix least-squares refinement based on F^2 converged at $R1 = 0.0262$ and $wR2 = 0.0668$ [based on $I > 2\sigma(I)$], $R1 = 0.0290$ and $wR2 = 0.0689$ for all data.

Sheldrick, G.M. SHELXTL, v. 2008/4; Bruker Analytical X-ray, Madison, WI, 2008.

CrystalClear Expert 2.0 r12, Rigaku Americas and Rigaku Corporation (2011), Rigaku Americas, 9009, TX, USA 77381-5209, Rigaku Tokyo, 196-8666, Japan.

Table 3.8. Crystal Data and Structure Refinement for 3.

Empirical formula	C ₃₀ H ₂₄ F ₁₀ N ₂ Pd
Formula weight	708.91
Temperature	85(2) K
Wavelength	0.71073 Å
Crystal system	Triclinic
Space group	P-1
Unit cell dimensions	a = 10.3964(2) Å alpha = 97.4490(10)° b = 10.9403(2) Å beta = 92.6340(10)° c = 12.4107(3) Å gamma = 97.7850(10)°
Volume	1383.87(5) Å ³
Z	2
Calculated density	1.701 mg/mm ³
Absorption coefficient	0.762 mm ⁻¹
F(000)	708
Crystal size	0.31 x 0.28 x 0.17 mm ³
Theta range for data collection	1.66 to 35.01°
Limiting indices	-16<=h<=16, -17<=k<=17, -20<=l<=20
Reflections collected / unique	65510
Unique Refelctions	12093 [R(int) = 0.0487]
Completeness to $\theta = 35.01$	99.2 %
Absorption correction	Semi-empirical from equivalents
Max. and min. transmission	0.8813 and 0.7980
Refinement method	Full-matrix least-squares on F ²
Data / restraints / parameters	12093 / 0 / 394
Goodness-of-fit on F ²	1.057
Final R indices [$I > 2\sigma(I)$]	R ₁ = 0.0262, wR ₂ = 0.0668
R indices (all data)	R ₁ = 0.0290, wR ₂ = 0.0689
Largest diff. peak and hole	1.047 and -1.031 e.Å ⁻³

References

- (1) Lunsford, J. H. *Catal. Today* **2000**, *63*, 165.
- (2) Lyons, T. W.; Sanford, M. S. *Chem. Rev.* **2010**, *110*, 1147.
- (3) Ackermann, L. *Chem. Rev.* **2011**, *111*, 1315.
- (4) Yamaguchi, J.; Yamaguchi, A. D.; Itami, K. *Angew. Chem. Int. Ed.* **2012**, *51*, 8960.
- (5) Neufeldt, S. R.; Sanford, M. S. *Acc. Chem. Res.* **2012**, *45*, 936.
- (6) Yeung, C. S.; Dong, V. M. *Chem. Rev.* **2011**, *111*, 1215.
- (7) Weibel, J. M.; Blanc, A.; Pale, P. In *Silver in Organic Chemistry*; 2010; pp 285–328.
- (8) Hussain, I.; Singh, T. *Adv. Synth. Catal.* **2014**, *356*, 1661.
- (9) Lafrance, M.; Gorelsky, S. I.; Fagnou, K. *J. Am. Chem. Soc.* **2007**, *129*, 14570.
- (10) Lafrance, M.; Fagnou, K. *J. Am. Chem. Soc.* **2006**, *128*, 16496.
- (11) Liégault, B.; Lapointe, D.; Caron, L.; Vlassova, A.; Fagnou, K. *J. Org. Chem.* **2009**, *74*, 1826.
- (12) Gorelsky, S. I.; Lapointe, D.; Fagnou, K. *J. Am. Chem. Soc.* **2008**, *130*, 10848.
- (13) Lapointe, D.; Fagnou, K. *Chem. Lett.* **2010**, *39*, 1118.
- (14) Lafrance, M.; Shore, D.; Fagnou, K. *Org. Lett.* **2006**, *8*, 5097.
- (15) Gorelsky, S. I.; Lapointe, D.; Fagnou, K. *J. Org. Chem.* **2012**, *77*, 658.
- (16) Arroniz, C.; Denis, J. G.; Ironmonger, A.; Rassias, G.; Larrosa, I. *Chem. Sci.* **2014**, *5*, 3509.
- (17) Anand, M.; Sunoj, R. B.; Schaefer, H. F. *J. Am. Chem. Soc.* **2014**, *136*, 5535.
- (18) Lohr, T. L.; Piers, W. E.; Sgro, M. J.; Parvez, M. *Dalt. Trans.* **2014**, *43*, 13858.
- (19) Potavathri, S.; Dumas, A. S.; Dwight, T. A.; Naumiec, G. R.; Hammann, J. M.; DeBoef, B. *Tetrahedron Lett.* **2008**, *49*, 4050.
- (20) Font, M.; Acuña-Parés, F.; Parella, T.; Serra, J.; Luis, J. M.; Lloret-Fillol, J.; Costas, M.; Ribas, X. *Nature* **2014**, *5*, 4373.
- (21) He, C. Y.; Min, Q. Q.; Zhang, X. *Organometallics* **2012**, *31*, 1335.
- (22) Wang, G. W.; Zhou, A. X.; Li, S. X.; Yang, S. D. *Org. Lett.* **2014**, *16*, 3118.

- (23) Patrick, S. R.; Boogaerts, I. I. F.; Gaillard, S.; Slawin, A. M. Z.; Nolan, S. P. *Beilstein J. Org. Chem.* **2011**, *7*, 892.
- (24) Tang, S.; Yu, H.; You, W.; Guo, Q. *Chinese J. Chem. Phys.* **2013**, *26*, 415.
- (25) Remy, M. S.; Cundari, T. R.; Sanford, M. S. *Organometallics* **2010**, *29*, 1522.
- (26) Zhang, L.; Fang, D. C. *J. Org. Chem.* **2013**, *78*, 2405.
- (27) Masui, K.; Ikegami, H.; Mori, A. *J. Am. Chem. Soc.* **2004**, *126*, 5074.
- (28) Takahashi, M.; Masui, K.; Sekiguchi, H.; Kobayashi, N.; Mori, A.; Funahashi, M.; Tamaoki, N. *J. Am. Chem. Soc.* **2006**, *128*, 10930.
- (29) Li, H.; Liu, J.; Sun, C. L.; Li, B. J.; Shi, Z. *J. Org. Lett.* **2011**, *13*, 276.
- (30) He, C. Y.; Fan, S.; Zhang, X. *J. Am. Chem. Soc.* **2010**, *132*, 12850.
- (31) Hull, K. L.; Sanford, M. S. *J. Am. Chem. Soc.* **2009**, *131*, 9651.
- (32) Miao, T.; Wang, L. *Adv. Synth. Catal.* **2014**, *356*, 429.
- (33) Yang, S.; Li, B.; Wan, X.; Shi, Z. *J. Am. Chem. Soc.* **2007**, *129*, 6066.
- (34) Stuart, D. R.; Villemure, E.; Fagnou, K. *J. Am. Chem. Soc.* **2007**, *129*, 12072.
- (35) Potavathi, S.; Pereira, K. C.; Gorelsky, S. I.; Pike, A.; Lebris, A. P.; Deboef, B. *J. Am. Chem. Soc.* **2010**, *132*, 14676.
- (36) Campbell, A. N.; Meyer, E. B.; Stahl, S. S. *Chem. Commun.* **2011**, *47*, 10257.
- (37) Hull, K. L.; Sanford, M. S. *J. Am. Chem. Soc.* **2007**, *129*, 11904.
- (38) Han, W.; Mayer, P.; Ofial, A. R. *Angew. Chem. Int. Ed.* **2011**, *50*, 2178.
- (39) Yu, M.; Liang, Z.; Wang, Y.; Zhang, Y. *J. Org. Chem.* **2011**, *76*, 4987.
- (40) Mori, A.; Sugie, A. *Bull. Chem. Soc. Jpn.* **2008**, *81*, 548.
- (41) Wang, C.; Piel, I.; Glorius, F. *J. Am. Chem. Soc.* **2009**, *131*, 4194.
- (42) Cho, S. H.; Hwang, S. J.; Chang, S. *J. Am. Chem. Soc.* **2008**, *130*, 9254.
- (43) Aufiero, M.; Proutiere, F.; Schoenebeck, F. *Angew. Chem. Int. Ed.* **2012**, *51*, 7226.
- (44) Suresh, R.; Kumaran, R. S.; Senthilkumar, V.; Muthusubramanian, S. *RSC Adv.* **2014**, *4*, 31685.
- (45) Lanci, M. P.; Remy, M. S.; Kaminsky, W.; Mayer, J. M.; Sanford, M. S. *J. Am. Chem. Soc.* **2009**, *131*, 15618.

- (46) Lotz, M. D.; Remy, M. S.; Lao, D. B.; Ariafard, A.; Yates, B. F.; Canty, A. J.; Mayer, J. M.; Sanford, M. S. *J. Am. Chem. Soc.* **2014**, *136*, 8237.
- (47) Koizumi, T.; Yamazaki, A.; Yamamoto, T. *Dalton Trans.* **2008**, *2*, 3949.
- (48) Chen, F.; Zhang, X. *Chem. Lett.* **2011**, *40*, 978.
- (49) Guo, F.; Han, J.; Mao, S.; Li, J.; Geng, X.; Yu, J.; Wang, L. *RSC Adv.* **2013**, *3*, 6267.
- (50) He, M.; Soulé, J.-F.; Doucet, H. *ChemCatChem* **2014**, *6*, 1824.
- (51) Wei, Y.; Su, W. *J. Am. Chem. Soc.* **2010**, *132*, 16377.
- (52) Rousseaux, S.; Davi, M.; Sofack-Kreutzer, J.; Pierre, C.; Kefalidis, C. E.; Clot, E.; Fagnou, K.; Baudoin, O. *J. Am. Chem. Soc.* **2010**, *132*, 10706.
- (53) Miller, W. T.; Sun, K. K. *J. Am. Chem. Soc.* **1970**, *92*, 6985.
- (54) Liu, C.; Zhang, H.; Shi, W.; Lei, A. *Chem. Rev.* **2011**, *111*, 1780.
- (55) Kobayashi, K.; Sugie, A.; Takahashi, M.; Masui, K.; Mori, A. *Org. Lett.* **2005**, *7*, 5083.
- (56) Masuda, N.; Tanba, S.; Sugie, A.; Monguchi, D.; Koumura, N.; Hara, K.; Mori, A. *Org. Lett.* **2009**, *11*, 2297.
- (57) Zhang, X.; He, C.-Y.; Wang, Z.; Wu, C.-Z.; Qing, F.-L. *Chem. Sci.* **2013**, *13*, 3508.
- (58) Masui, K.; Mori, A.; Okano, K.; Takamura, K.; Kinoshita, M.; Ikeda, T. *Org. Lett.* **2004**, *6*, 2011.
- (59) Crabtree, R. H. *Chem. Rev.* **1995**, *95*, 987.
- (60) Shilov, A. E.; Shul, G. B. *Chem. Rev.* **1997**, *97*, 2879.
- (61) Conley, B. L.; Tenn, W. J.; Young, K. J. H.; Ganesh, S.; Meier, S.; Ziatdinov, V.; Mironov, O.; Oxgaard, J.; Gonzales, J.; Goddard, W. A.; Periana, R. A. In *Activation of Small Molecules: Organometallic and Bioinorganic Perspectives*; Wiley-VCH Verlag GmbH & Co. KGaA, 2006; pp 235–285.
- (62) Jones, C. J.; Taube, D.; Ziatdinov, V. R.; Periana, R. a.; Nielsen, R. J.; Oxgaard, J.; Goddard, W. A. *Angew. Chem. Int. Ed.* **2004**, *43*, 4626.
- (63) Hashiguchi, B. G.; Konnick, M. M.; Bischof, S. M.; Gustafson, S. J.; Devarajan, D.; Gunsalus, N.; Ess, D. H.; Periana, R. a. *Science* **2014**, *343*, 1232.
- (64) MacLean, E. J.; Robinson, R. I.; Teat, S. J.; Wilson, C.; Woodward, S. *J. Chem. Soc. Dalton Trans.* **2002**, *18*, 3518.
- (65) Stromnova, T. *Inorg. Chim. Acta* **2003**, *350*, 283.
- (66) Sarria Toro, J. M.; den Hartog, T.; Chen, P. *Chem. Commun.* **2014**, *50*, 10608.

- (67) Bernhardt, S.; Knochel, P.; Manolikakes, G. Organozinc complexes and processes for making and using the same. US20140031545, June 28, 2012.
- (68) *Org. Synth.* **1945**, 25, 53.
- (69) Coyle Lee, C.; Halbert, T. R.; Pan, W.-H.; Harmer, M. A.; Wei, L.; Leonowicz, M. E.; Dim, C. O. B.; Miller, K. F.; Bruce, A. E.; McKenna, S.; Corbin, J. L.; Wherland, S.; Stiefel, E. I. *Inorganica Chim. Acta* **1996**, 243, 147.

CHAPTER 4

Conversion of Methane to Ethane: High Throughput Experimentation and Resulting Studies

Background

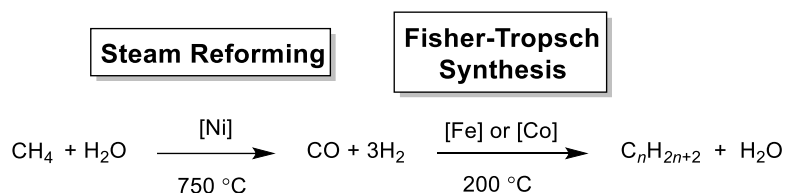
Natural gas is an abundant resource in the United States, and with improved extraction methods, has become even more accessible in the last ten years.¹ Since 2005, domestic natural gas production has increased by 6.3 quadrillion BTUs (British thermal units), making the US the largest producer of dry natural gas in the world.² As methane is the predominant component of natural gas, methane could be a promising C₁ feedstock to fuels and commodity chemicals.³⁻⁶

Significant research has focused on various approaches to upconvert methane to value-added products. Current industrial methods employ heterogeneous catalysts, such as the two-step process of steam reforming to generate syngas (CO+H₂) and subsequent Fischer-Tropsch synthesis (FT) to access higher alkanes (Figure 4.1).⁷ However, FT plants remain relatively scarce due to their high capital cost⁸s as well as due to a number of inherent disadvantages associated with this process. One disadvantage is that this two-step process requires high temperatures (250 to 700 °C), often resulting in formation of the thermodynamically favored product, CO₂.⁶ Another challenge

of this approach is the poor selectivity in the Fisher-Tropsch step, resulting in a range of alkane products.³ To improve the efficiency of the overall conversion of CH₄ to higher alkanes, we sought a more direct route using to circumvent the challenges associated with this heterogeneous process.

The direct functionalization of methane has been extensively studied using heterogeneous metal oxide catalysts.⁶ However, these catalysts have failed to become industrially relevant due to issues in selectivity and overall conversion, due to high temperatures required, resulting in over oxidation of products and catalyst degradation.⁴ Mechanistic studies could provide needed insight to improve this oxidative coupling process. To gain a better mechanistic understanding of the functionalization of methane, we envision an alternate approach using homogeneous catalysts operating under more mild reaction conditions.

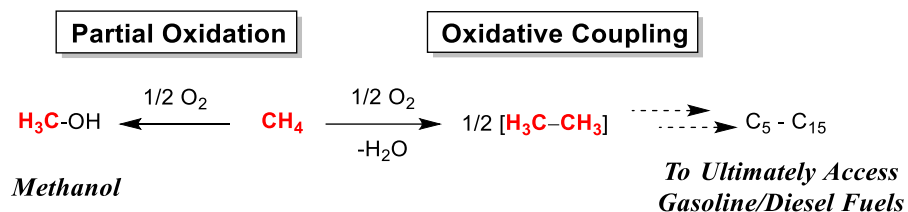
Figure 4.1. Industrial Process for Accessing Alkanes from Methane



Utilization of homogeneous catalysts can provide several advantages over heterogeneous processes.⁹ Typically, homogeneous systems operate at significantly lower temperatures, potentially minimizing the formation of CO₂. Additionally, well-established solution-phase techniques can facilitate mechanistic studies with homogeneous catalysts, thereby providing insight to enable enhancements of selectivity and reactivity.

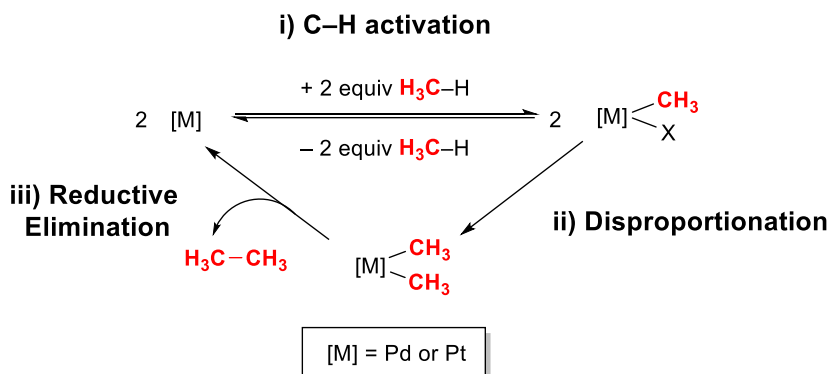
Homogeneous catalysts containing Pd and Pt metal centers have been utilized in methane functionalization, commonly through partial oxidation to generate the oxygenated product methanol (Figure 4.2).¹⁰⁻¹³ However, under conditions typically shown to activate methane, methanol is inherently biased to undergo facile oxidation to generate CO₂.¹⁴ To circumvent this challenge, we envisioned an alternate approach through oxidative C–C coupling of methane to form ethane, followed by subsequent couplings to generate higher alkanes (Figure 4.2).

Figure 4.2. Potential Routes to Functionalization of Methane



Our proposed approach proceeds through: (i) methane activation with Pd or Pt catalysts to generate M-Me bond; (ii) disproportionation to generate a dimethyl metal intermediate; and (iii) reductive elimination to liberate C–C coupled product (Scheme 4.1). In the development of this process, our group^{15–18} and others^{19–21} have demonstrated steps ii and iii with Pd and Pt complexes, further discussed in Chapter 2. Additionally, studies using a model system with palladium complexes in Chapter 3 have provided insight into the role of additives in C–H activation, relating to the first step of our proposed catalytic cycle (scheme 4.1, step i). With our stoichiometric studies of steps *i* - *iii*, we sought to combine these steps to investigate catalysis with this system, forming ethane from methane as the first product in this process.

Scheme 4.1. Proposed Catalytic Cycle for Methane Dimerization



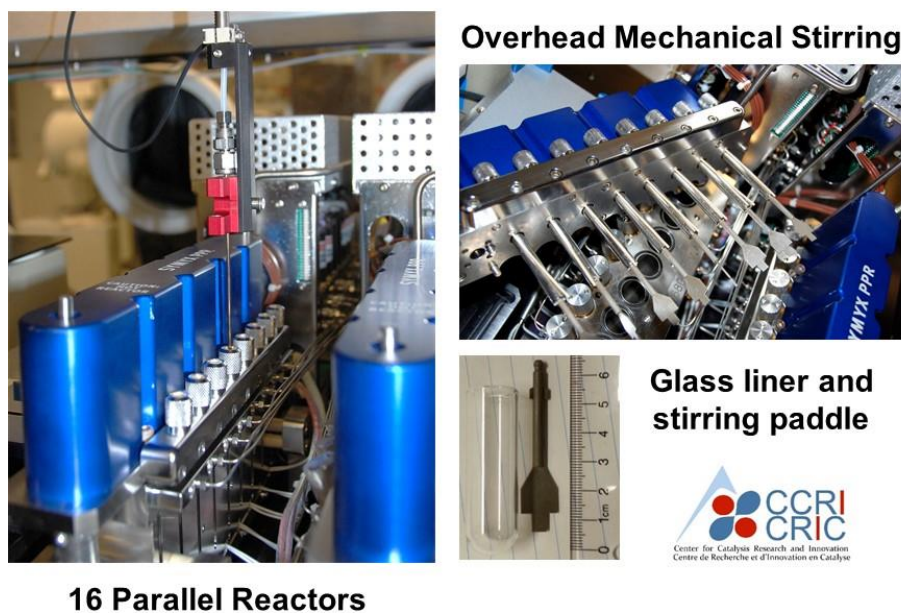
In efforts to investigate the overall conversion of methane to ethane, a number of logistical challenges had to be addressed. First, methane activation often requires high pressures and elevated temperatures, and special reactors are required to handle these conditions. Second, we sought an efficient and rapid method to examine a variety of catalysts and conditions previously demonstrated in steps *i*, *ii* or *iii* of this transformation. Finally, the analysis of our product, ethane, could prove challenging in these mixtures of gases. The detection of trace ethane in high pressures

of methane needed to be addressed to ensure accurate identification of promising catalysts and conditions.

Results and Discussion

Initially, we did not have the capabilities in the Sanford lab to address all of these issues. However, all of these criteria for the experimental setup could be achieved through the use of high pressure parallel reactors at the Center for Catalysis Research and Innovation (University of Ottawa). These 16 parallel reactors tolerate elevated pressures and temperatures well above the requirements for our experimentation (Figure 4.3). Each reactor well contained an independent headspace, avoiding cross-contamination of the gaseous products of each reactor, while allowing efficient screening of a variety of reactions. Additional details about the reactors and experimental protocol can be found on p. 129.

Figure 4.3. High Throughput Experiment – Reactor Setup⁴



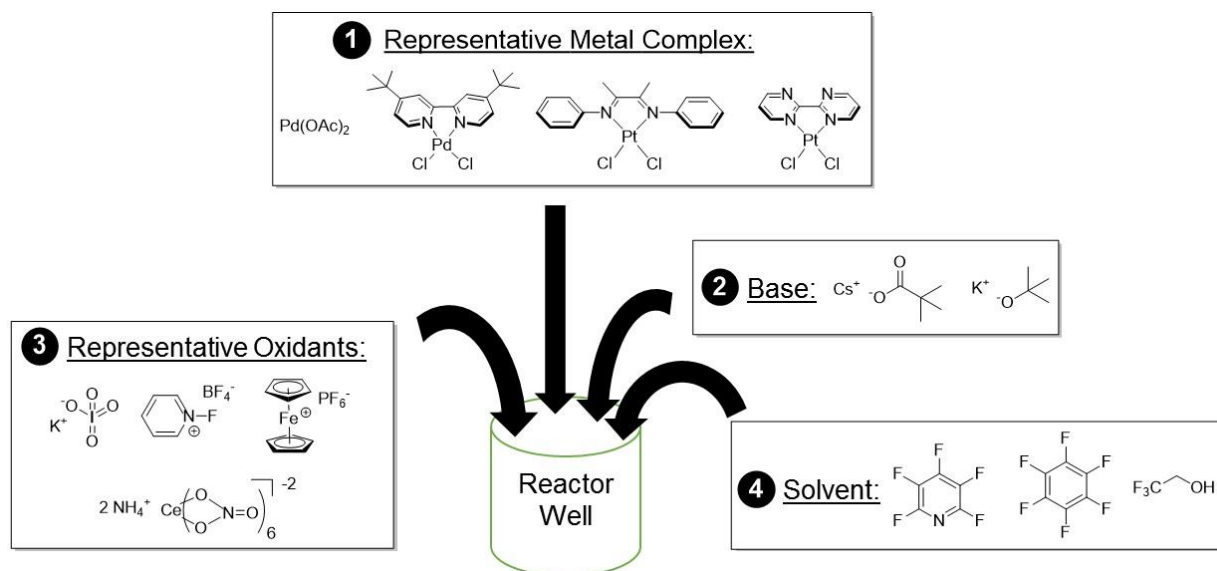
To address the last challenge in the detection of ethane, our collaborators at the University of Washington, specifically Dr. Johanna Blaquiere, conducted a series of tests with mixtures of CH_4 and C_2H_6 . With these studies, Dr. Blaquiere developed a sampling protocol, venting the headspace

⁴ Pictures courtesy of Roxanne Clement, Center for Catalysis Research and Innovation, University of Ottawa

from pressure reactors into gas bags, and subsequent sampling of the gas via a gas tight syringe. The gases in the syringe were then injected onto a Gas Chromatography instrument with a GS-CarbonPLOT column to separate the gaseous components of the reaction mixture. This work established the limits on maximum pressures of methane (10 bar) and minimum catalyst loading of 20 μ moles to ensure reproducible detection of ethane.

Concurrently in the Sanford lab, we focused on the experimental design for the high throughput experimentation (HTE). For these studies, a series of metal complexes and a variety of conditions were chosen based on prior work in our group and others.^{10,12,15,17,22–24} To more efficiently examine a series of reactions, our approach combined several metal complexes under one set of conditions, as previously demonstrated by Wieland and coworkers²⁵. Upon detection of ethane, subsequent studies on individual metal species were used to elucidate the complex generating the highest yields of ethane. Thus, for each experiment, several metal complexes (1) were combined with a base (2), an oxidant (3), an additive, and a solvent (4) in each reactor well, shown in Figure 4.4.

Figure 4.4. Representative Conditions for the Conversion of Methane to Ethane



Each of the four components, metal complex, base, oxidant and solvent (Figure 4.4), were chosen based on rational design for each reaction. For example, several palladium and platinum species were examined in these reactions, as shown in Figure 4.4. These metal complexes were selected based on prior reports of methane activation or methyl coupling, in either stoichiometric or

catalytic studies. These complexes included Pd and Pt salts as well as isolated Pd and Pt complexes bearing mono- and bidentate ligands.

The second component, base was included to drive the methane activation forward by facilitating deprotonation of alkane σ -complex intermediates. Two bases of varying strength, CsOPiv and KO^tBu were selected based on prior use in C–H activation chemistry. The third component, oxidant, was employed to facilitate H₃C–CH₃ reductive elimination from potential M–CH₃ intermediates in this transformation. Based on the studies discussed in Chapter 2, the addition of oxidants allows access to high valent metal intermediates from M^{II}-CH₃ species. These less stable high valent M-CH₃ intermediates then undergo H₃C–CH₃ coupling more easily than the analogous Pd^{III} complex. Oxidants commonly shown to react with palladium and platinum complexes were selected for these experiments.

The fourth component added to the reaction was solvent. Solvent choice is crucial in methane activation reactions due to limited solubility of methane in many polar organic solvents. A number of gases have been shown to have enhanced solubility in fluorinated solvents versus more polar organic solvents.²⁶ Additionally, homogeneous catalysts are likely to activate weaker C–H bonds in solvent molecules over the strong C–H bonds of methane. Thus, we chose a series of fluorinated solvents to mitigate activation of solvent and maximize the solubility of CH₄. In Chapter 3, Ag additives were shown to participate in C–H activation through deprotonation of the substrate or halide abstraction to access a more active catalyst. Thus, 2 equiv of AgOPiv was added to each of the reactions. With these rationally designed reaction conditions in hand, high throughput experiments were conducted on the parallel pressure reactor system.

Experiments were performed over 4 days, slightly modifying conditions based upon the prior day's results, and all results can be seen in the General Experimentation and Characterization section (p 131). Based on prior reports, methane functionalization reactions are conducted under a wide range of conditions including pressures from 1 to 30 bar and temperatures of between 60 - 180 °C. As mentioned previously in this chapter, our HTE reactions were performed at pressures of 10 bar CH₄ based on studies by our collaborators. For these reactions, we chose a temperature regime starting at lower temperatures (50 – 100 °C) with the temperature ramping to 120 – 150 °C after 1 h. We proposed these lower initial temperatures should enable the formation of the active

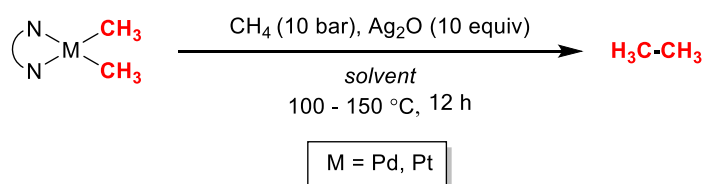
catalysts under these conditions, ultimately reaching higher temperatures required for methane activation. Reactions were conducted under these conditions, and upon completion, the headspace of each was individually vented from the reactor into a gas bag, shown on the right in Figure 4.5. The gas bags were sampled manually via gas-tight syringe and injected into the GC to detect ethane and ethylene. Using these outlined conditions and methods, we conducted a series of reactions at the high throughput facility, analyzing for hydrocarbon gases ethane and ethylene.

Figure 4.5. Sampling of Reaction Headspace from Parallel Reactor to Gas Bag



Initially, we ran a series of control reactions to confirm the detection of ethane using the instrumentation at the high throughput facility. These reactions employed a combination of dimethyl catalysts and oxidants previously shown to liberate ethane¹⁵⁻¹⁷ (Scheme 4.2). As anticipated, ethane was observed from these reactions under 10 bar CH₄, confirming that trace ethane could be detected under these conditions at the high throughput facility.

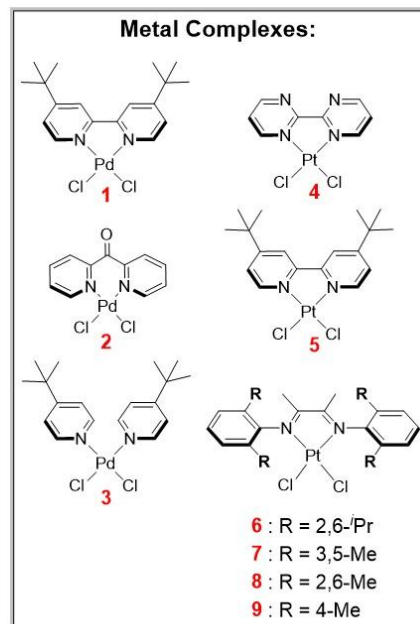
Scheme 4.2. Representative Control Reaction under 10 bar CH₄



Next, reactions were conducted with the four components required to convert methane to ethane. We were pleased to find that ethane was observed from several of reactions containing palladium and platinum dichloride complexes with various oxidants and solvents, shown below in Table 4.1. Interestingly, ethylene was also detected in these reactions, possibly arising from ethane activation and subsequent β -hydride elimination. Due to limited time at the HTE facility, we were unable to conduct the necessary tests to confirm that the observed C_2 products originated from CH_4 . Thus, we sought to follow up these results at our home universities, conducting necessary control reactions and determining the complex affording the highest yields of each C_2 product.

Table 4.1. HTE Hits Generating Ethane and Ethylene

Entry	Metal Complex	Oxidant	Ethane Peak Area	Ethylene Peak Area
1 ^a	1, 2, 3	KIO ₄	0.5	0
2 ^a	1, 2, 3	NOBF ₄	0.5	0
3 ^a	1, 2, 3	N-fluoropyridinium BF ₄	0.5	0
4 ^b	1, 2, 3	N-fluoropyridinium BF ₄	0.5	0
5 ^c	Pd(TFA) ₂ , Pd(OPiv) ₂ , Pd(OAc) ₂	Ag ₂ O	0	1.3
6 ^a	K ₂ PtCl ₆ + tbutylbiscarbene	AgOPiv, KIO ₄	0	1.3
7 ^a	4	N-fluoropyridinium BF ₄	0.5	0
8 ^b	5, 6, 7	Ag ₂ O	0	0.5
9 ^b	5, 6, 7	N-fluoropyridinium BF ₄	0.5	0.5
10 ^d	6, 9	Ag ₂ O	2.4	1.7
11 ^d	4, 8, 9	CAN	1.1	0
12 ^e	6, 9	KIO ₄	1.1	4.8



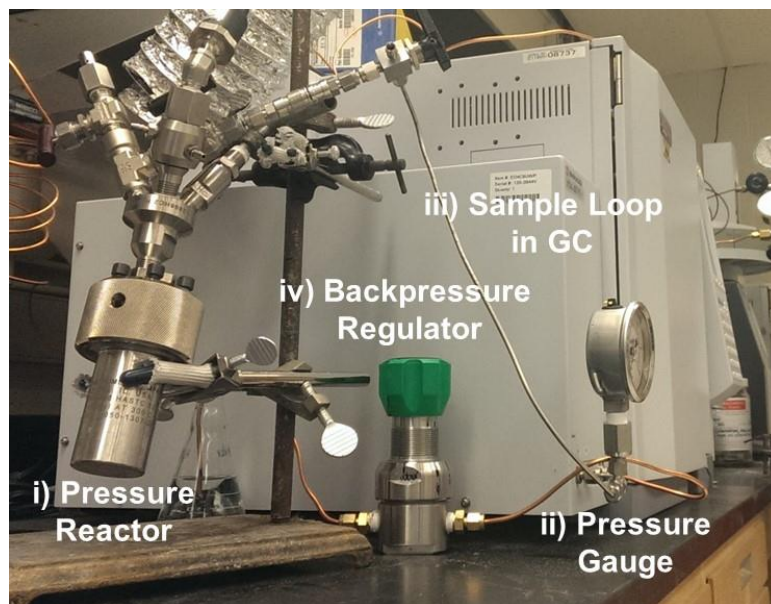
^aConditions: 120°C, 14h, trifluoroethanol; ^bConditions: 150°C, 14h, C₃F₅N; ^cConditions: 150°C, 14h, C₃F₅N : trifluoroethanol (1:9); ^dConditions: 150°C, 14h, trifluoroethanol; ^eConditions: 150°C, 14h, C₃F₅N

Initial work by our collaborators in the Mayer lab further characterized the reaction shown to generate the highest yields of ethane in the high throughput studies (Table 4.1, entry 10). They were able to reproduce the observation of ethane and ethylene from this reaction, and determined that complex **6** generated the highest amount of ethane under these conditions. Based on these

results, we sought to further investigate other reactions shown in the HTE to generate ethane and ethylene.

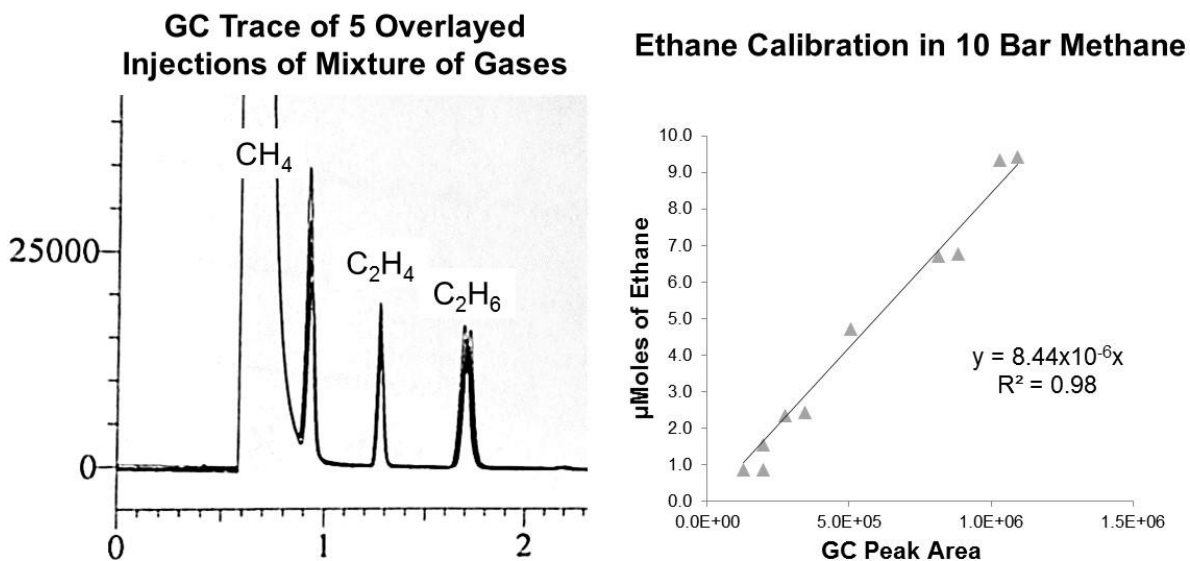
In our lab, we sought to establish a similar method to both conduct and analyze these reactions to convert methane to ethane. We envisioned a system similar to that in the Mayer lab, using Parr® pressure vessels and analyzing products via gas chromatography using a Carbon-PLOT column. However, we included some modifications to enhance the sampling capabilities and more accurately quantify the product yields. Some of the key design criteria included: (a) detection and separation of trace ethane in 10 bar CH₄, similar to studies in the Mayer group; (b) attaining reproducible amounts of sample from each injection; (c) generating accurate and calibrated yields of ethane from reaction mixtures; and (d) sampling of both the headspace (gaseous portion of the reaction) and the solution phase of the reaction, facilitating the collection of kinetic data during the course of the reaction. To design a system meeting these criteria, the following equipment was established with guidance from the Thompson Chemical Engineering Lab at the University of Michigan. Reactions were conducted in 50 mL Parr® pressure vessels, and upon cooling, were connected to a GC instrument via Swagelock® connections (figure 4.6). The headspace from the reactor was sampled through a gas outlet in the pressure reactor (i) that then flowed through a pressure gauge (ii), into a 1 mL sample loop of the GC (iii), and finally through a backpressure regulator (iv), shown in Figure 4.6. The pressure gauge and backpressure regulator ensured that equal pressures of sample filled the sample loop, and thus, controlled the amount of sample injected onto the GC column each time. Components ii and iv were incorporated to ensure reproducibility among injections and facilitate accurate quantification of these gaseous products.

Figure 4.6. Setup for Sampling of Gaseous Products From Pressure Vessel



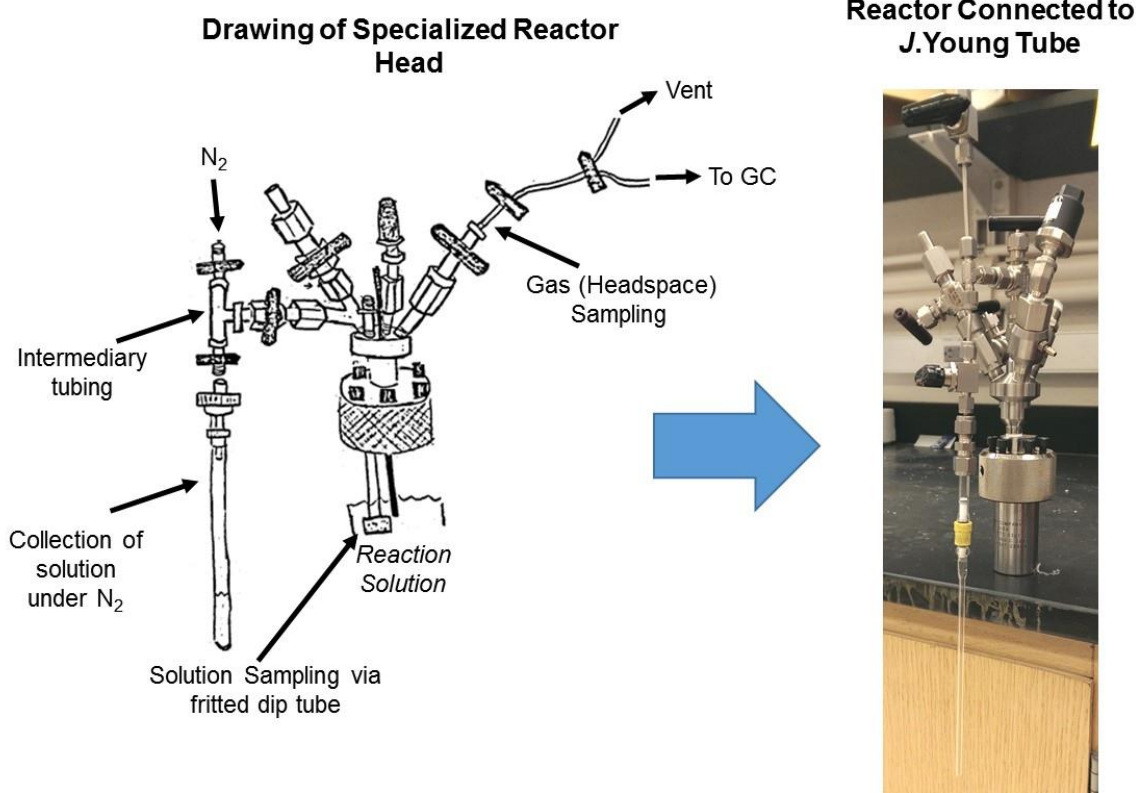
With a method to analyze these reactions in hand, we sought to demonstrate separation of the gaseous mixtures and detection of trace ethane in methane. A mixture of gases containing methane with trace ethane and ethylene was sampled on the newly established system. Before each injection, the sample loop was purged multiple times to ensure that pure sample was injected onto the GC column. As shown in Figure 4.7 (left), ethane and ethylene were observed using an isothermal GC method with good separation among the three gases (see p. 132 for full details). The GC trace shown in Figure 4.7 represents five overlaid injections from the same reactor, showing good reproducibility among the injections. To enable the quantification of gases generated in our reactions, we sought to calibrate this system and fulfill our third requirement. A calibration curve was obtained using a premixed tank of ethane in methane (0.11 wt% ethane in methane), shown in Figure 4.7 (right).

Figure 4.7. Reproducibility of Sampling and Calibration of System



To address our last criteria, we modified a reactor to facilitate sampling of the solution-phase of the reaction via a dip tube (Figure 4.8). A frit was added to the end of the dip tube to prevent particles from clogging the tube. Sampling of the solution was achieved by leveraging the high pressures in the reactor, which forced the reaction solution through the fritted dip tube and into the t-shaped section of tubing, which is closed off from the glass collecting tube. This intermediary tubing was crucial to permit only a small aliquot of the solution to be collected, and prevented overpressurization of the glass collection tube. After the reaction was closed off from the t-shaped tubing, the sample was then collected in the tube (shown here is a J. Young NMR tube) under ambient pressures of N_2 .

Figure 4.8. Modifications to Pressure Vessel to Enable Solution Phase Sampling

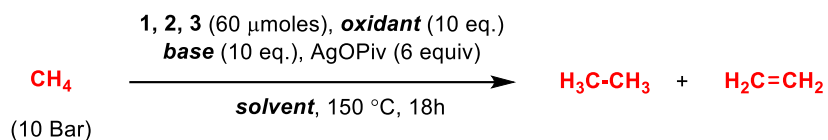


All of these design modifications allowed us to quantitatively analyze reactions to access the conversion of methane to ethane. We have obtained good separation of gaseous mixtures of ethane, ethylene and methane with high sensitivity, detecting $<1 \mu\text{mole}$ of ethane in 10 bar methane. Additionally, this new equipment afforded reproducible sampling of the reaction headspace, providing calibrated yields of ethane from these reactions. Also, modifications included in the pressure reactors facilitated sampling of both the gases in the headspace and solution phase species. Thus, we satisfied all of the criteria for this apparatus, and next sought to quantify yields of ethane from promising HTE results.

Our studies initially focused on reactions shown to generate ethane using Pd complexes (Table 4.1, entries 1-4). These complexes can be easily synthesized from commercially available ligands and palladium dichloride.²⁷⁻²⁹ The purity of these complexes was assessed through ^1H NMR spectroscopy and elemental analysis. Upon subjecting these complexes to the reaction conditions, no ethane or ethylene was observed from any of palladium complexes under conditions from the THE (Table 4.2). Thus, the trace gases we observed during the high throughput experiments appear

to be artifacts from either the reaction setup or some contamination, although further investigation of the source of these false-positive results has not been pursued.

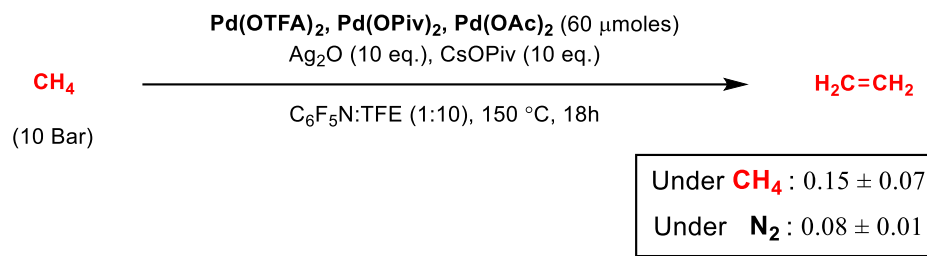
Table 4.2. Ethane and Ethylene Generated using Palladium Complexes



Entry	Oxidant	Base	Solvent	Ethane (μmoles)	Ethylene (μmoles)
1	KIO ₄	CsOPiv	TFE	not observed	not observed
2	NOBF ₄	CsOPiv	TFE	not observed	not observed
3	NFPBF ₄	KO ^t Bu	TFE	not observed	not observed
4	NFPBF ₄	CsOPiv	C ₆ F ₆	not observed	not observed

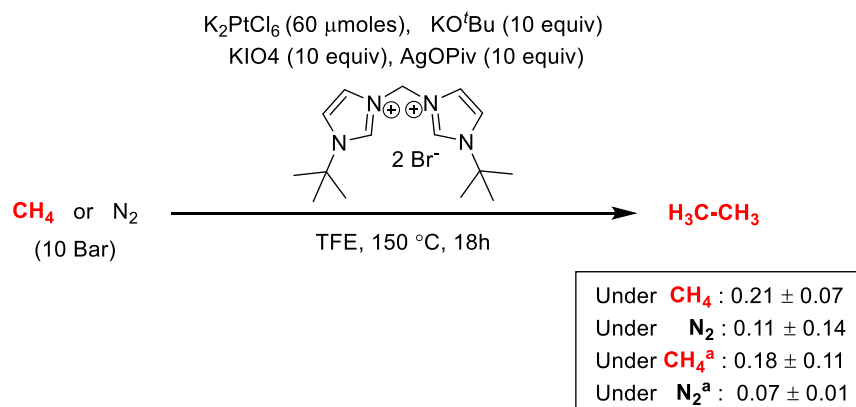
Next, we examined palladium salts in combination with silver oxide as an oxidant (Table 4.1, entry 5). Upon repeating this reaction in triplicate, we observed only ethylene, similar to the results from the high throughput experiments. To elucidate the source of ethylene in these reactions, we ran the reaction under 10 bar N₂ rather than methane, using otherwise analogous conditions. If the ethylene generated in our original conditions was derived from CH₄, then no C₂ products would be expected under N₂. When the reaction was run under nitrogen, the amount of ethylene obtained was within error of the ethylene formed under CH₄ pressures (Scheme 4.3). These results indicate that ethylene is not a result of methane coupling, but potentially generated from a decomposition pathway of the pivalate base or the ligands on palladium.

Scheme 4.3. Ethylene Generated from Palladium Salts, Under CH₄ and N₂ Pressures



We then turned our focus to several results with platinum complexes that generated ethane and ethylene in the high throughput studies. The first result we examined involved potassium hexachloroplatinate (K_2PtCl_6) and a *tert*-butyl biscarbene ligand (Table 4.1, entry 6). To pursue this reaction, we synthesized the carbene ligand based on prior literature reports.³⁰ Subjecting this platinum salt/ligand to conditions analogous to the HTE, we observed only ethane generated under pressures of CH_4 (Scheme 4.4). This result was unexpected as only ethylene was observed during the high throughput experiments under analogous conditions. The reaction was performed under N_2 pressures, resulting in comparable ethane yields to reactions conducted under methane. This suggests the ethylene observed was not derived from CH_4 coupling, but rather a side reaction. Further studies to modify the reaction conditions, such as removal of AgOPiv , did not mitigate the detection of C_2 products in the background reactions (under N_2). This suggests that the ethane is likely derived from ligand decomposition.

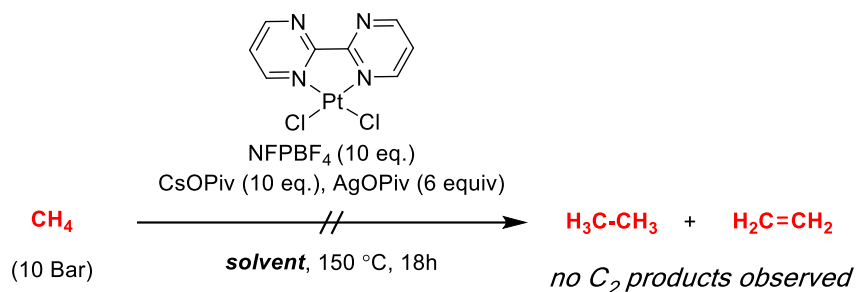
Scheme 4.4. Yields of C₂H₆ and C₂H₄ from K₂PtCl₆ and a Biscarbene Ligand



^aIn the exclusion of AgOPiv

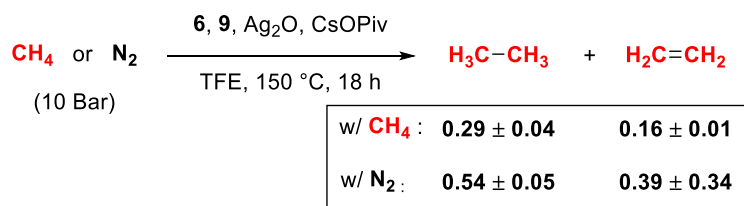
Next, we examined results from the HTE containing preformed Pt species with bidentate nitrogen donor ligands (Table 4.1, entries 7-12). To examine these reactions, we synthesized ligands and complexes using established procedures³¹⁻³³. The structure and purity of these complexes was then determined by ¹H NMR spectroscopy and elemental analysis. Our studies revealed that the reaction of methane with (bipyrimidine)Pt^{II}Cl₂ and N-fluoropyridinium tetrafluoroborate in 2,2,2-trifluoroethanol did not afford any C₂ products (Scheme 4.5). Similar to the results with palladium complexes, we hypothesize that the observed ethane at the high throughput facility was a result of an artifact in the sample preparation or cleaning of the reactors.

Scheme 4.5. Yields of C₂H₄ and C₂H₆ Using (bipyrimidine)Pt^{II}Cl₂



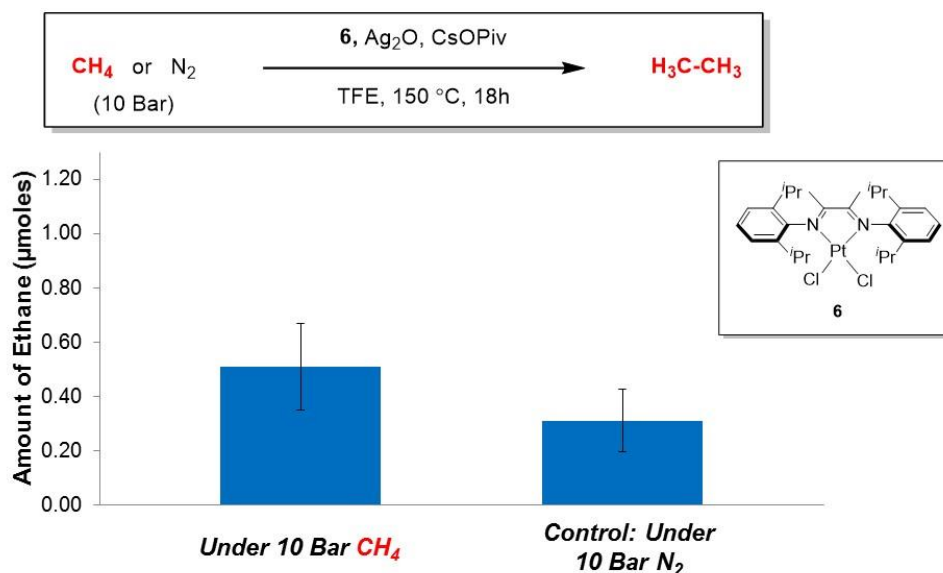
Next, we examined the reaction that generated the highest yields of ethane and ethylene in the HTE, shown in entry 10 (Table 4.1). Upon repeating this reaction, we observed ethane and ethylene using Pt^{II}(DAB) catalysts **6** and **9**, as shown in Scheme 4.6. Notably, significant ethane and ethylene were also observed under pressures of N₂. Thus, we sought to elucidate the source of ethane from this reactions under N₂ before repeating the remaining reactions, all of which contained similar Pt(DAB)Cl₂ complexes. A better understanding of the source of C₂ products under N₂ pressures could provide insight into future efforts to convert methane to ethane.

Scheme 4.6. Generation of C₂H₆ and C₂H₄ Using (DAB)PtCl₂ Complexes



Based on work by our collaborators, complex **6** generated the highest yields of ethane under these conditions. Thus we pursued studies to investigate the background reaction with **6** under N₂ pressures. First, we examined the reactivity of **6** under slightly modified conditions, i.e. higher catalyst loading to more easily detect trace products. The reaction of complex **6** with CH₄ in the presence of Ag₂O in TFE generated 0.5 μmoles of ethane and 0.3 μmoles of ethylene under these modified conditions (Figure 4.9). The analogous reaction was conducted under 10 bar N₂ rather than methane, generating 0.3 μmoles of ethane and 0.2 μmoles of ethylene, confirming a significant background reaction occurs with complex **6**. The yields of both ethane and ethylene from the reaction under CH₄ were within error of those observed under N₂, suggesting these C₂ products were not derived from methane coupling. In further studies, we focused predominantly on elucidating the source of ethane generated in these reaction. Details about the ethylene from these reactions can be found in the General Experimental Procedures and Characterization Section (p. 133).

Figure 4.9. Ethane Generated Using Complex 6 under Pressures of CH₄ and N₂^a



^aConditions: **6** (80 μmoles, 53 mgs, 1 equiv), CsOPiv (187 mgs, 10 equiv), Ag₂O (185 mgs, 10 equiv), CH₄ (10 bar) or N₂ (10 bar), in TFE (2 mL), 150 °C, 18 h.

To mitigate the apparent decomposition of the (DAB)Pt complexes to form ethane, the reactions were examined under reduced temperatures and at shorter reaction times. At 120 °C, we observed reduced ethane generated from reactions with **6** under N₂ pressures (Table 4.3, entries 1-2).

However, we also saw similarly reduced yields of ethane from analogous reactions run under CH₄. At 100 °C, no ethane was detected under CH₄ pressures, and thus reactions under N₂ were not performed (entry 4). Additionally, the reaction with **6** under N₂ was stopped after 3 h and 6 h, affording comparable ethane as detected at 18 h (see p. 133). Thus, it appears this side reaction to generate ethane occurs rapidly but diminishes at lower temperatures, and ethane yields from reactions under CH₄ also diminish with lowered temperatures. Lower temperatures or shorter reaction times were not effective in inhibiting this side reaction without also reducing reactivity under CH₄. We next sought to identify the source of ethane to better understand and inhibit this background reaction.

Table 4.3. Modifying Conditions to Impede Formation of Ethane Under N₂

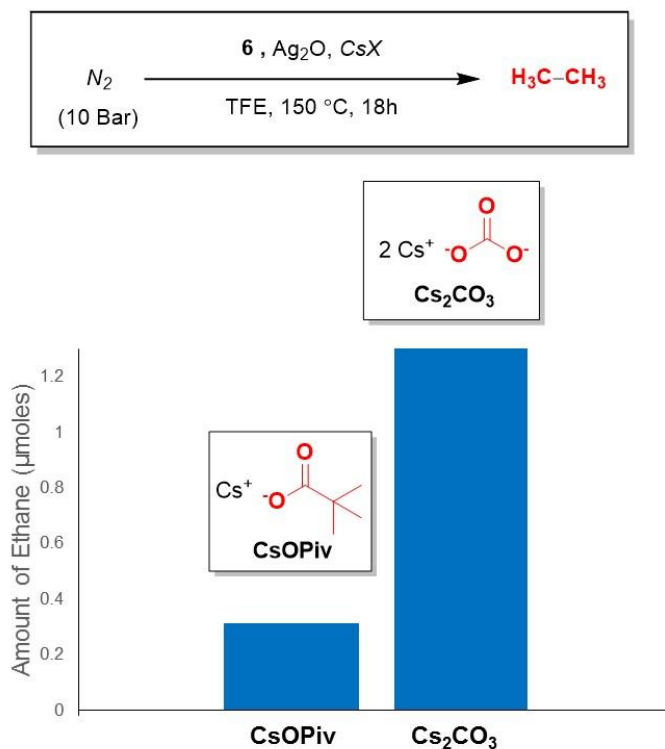
CH₄ or N ₂ (10 Bar)	$\xrightarrow[\text{TFE, } T \text{ } ^\circ\text{C, 18h}]{\text{6 (80 } \mu\text{moles), Cs}_2\text{CO}_3 \text{ (10 equiv)}Ag_2O \text{ (10 equiv)}}$	H₃C-CH₃
---	---	--------------------------------------

Entry	CH ₄ or N ₂	Temperature	Ethane (μ moles)
1	N ₂	150 °C	1.33
2	N ₂	120 °C	0.44
3	CH ₄	120 °C	0.07
4	CH ₄	100 °C	not detected

To investigate the source of ethane, we examined each of the components in the reaction, specifically those likely to generate ethane upon decomposition. A series of reactions were conducted under 10 bar N₂, systematically modifying the base and the ligand scaffold of complex **6**. First, we studied the pivalate base, modifying CsOPiv to Cs₂CO₃ under otherwise analogous conditions. This variation should not significantly impact the basicity or the solubility under these conditions, however, the degradation of carbonate should result in significantly different products than that of pivalate. We proposed diminished yields of ethane would be observed with this modification if ethane is derived from pivalate base. Interestingly, when the reaction was

conducted with Cs_2CO_3 under N_2 , higher amounts of ethane were observed, shown in Figure 4.10. This suggests that the background reaction does not arise from decomposition of the pivalate base.

Figure 4.10. Probing the Background Reaction – Modification of the Base

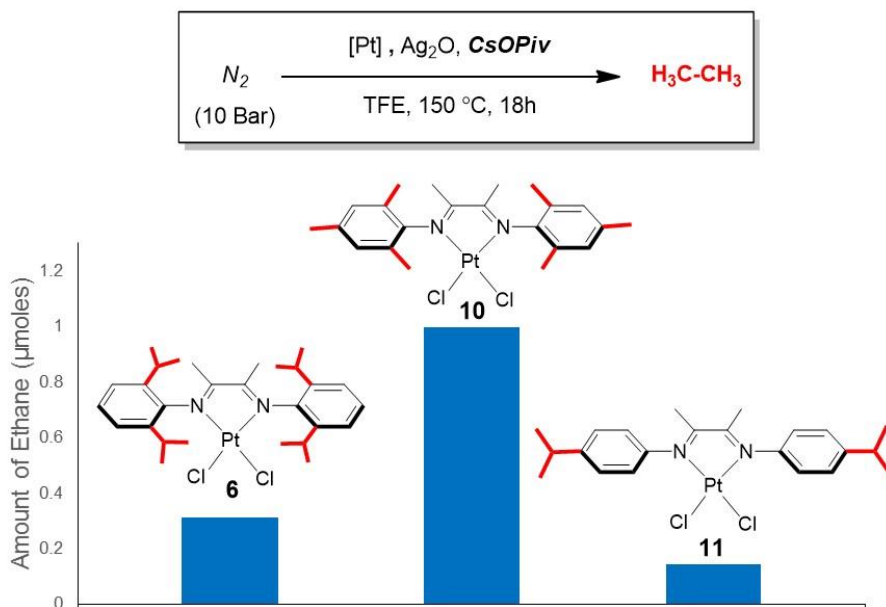


We next looked to the modification of complex **6**, or more specifically the ligand scaffold. Complex **6** could decompose in at least two ways: (i) decomposition of the isopropyl substituent on the aryl ring, or (ii) degradation of the diimine backbone. Hence, we synthesized a series of platinum complexes with modified ligands to inhibit degradation at each of these positions.

To address the possibility of ethane formation via degradation at the *o*-isopropyl groups, the analogous mesityl complex **10** and *p*-isopropyl species **11** were synthesized based on prior reports^{31,33,34} of similar complexes. Decomposition involving activation of the isopropyl substituent could occur, thus modification of the *ortho*-isopropyl groups on the aryl ring could help suppress this background reaction. Complex **10** has similar solubility to **6**, but with *ortho*-methyl groups which have an increased distance from the Pt metal center to prevent activation. Complex

11 also has comparable solubility but contains no alkyl substituents at the ortho-positions of the aryl ring. Thus, complex **10** and **11** were subjected to the reaction conditions, under 10 bar N₂, and the headspace was analyzed using the previously mentioned GC techniques. Both complex **10** and **11** resulted in similar or increased amounts of ethane compared to reactions with **6**. These data suggest that decomposition of the ortho-isopropyl substituents on the aryl ring of **6** does not significantly contribute the background reaction (Figure 4.11).

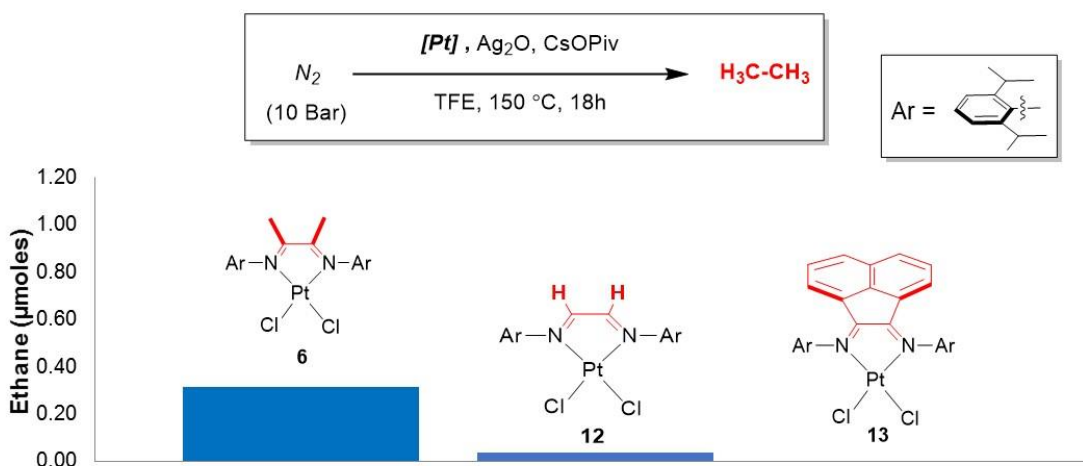
Figure 4.11. Methods for Modification of the Aryl Substituent of 6 to Inhibit the Observed Background Reaction



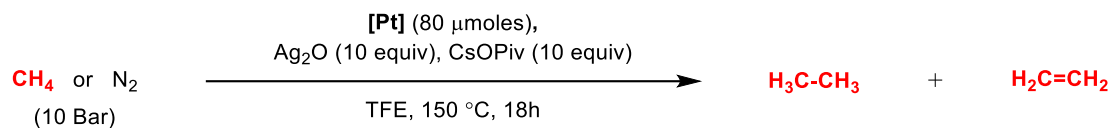
Next, we examined alterations of the diimine backbone to inhibit the formation of ethane in reactions conducted under N₂. Thus, the methyl groups on the backbone were changed to a smaller hydrogen substituents. This change should affect the products generated in decomposition of the ligand backbone, resulting in reduced amounts of ethane. The complex (**12**) was synthesized based on previous reports,³³ and characterized by ¹H NMR spectroscopy and elemental analysis. Complex **12** was subjected to the reaction conditions under 10 bar of N₂. Gratifyingly, a significantly lower amount of ethane, 0.03 μmoles, was observed in reactions containing **12**, shown in Figure 4.12, suggesting that degradation of the backbone generates ethane under these conditions. To gain evidence in support of this proposal, complex **13**, bearing a larger, more

hindered fused naphthyl backbone was synthesized. This complex could also mitigate ethane formation by inhibiting the degradation of the ligand backbone. Subjecting **13** to similar reaction conditions under 10 bar of N₂ resulted in no detectable formation of ethane (Figure 4.12). Thus, these studies strongly suggest that the ethane observed in these background reactions derives from degradation of the ligand backbone. However, further work to elucidate the mechanism of decomposition has not been conducted.

Figure 4.12. Modifications in the Backbone of the Ligand Scaffold for **6 to Minimize the Background Ethane Observed.**



Moving forward, we pursued further studies with these complexes shown to exhibit a limited background reaction under N₂. Preliminary studies with both **12** and **13** afforded only trace ethane and ethylene under CH₄ pressures. However, further studies with **12** and **13** using other oxidants, bases and solvents could be pursued to generate higher yields of ethane and ethylene.

Table 4.4. Ethane and Ethylene Observed from **12 and **13** under CH₄ and N₂**

Entry	Complex	CH ₄ or N ₂	Ethane (μmoles)	Ethylene (μmoles)
1	12	CH ₄	0.06	0.07
2	12	N ₂	0.03	0.03
3	13	CH ₄	0.06	0.07
4	13	N ₂	not detected	not detected

After elucidating the main source of ethane in these background reactions conducted under N₂ pressures, further investigation into the conversion of methane to ethane could be pursued with metal complexes containing modified backbone functionality, such as **12**, **13** and **14** ((^{Mes}DAB^H)PtCl₂). Further ligand design to generate complexes less likely to form C₂ products upon decomposition, such as with trifluoromethyl substituents, could also be pursued in this transformation.

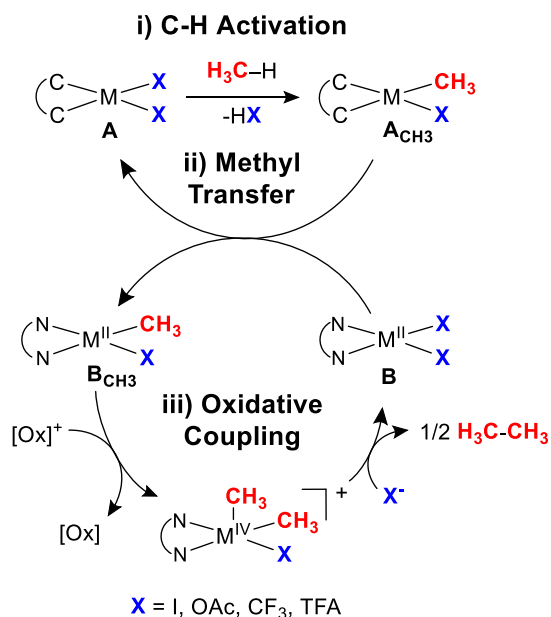
Conclusions

From this work, we have identified a series of reactions from high throughput experimentation that resulted in ethane and ethylene. Furthermore, we established a method to efficiently analyze and quantify the products of these reactions, through gaseous headspace and solution-phase sampling techniques. With these developments, we have pursued several of the HTE reactions shown to generate ethane and ethylene, identifying and mitigating a background reaction observed with several of the diimine ligands. Interestingly, these diimine ligands have been used by Bercaw and others in stoichiometric studies of methane functionalization, however, to our knowledge there are no reports of this decomposition pathway to generate ethane.^{24,32,33,35} Overall, these studies could provide insight into ligand design in future studies on methane functionalization.

Future Directions

In pursuing future routes to methane oligomerization, the activation of methane remains a challenge. To achieve this key C–H activation step, one alternate approach could combine two catalysts, **A** and **B**, in a tandem process, as shown in Scheme 4.7. This type of process would involve: (1) activation of methane by complex **A** to form **A**CH₃; (2) subsequent methyl transfer from complex **A**CH₃ to complex **B**, resulting in **B**CH₃; and (3) oxidation/reductive elimination at **B**CH₃ to generate ethane. Using this system, the most proficient metal complexes could be chosen for each step, circumventing the requirement for one catalyst to efficiently perform all of the steps in the catalytic cycle. Additionally, improvement of each step could be achieved by tuning complex **A** and **B** independently to improve both methane activation and C–C reductive elimination.

Scheme 4.7. A Tandem Catalytic Approach to Methane Coupling



Initially, we would envision applying complexes previously demonstrated to achieve each step of this process to the tandem catalytic cycle. For example, several palladium and platinum complexes have been used in methane functionalization reactions or H/D exchange studies with methane, implicating their propensity for the methane activation. Thus, similar complexes could

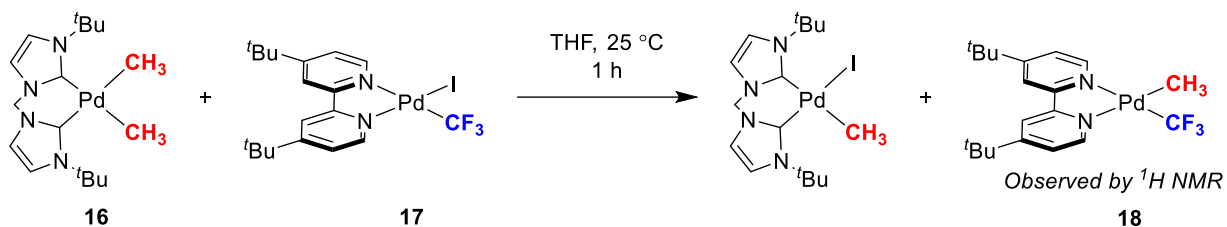
be employed in this tandem system as **A**, for methane activation step. In Chapter 2, we demonstrated generation of ethane from the oxidation of Pd^{II}-CH₃ species. Additional work in our group^{15,16} and others^{19,20,35} has shown the oxidation of dimethyl Pd and Pt species under mild conditions also generates ethane. Based on this work, similar catalysts for **B** would be promising in facilitating the oxidative coupling.

One main challenge introduced with tandem catalysis involves methyl transfer between two different metal centers, proceeding from **A** to **B**. To address this, stoichiometric studies on this methyl transfer could provide optimal conditions and metal complexes for the overall transformation to generate ethane. Insight gained from stoichiometric work could be applied to catalytic studies to convert methane to ethane.

To explore methyl transfer between **A** and **B**, we conducted very preliminary stoichiometric studies with a biscarbene Pd complex (**16**) and tppy Pd complex (**17**), representing ACH₃ and **B**, respectively. Complex **16** was chosen for ACH₃ as biscarbene Pd complexes analogous to **16** have been used in the partial oxidation of methane, a process that is believed to involve initial methane activation.¹² Thus, biscarbene Pd complexes similar to **16** could be promising as catalyst **A** in this tandem system. In Chapter 2, we have shown that the treatment of **18** with 1 and 2 *e*⁻ oxidants affords ethane in good yields. As **18** has been shown in the oxidative coupling to access ethane, this complex likely could perform as catalyst **B** in the tandem system. With these two promising complexes representing **A** and **B**, we wanted to examine the methyl transfer step from **16** to **17**, required to realize a tandem approach.

In preliminary studies, **16** and **17** were combined under mild conditions, affording complex **18** after 1 h. This reaction provides some initial proof-of-principle for the methyl transfer step, however further mechanistic studies will provide necessary insight to achieve methane coupling with a tandem system. Using complexes similar to **16** and **17**, tandem catalysis could provide a promising alternate route to methane coupling.

Scheme 4.8. Tandem Catalysis to Convert Methane to Ethane

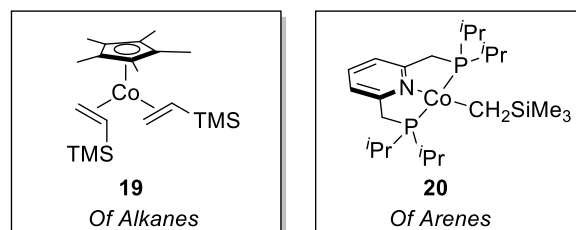


Another approach to address the challenge of methane activation would employ the use of other metal centers. A number of metal complexes have been shown to perform alkane functionalization,^{36–38} and perhaps the different properties of these metal centers could be exploited in methane activation. For example, cobalt complexes have been shown to facilitate both C–H activation of alkanes and oxidative coupling to generate ethane.^{39–41} Thus, application of similar cobalt complex to our proposed catalytic cycle could provide an alternate route to methane coupling with Pd or Pt species.

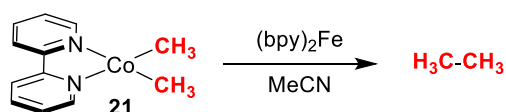
Based on prior reports, cobalt complexes can facilitate the non-directed C–H activation of arenes and alkanes. Brookhart and coworkers demonstrated C–H activation of alkanes with **19**, to access alkane dehydrogenation products.³⁹ Additionally, cobalt pincer complexes such as **20** have been shown by Chirik⁴² to facilitate borylation of benzene, proposed to proceed through oxidative addition of the C–H bond. Thus, similar bidentate and tridentate cobalt complexes could be applied to methane activation in our catalytic cycle. Furthermore, stoichiometric studies^{41,41} with Co^{III} - CH_3 species, such as **21**, have selectively afforded ethane, as shown in Figure 4.1. Based on these precedents, similar cobalt complexes containing bidentate or pincer ligands could be used in efforts to oxidatively couple methane.

Figure 4.13. Precedents for Cobalt Mediated C–H Functionalization and H₃C–CH₃ Coupling

For C–H Activation/Functionalization:



For H₃C–CH₃ Reductive Elimination:



General Experimental Procedures and Characterization

General Instrumentation.

NMR spectra were obtained on Varian vnmrs 700 (699.76 MHz for ¹H; 175.95 MHz for ¹³C), Varian vnmrs 500 (500.1 MHz for ¹H; 125.75 MHz for ¹³C), Varian MR 400 (400.52 MHz for ¹H; 125.70 MHz for ¹³C; 376.87 MHz for ¹⁹F) or Varian Inova 500 (499.90 MHz for ¹H) spectrometers. ¹H and ¹³C chemical shifts are reported in parts per million (ppm) relative to the referenced solvent peak. Multiplicities are reported as singlet (s), doublet (d), triplet (t), quartet (q), doublet of doublets (dd), heptet (h) and multiplet (m). Gas chromatography was carried out on a GC-FID (Shimadzu GC-2010 Plus) using a 1 mL sample loop and a GS-CarbonPLOT (30 m, 0.32 mm ID, 3.00 μm df,) column obtained from Agilent with high purity helium as the carrier gas. In all reactions, the back-pressure regulator was set at atmospheric pressure. The method for analyzing gases utilized a split injection (20:1) and an isothermal method (60 °C, 5 min) with an FID detector (250 °C). GC yields were calibrated based on a mixed tank of ethane in methane (0.11%), obtained from Metro Welding. All pressure reactions were prepared in an N₂-filled glovebox, sealed, and then pressurized with N₂ or CH₄. The synthesis of metal complexes was conducted in air, and the complexes were dried overnight under vacuum before transferring into the glovebox.

Materials and Methods

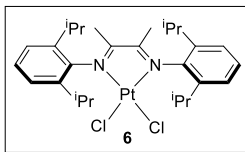
Acetone, dichloromethane, methanol, pentanes and tetrahydrofuran were obtained from Fisher Scientific or VWR and used without further purification. All deuterated solvents were obtained from Cambridge Isotope Laboratories and used without further purification., 2,3-butanedione (Alfa Aesar), cesium carbonate (Aldrich), cesium pivalate (Aldrich), hexafluorobenzene (TCI), 4-isopropyl aniline (Aldrich), N-fluoropyridinium tetrafluoroborate (TCI), palladium acetate (Pressure Chemical), palladium pivalate (Aldrich), palladium trifluoroacetate (Strem), pentafluoropyridine (Matrix), potassium hexachloroplatinate (Pressure), potassium periodate (Aldrich), potassium *t*-butoxide (Acros), silver oxide (Acros), 2,2,2-trifluoroethanol (Alfa Aesar) and Zeise's dimer (Strem) were obtained from commercial vendors and used without further purification. Silver pivalate was prepared based on literature procedure.

Synthesis and Characterization of Complexes

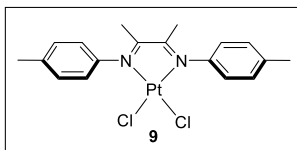
Diimine ligands (*oiPr*DAB^{Me}),⁴³ (*oiPr*DAB^H),⁴⁴ (*oiPr*DAB^{Nap}),⁴⁵ (*oMe*DAB^{Me}),²⁴ (*mMe*DAB^{Me}),²⁴ (*pMe*DAB^{Me}),⁴⁶ (*Mes*DAB^{Me}),²⁴ and (*Mes*DAB^H)⁴⁷ were synthesized based on precedent reports. The palladium and platinum complexes (4,4'-di-*tert*-butyl-2,2'-bipyridine)PdCl₂ (**1**),²⁷ (dipyridyl ketone)PdCl₂ (**2**),²⁸ (4-*tert*-butylpyridine)₂PdCl₂ (**3**),²⁹ (2,2'-bipyrimidine)PtCl₂ (**4**),⁴⁸ (4,4'-di-*tert*-butyl-2,2'-bipyridine)PtCl₂ (**5**),⁴⁹ (*mMe*DAB^{Me})PtCl₂ (**7**),³³ and (*oMe*DAB^{Me})PtCl₂ (**8**)³⁴ were prepared based on literature procedures.

General procedure for synthesis of DABPtCl₂ complexes

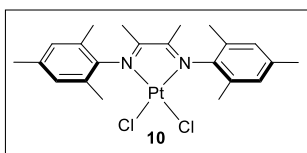
The synthesis of Pt complexes is based on established procedures for the synthesis of (*mMe*DAB^{Me})PtCl₂ (**7**).³³ Zeise's dimer [(C₂H₄)PtCl₂]₂ (1 equiv) was suspended in THF at 25 °C, resulting in an orange solution after 10 m. Diimine ligand (2 equiv) was then added to the suspension and the solution was stirred at 25 °C for 24 h, affording a color change (dark red or brown depending on the ligand). The solution was then concentrated to 0.5 mL and 10 mL of pentanes was added to precipitate the product. The solids were collected on a glass frit and dried overnight under vacuum.



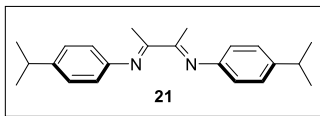
(*oiPrDABMe*)PtCl₂ (6). A brown powder (167 mgs, 74% yield) was isolated. ¹H NMR (401 MHz, 298 K, Acetone-*d*₆) δ 7.50 – 7.16 (m, 6H), 3.19 (h, *J* = 7 Hz, 4H), 1.95 (s, 6H), 1.40 (d, *J* = 7 Hz, 12H), 1.18 (d, *J* = 7 Hz, 12H). Elemental Analysis: calculated for C₂₈H₄₀Cl₂N₂Pt, C: 50.15, H: 6.01, N: 4.18; Found: C: 49.98, H: 5.95, N: 4.12.



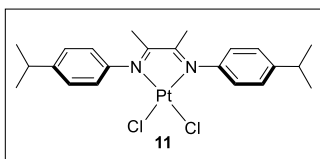
(*pMeDABMe*)PtCl₂ (9). A brown powder (115 mgs, 36% yield) was isolated. ¹H NMR (700 MHz, 298 K, Acetone-*d*₆) δ 7.30 (d, *J* = 8 Hz, 4H), 7.03 (d, *J* = 8 Hz, 4H), 2.37 (s, 6H), 1.81 (s, 6H). ¹³C NMR (176 MHz, 298 K, DMSO-*d*₆) δ 180.43, 142.92, 137.10, 128.84, 123.15, 20.71, 20.58.



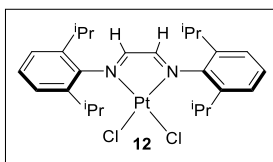
(*MesDABMe*)PtCl₂ (10). A brown powder (182 mgs, 47% yield) was isolated. ¹H NMR (401 MHz, 298 K, Acetone-*d*₆) δ 6.52 (s, 4H), 1.83 (s, 6H), 1.70 (s, 12H), 1.28 (s, 6H). ¹³C NMR (175.95 MHz, 298 K, DMSO-*d*₆): 180.42, 141.02, 136.53, 129.61, 128.28, 20.51, 19.16, 17.08.



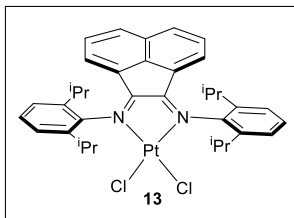
(*piPrDABMe*) (21). Dissolved *para*-isopropyl aniline (0.73 mL, 5.3 mmol, 2 equiv), 2,3-butanedione (0.23 mL, 2.7 mmol, 1 equiv) and trifluoroacetic acid (3 drops) in methanol (10 mL) and let stand at 25 °C for 6 h. The precipitate was isolated on a glass frit and washed with additional methanol. A yellow powder (424 mgs, 50% yield) was collected. ^1H NMR (700 MHz, 298 K, Acetone- d_6) δ 7.27 (d, $J = 8$ Hz, 4H), 6.76 (d, $J = 8$ Hz, 4H), 2.92 (hept, $J = 7$ Hz, 2H), 2.12 (s, 6H), 1.24 (d, $J = 7$ Hz, 12H). ^{13}C NMR (176 MHz, 298 K, Acetone- d_6) δ 168.65, 149.88, 145.05, 127.65, 119.74, 34.33, 24.46, 15.32.



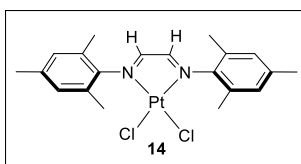
(*piPrDABMe*)PtCl $_2$ (11). A yellow powder (296 mgs, 51% yield) was isolated. ^1H NMR (700 MHz, 298 K, DMSO- d_6) δ 7.37 (d, $J = 8$ Hz, 4H), 7.08 (d, $J = 8$ Hz, 4H), 2.97 (hept, $J = 7$ Hz, 2H), 1.80 (s, 6H), 1.25 (d, $J = 7$ Hz, 12H). ^{13}C NMR (175.97 MHz, 298 K, DMSO- d_6) δ 180.48, 147.78, 143.17, 126.15, 123.23, 32.98, 23.74, 20.66.



(*oiPrDABH*)PtCl $_2$ (12). A red-brown powder (62 mgs, 91% yield) was isolated. ^1H NMR (401 MHz, Acetone- d_6) δ 9.82 (s, 2H), 7.96 – 7.69 (m, 6H), 3.80 (h, $J = 7$ Hz, 4H), 1.84 (d, $J = 7$ Hz, 12H), 1.65 (d, $J = 7$ Hz, 12H). ^{13}C NMR (175.97 MHz, 298 K, DMSO- d_6) δ 183.38, 140.89, 132.94, 129.07, 123.30, 28.04, 24.21, 23.08.



(oiPrDAB^{Naph})PtCl₂ (13). A dark red powder (232 mgs, 90% yield) was isolated. ¹H NMR (700 MHz, 298 K, Acetone-*d*₆) δ 8.07 (d, *J* = 8 Hz, 2H), 7.19 (t, *J* = 8 Hz, 2H), 7.13 (t, *J* = 8 Hz, 2H), 7.02 (d, *J* = 8 Hz, 4H), 6.13 (d, *J* = 7 Hz, 2H), 2.99 (hept, *J* = 7 Hz, 4H), 0.92 (d, *J* = 7 Hz, 12H), 0.46 (d, *J* = 7 Hz, 12H). ¹³C NMR (175.97 MHz, 298 K, DMSO-*d*₆) δ 176.84, 146.15, 140.48, 140.10, 132.11, 132.79, 130.02, 129.42, 125.68, 124.27, 123.73, 28.05, 23.58, 23.38.



(MesDAB^H)PtCl₂ (14). (SMe₂)₂PtCl₂ complex (200 mgs, 0.51 mmol, 1 equiv) was dissolved in acetone (10 mL) and the DAB ligand (165 mgs, 0.56 mmol, 1.1 equiv) was added to solution. The reaction was stirred at 25 °C for 24 h and then concentrated to ~0.5 mL. Pentanes (10 mL) was added and the solution was cooled to -33 °C to precipitate out the product. A brown powder (223 mgs, 78% yield) was isolated on a glass frit. ¹H NMR (500 MHz, 298 K, DMSO-*d*₆) δ 9.00 (s, 2H), 6.98 (s, 4H), 2.29 (s, 6H), 2.21 (s, 12H).

General Procedure for High Throughput Experiments

All solids were weighed out into 5 mL glass liners in the N₂-filled glovebox. The well of each reactor was then filled with 0.1 mL of solvent, followed by insertion of the glass liner into the well. Solvent was added outside the liner to prevent evaporation of the solvent from the reaction inside the liner. Subsequently, the reactors were sealed and pressurized with N₂ to ensure each reactor maintained pressure. If any of the reactors failed to hold pressure, the o-ring inside the reactor was replaced and this test was repeated. The N₂ pressure was vented and the reactors were pressurized

with 10 bar CH₄. Then approximately 2 mL of solvent was added to the pressurized reactions, and the reactors were heated to the appropriate temperatures. On day 1 – 3 of HTE studies, the reactors were heated at 50 °C for 1 h and then the temperature was increased to 120 °C for 12 -13 h. On the final day of experiments, the temperature was modified to 100 °C for 6 h and 150 °C for 6 additional hours, to attain more methane activation at higher temperatures. The reactors were then cooled to 25 °C over 3 h and sampled.

General Procedure for Sampling of Headspace for HTE

The sampling of each headspace was performed in a similar manner to the procedures established by our collaborators, Dr. Johanna Blaquiere and Dr. James Mayer. Each reactor was vented directly into a gas bag, and the reactor was then pressurized with 10 bar N₂ and vented into the same bag to flush out any remaining gaseous products in the reactor. A gas tight needle was used to remove 10 µL of the gaseous mixture via a septum on the gas bag. The gaseous mixture was then manually injected into the GC instrument, using an J&W Carbon-PLOT column.

Figure 4.14. HTE Generating C₂ Products

Entry	Metal Complex	Oxidant	Ethane Peak Area	Ethylene Peak Area
1 ^a	1, 2, 3	KIO ₄	0.5	0
2 ^a	1, 2, 3	NOBF ₄	0.5	0
3 ^a	1, 2, 3	N-fluoropyridinium BF ₄	0.5	0
4 ^b	1, 2, 3	N-fluoropyridinium BF ₄	0.5	0
5 ^c	Pd(TFA) ₂ , Pd(OPiv) ₂ , Pd(OAc) ₂	Ag ₂ O	0	1.3
6 ^a	K ₂ PtCl ₆ + tbutylbiscarbene	AgOPiv, KIO ₄	0	1.3
7 ^a	4	N-fluoropyridinium BF ₄	0.5	0
8 ^b	5, 6, 7	Ag ₂ O	0	0.5
9 ^b	5, 6, 7	N-fluoropyridinium BF ₄	0.5	0.5
10 ^d	6, 9	Ag ₂ O	2.4	1.7
11 ^d	4, 8, 9	CAN	1.1	0
12 ^e	6, 9	KIO ₄	1.1	4.8
13	Control: (^{Ar} DAB ^{Me})Pt(CH ₃) ₂ , (Ar = mCF ₃)	Ag ₂ O	5.9	1.1
14	Control: (^{Ar} DAB ^{Me})Pt(CH ₃) ₂ , (Ar = mCF ₃)	Ag ₂ O	3.2	1.2
15	Control: (^{Ar} DAB ^{Me})Pt(CH ₃) ₂ , (Ar = mCF ₃)	Ag ₂ O	6.7	1.5
16	Control: (Tetramethylethylenediamine)Pd(CH ₃) ₂	Ag ₂ O	9.5	0
17	Control: (1,5-cyclooctadiene)Pt(CH ₃) ₂	Ag ₂ O	7.2	13.1
18	Control: (1,5-cyclooctadiene)Pt(CH ₃) ₂	KIO ₄	165.4	1.9
19	Control: (C ₂ H ₄)PdCl ₂	Ag ₂ O	1.2	185.7
20	Control: (C ₂ H ₄)PdCl ₂	Ag ₂ O	2.1	170.7
21	Control: Pt(OAc) ₂ , (C ₂ H ₄)PdCl ₂	Ag ₂ O, KIO ₄	1.4	22.2

Metal Complexes:

6 : R = 2,6-Pr
7 : R = 3,5-Me
8 : R = 2,6-Me
9 : R = 4-Me

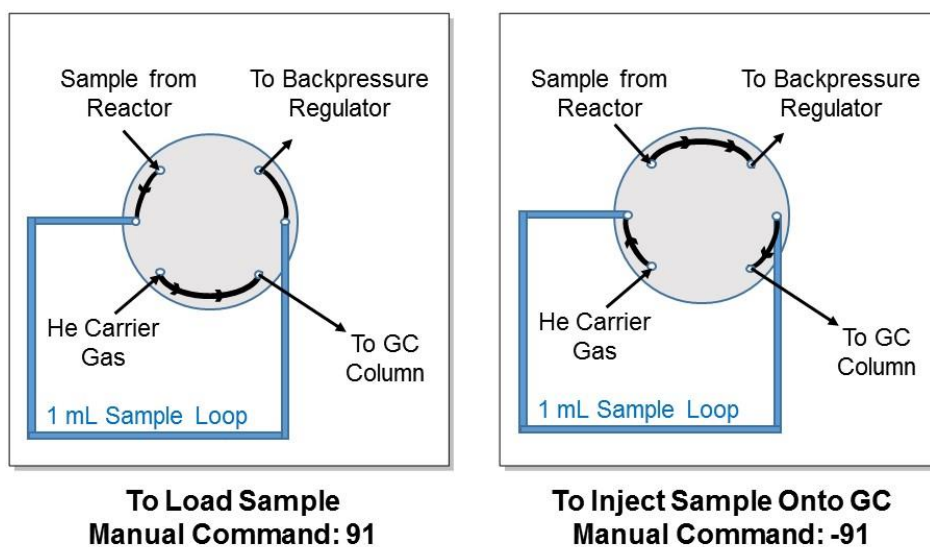
General Procedure for Conversion of CH₄ to C₂H₆ Conducted in the Sanford Lab

All components of the reaction were dried overnight under reduced pressure before transferring into the glovebox. To prevent background contamination, the Hastelloy® well, glass liner, and Teflon® stirbar were dried in the oven for at least 3 h, and then pumped into the glovebox while still hot. All reactions were prepared in an N₂-filled glovebox. The metal complex (60 μmoles), oxidant (600 μmoles, 10 equiv), base (600 μmoles, 10 equiv) and AgOPiv (126 μmoles/ complex, 2.1 equiv/complex) were weighed into the glass liner. Dry solvent (2 mL) was added to the glass liner along with ~5 mL of solvent in the well to prevent the reaction from drying out. The glass liner was then inserted into the well of the reactor, and sealed before removing the pressure vessel from the glovebox. Each vessel was then pressurized with 10-12 bar of CH₄, and heated to 165 °C on a custom built aluminum block (to reach an internal temperature of 150 °C). The vessels were stirred at 165 °C for 18 h, then removed from the heating block and submerged in ice until reaching 25 °C. The cooled reactors were sampled via GC-FID using a GS carbon-PLOT column. Each reaction was performed in duplicate or triplicate.

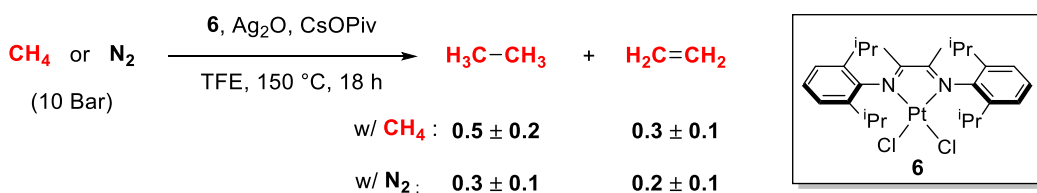
General Procedure for Sampling of Headspace in the Sanford Lab (Modified System)

Each reactor was directly connected to the GC sample loop via Swagelok® quick-connect fittings and vented into a section of tubing closed off from the GC by a two-way valve. The reactor was then closed and the sample in the tube was released into the GC sample loop upon opening the two way valve. This step is repeated 10 times to ensure a complete purge of the prior sample. The sample loop must be in the correct position to allow the sample to flow into the loop (position 91). The GC program includes the switching of the sample loop between the two positions (-91 inject to column, 91 load), however it can be manually changed using the function button, pressing 5 and then 91 enter to access the load position. After the sample is purged through the sample loop, the green start button must be pressed to turn the sample loop and inject the sample onto the GC column. The yield from each reactor is an average of 5 injections.

Figure 4.15. Diagram of the Sample Loop on the GC-2010 Plus



Scheme 4.9. Ethane and Ethylene Generated from **6** Under Pressure of CH₄ or N₂



General Procedure for Investigating Background C₂ Products

All components of the reaction were dried overnight under reduced pressure before transferring into the glovebox. To prevent background contamination, the Hastelloy® well, glass liner, and Teflon® stirbar were dried in the oven for at least 3 h, and then pumped into the glovebox while still hot. All reactions were prepared in an N₂-filled glovebox. The platinum complex (80 μmoles), Ag₂O (184 mgs, 800 μmoles, 10 equiv) and CsX (800 μmoles, 10 equiv) were weighed into the glass liner. Dry 2,2,2-trifluoroethanol (2 mL) was added to the glass liner along with ~5 mL of solvent in the well to prevent the reaction from drying out. The glass liner was then inserted into the well of the reactor, and sealed prior to removing the pressure vessel from the glovebox. Each vessel was then pressurized with 10-12 bar of CH₄ or N₂, and heated to 165 °C on an custom built aluminum block (to reach an internal temperature of 150 °C). The vessels were stirred at 165 °C for 18 h, then removed from the heating block and submerged in ice until reaching approximately 25 °C. The cooled reactors were sampled via GC-FID using a GS carbon-PLOT column. Each reaction is performed in duplicate.

Scheme 4.10. Ethane and Ethylene Generation from Complex 6 at Reduced Times

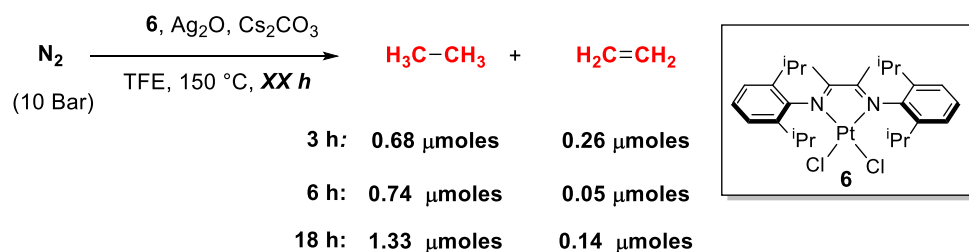


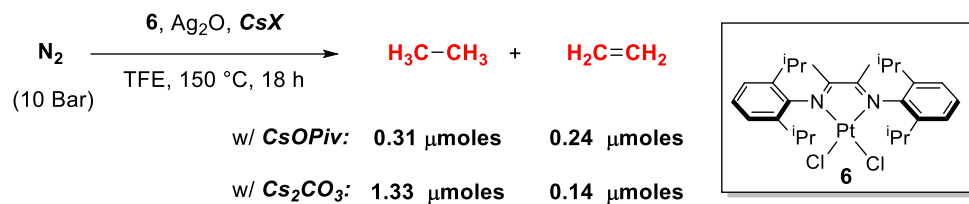
Table 4.5. Ethane and Ethylene Formed at Reduced Temperatures

$$\text{CH}_4 \text{ or } \text{N}_2 \xrightarrow[\text{TFE, } T \text{ } ^\circ\text{C, 18h}]{\mathbf{6} \text{ (80 } \mu\text{moles), Cs}_2\text{CO}_3 \text{ (10 equiv), Ag}_2\text{O (10 equiv)}} \text{H}_3\text{C}-\text{CH}_3 + \text{H}_2\text{C}=\text{CH}_2$$
 (10 Bar)

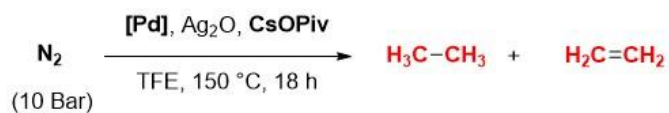
Entry	CH ₄ or N ₂	Temperature	Ethane (μmoles)	Ethylene (μmoles)
1	N ₂	150 °C	1.33	0.14

2	N ₂	120 °C	0.44	0.25
3	CH ₄	120 °C	0.07	0.02
4	CH ₄	100 °C	not detected	not detected

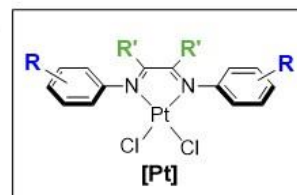
Scheme 4.11. Ethane and Ethylene Generation Using CsOPiv or Cs₂CO₃ with Complex 6



Scheme 4.12. Generation of Ethane and Ethylene from Pt Complexes Under N₂



Entry	Complex	R =	R' =	Ethane	Ethylene
1	6	2,6-iPr	Me	0.31	0.24
2	10	2,4,6-Me	Me	1.00	0.40
3	11	4-iPr	Me	0.14	0.09
4	12	2,6-iPr	H	0.03	0.04
5	13	2,6-iPr	Naphthyl	not detected	not detected



References

- (1) Kerr, R. A. *Science* **2010**, *329*, 780.
- (2) U.S. Energy Information Administration. International Energy Statistics - EIA <http://www.eia.gov/cfapps/ipdbproject/iedindex3.cfm?tid=3&pid=26&aid=1&cid=regions&syid=1980&eyid=2013&unit=QBTU> (accessed Mar 25, 2015).
- (3) Ma, D. *Energy Environ. Sci.* **2014**, *7*, 2580.
- (4) Hammond, C.; Conrad, S.; Hermans, I. *ChemSusChem* **2012**, *5*, 1668.
- (5) McFarland, E. *Science* **2012**, *338*, 340.
- (6) Lunsford, J. H. *Catal. Today* **2000**, *63*, 165.
- (7) Kaneko, T.; Derbyshire, F.; Makino, E.; Gray, D.; Tamura, M.; Li, K. In *Ullmann's Encyclopedia of Industrial Chemistry*; Wiley-VCH, 2000.
- (8) Holmen, A. *Catal. Today* **2009**, *142*, 2.
- (9) Cornils, B.; Herrmann, W. a. *J. Catal.* **2003**, *216*, 23.
- (10) Shilov, A. E.; Shul'pin, G. B. *Chem. Rev.* **1997**, *97*, 2879.
- (11) Kua, J.; Xu, X.; Periana, R. A.; Goddard, W. A. *Organometallics* **2002**, *21*, 511.
- (12) Muehlhofer, M.; Strassner, T.; Herrmann, W. A. *Angew. Chem. Int. Ed.* **2002**, *41*, 1745.
- (13) Kao, L. C.; Hutson, A. C.; Sen, A. *J. Am. Chem. Soc.* **1991**, *113*, 700.
- (14) Crabtree, R. H. *Chem. Rev.* **1995**, *95*, 987.
- (15) Lanci, M. P.; Remy, M. S.; Lao, D. B.; Sanford, M. S.; Mayer, J. M. *Organometallics* **2011**, *30*, 3704.
- (16) Lanci, M. P.; Remy, M. S.; Kaminsky, W.; Mayer, J. M.; Sanford, M. S. *J. Am. Chem. Soc.* **2009**, *131*, 15618.
- (17) Lotz, M. D.; Remy, M. S.; Lao, D. B.; Ariafard, A.; Yates, B. F.; Canty, A. J.; Mayer, J. M.; Sanford, M. S. *J. Am. Chem. Soc.* **2014**, *136*, 8237.
- (18) Remy, M. S.; Cundari, T. R.; Sanford, M. S. *Organometallics* **2010**, *29*, 1522.
- (19) Khusnutdinova, J. R.; Rath, N. P.; Mirica, L. M. *J. Am. Chem. Soc.* **2012**, *134*, 2414.
- (20) Khusnutdinova, J.; Rath, N.; Mirica, L. *J. Am. Chem. Soc.* **2010**, *132*, 7303.
- (21) Tang, F.; Zhang, Y.; Rath, N. P.; Mirica, L. M. *Organometallics* **2012**, *31*, 6690.
- (22) Periana, R. A.; Mironov, O.; Taube, D.; Bhalla, G.; Jones, C. J. *Science* **2003**, *301*, 814.

- (23) Lin, M.; Sen, A. *J. Am. Chem. Soc.* **1992**, *114*, 7307.
- (24) Zhong, H. A.; Labinger, J. A.; Bercaw, J. E. *J. Am. Chem. Soc.* **2002**, *124*, 1378.
- (25) Wieland, J.; Breit, B. *Nat. Chem.* **2010**, *2*, 832.
- (26) *Handbook of Green Chemistry and Technology*; Clark, J. H., Macquarrie, D. J., Eds.; John Wiley & Sons, 2008.
- (27) Foley, S. R.; Shen, H.; Qadeer, U. A.; Jordan, R. F. *Organometallics* **2004**, *23*, 600.
- (28) Annibale, G.; Canovese, L.; Cattalini, L.; Natile, G.; Biagini-Cingi, M.; Manotti-Lanfredi, A.-M.; Tiripicchio, A. *J. Chem. Soc. Dalton Trans.* **1981**, *12*, 2280.
- (29) Le Stang, S.; Paul, F.; Lapinte, C. *Inorg. Chim. Acta* **1999**, *291*, 403.
- (30) Scherg, T.; Schneider, S. K.; Frey, G. D.; Schwarz, J.; Herdtweck, E.; Herrmann, W. A. *Synlett* **2006**, *18*, 2894.
- (31) Hickman, A. J.; Cismesia, M. A.; Sanford, M. S. *Organometallics* **2012**, *31*, 1761.
- (32) Wong-Foy, A. G.; Henling, L. M.; Day, M.; Labinger, J. A.; Bercaw, J. E. *J. Mol. Catal. A Chem.* **2002**, *189*, 3.
- (33) Hickman, A. J. Catalyst Controlled Site-Selective C-H Functionalization, 2012.
- (34) Villalobos, J. M.; Hickman, A. J.; Sanford, M. S. *Organometallics* **2010**, *29*, 257.
- (35) Luo, J.; Rath, N. P.; Mirica, L. M. *Organometallics* **2013**, *32*, 3343.
- (36) Shul'pin, G. B. *Dalton Trans.* **2013**, *42*, 12794.
- (37) Gunsalus, N. J.; Konnick, M. M.; Hashiguchi, B. G.; Periana, R. A. *Isr. J. Chem.* **2014**, *54*, 1467.
- (38) Díaz-Requejo, M. M.; Pérez, P. J. *Chem. Rev.* **2008**, *108*, 3379.
- (39) Bolig, A. D.; Brookhart, M. *J. Am. Chem. Soc.* **2007**, *129*, 14544.
- (40) Xu, H.; Bernskoetter, W. H. *J. Am. Chem. Soc.* **2011**, *133*, 14956.
- (41) Ishikawa, K.; Fukuzumi, S.; Tanaka, T. *Inorg. Chem.* **1989**, *28*, 1661.
- (42) Obligacion, J. V.; Semproni, S. P.; Chirik, P. J. *J. Am. Chem. Soc.* **2014**, *136*, 4133.
- (43) Bhadbhade, M.; Clentsmith, G. K. B.; Field, L. D. *Organometallics* **2010**, *29*, 6509.
- (44) Briggs, A. J. *Synth. Commun.* **2013**, *43*, 3258.
- (45) Tu, T.; Fang, W.; Jiang, J. *Chem. Commun.* **2011**, *47*, 12358.

- (46) Alcazar, J.; Begtrup, M.; de la Hoz, A. *J. Chem. Soc. Perkin Trans.* **1995**, *19*, 2467.
- (47) Grasa, G. A.; Viciu, M. S.; Huang, J.; Nolan, S. P. *J. Org. Chem.* **2001**, *66*, 7729.
- (48) Kiernan. *J. Chem. Soc. Dalton Trans.* **1978**, 1127.
- (49) Achar, S.; Catalano, V. J. *Polyhedron* **1997**, *16*, 1555.